

# **INFLUENCE OF FIRE ON DC CORONA CURRENT**

By

**Ilunga Kayumba Grace**

Submitted in partial fulfilment of the requirement for the degree

Master of Science in Electrical Engineering

University of KwaZulu-Natal

Supervisor: Dr IE Davidson

Co-supervisor: Dr L Chetty

July 2014



## Declaration

I ILUNGA KAYUMBA Grace....., declare that

1. The research reported in this thesis, except where otherwise indicated is my original research.
2. This thesis has not been submitted for any degree or examination at any other university.
3. This thesis does not contain other persons' data, pictures, graphs or other information, unless specifically acknowledged as being sourced from other persons.
4. This thesis does not contain other persons' writing, unless specifically acknowledged as being sourced from other researchers. Where other written sources have been quoted, then:
  - a. Their words have been re-written but the general information attributed to them has been referenced
  - b. Where their exact words have been used, then their writing has been placed in italics and inside quotation marks, and referenced.
5. This thesis does not contain text, graphics or tables copied and pasted from the Internet, unless specifically acknowledged, and the source being detailed in the thesis and in the References sections.

Signed

.....

KG Ilunga

Signed

.....

IE Davidson

## **Acknowledgement**

My deepest gratitude to the Most High God, the Father the Creator of the heavens and earth for the grace He has bestowed upon me.

Thank you to my dear parents: A Kayumba and F Lenge for their continuous love, support and prayers.

Thank you to Dr IE Davidson, my supervisor, for his support and guidance during the research.

I would like to thank Dr L Chetty, my co-supervisor, for giving me the opportunity to study power transmission lines, and for his guidance, support and technical advice.

Thank you to my sisters IA Kayumba, BC Kayumba and NB Kayumba for their encouragement and prayers.

I am grateful to Pastor Ezekiel and his family for the support and prayers.

I would like to thank Charlain King and all my colleagues at the Eskom CoE in HVDC Engineering, Westville Campus, for encouragement and friendship.

I am grateful to my friends Alain, Blaise, Daniel, Pastor Caleb, Herve, Jimmy, Magalie, Pravesh and Taty for their support.

I wish to acknowledge UKZN, THRIP, NRF and ESKOM for the funding that supported this research.

KG ILUNGA

July 2014

## Abstract

Corona discharge is one of the undesirable consequences associated with HVDC transmission.

Corona discharges are the visible result of the partial electrical breakdown of ionised air in the non-uniform fields surrounding energised conductors. Corona produces undesirable effects such as corona loss, audible noise, radio interference, ozone and nitric oxides.

The performance of high voltage transmission lines is presumably affected by the occurrence of wild forest fires beneath these lines. Fire under transmission line generates heat and increases the temperature of the air surrounding the conductors.

The increase in temperature due to the presence of fire decreases the breakdown strength of air insulation that can result on flashovers and interruption of power supply.

This thesis presents the experimental results of the investigation conducted on a short test line using a small corona cage. The results of the corona current magnitudes obtained from the investigation on the dominant frequencies of the corona current pulses under the influence of high-temperature gas fire are presented.

The propagation of the dominant frequency signals is studied in isolation of other sources of high frequency signals within controlled laboratory conditions.

The corona current signature technique, which is the combination of the magnitudes of dominant frequencies and the repetition rate of the corona pulses, was introduced to evaluate the impact of fire on the corona current.

Results obtained from the dc corona current investigation are then compared with those obtained from ac corona current investigation and presented.

## Table of Contents

Declaration.....	I
Acknowledgement.....	II
Abstract.....	III
Abbreviations .....	VI
List of figures.....	VII
List of Tables.....	IX
CHAPTER 1.....	1
1.1 Problem Statement .....	2
1.2 Aims and Objectives .....	3
1.3 Scope of the dissertation.....	4
CHAPTER 2.....	5
2.1 Corona Process .....	5
2.2 Corona Onset Gradient .....	5
2.3 Corona Modes .....	7
2.3.1 Negative DC Corona.....	7
2.3.2 Positive DC Corona.....	7
2.3.3 AC Corona Modes.....	8
2.4 Phenomena of Ionisation in Air.....	9
2.4.1 Ionization by Collision .....	9
2.4.2 Photoionization .....	10
2.4.3 Secondary Ionisation.....	10
2.4.4 Thermal Ionisation.....	10
2.4.5 Attachment and Detachment.....	11
2.4.6 Recombination .....	11
2.4.7 Townsend First Ionisation Coefficient.....	11
2.4.8 Townsend Second Ionisation Coefficient.....	12
2.5 Consequences of Corona.....	14
2.5.1 Corona Loss (CL).....	14
2.5.2 Radio Interference (RI).....	14
2.5.3 Audible Noise (AN).....	14
2.5.4 Ozone and NO <sub>x</sub> .....	15
2.5.5 Corona Wind .....	15
2.6 Factors Influencing Corona Performance .....	15

CHAPTER 3.....	17
3.1 Thermal Ionization.....	17
3.2 Reduced Air Density .....	18
3.3 Combustion Particles .....	19
3.4 Flame Conductivity.....	19
3.5 Dielectric Strength.....	20
CHAPTER 4:.....	21
4.1 Experimental Procedure.....	21
4.1.1. Instruments .....	21
4.1.2. Apparatus .....	24
4.2 Test measurements .....	25
4.2.1 Background Noise.....	26
4.2.2 Experiment 1 - No Fire Condition (NFC).....	26
4.2.3 Experiment 2 - Fire Condition (FC).....	27
4.3 Results.....	28
4.3.1 No Fire Condition (NFC).....	28
4.3.2 Fire Condition (FC).....	40
4.3.3 Influence of Fire on Corona Current .....	52
4.3.4 Discussion.....	56
CHAPTER 5.....	57
5.1 Corona current tests.....	57
5.2 Future work.....	58
5.3 Recommendations .....	58
References.....	59
<b>APPENDIX A</b> .....	<b>62</b>
<b>APPENDIX B</b> .....	<b>74</b>
<b>APPENDIX C</b> .....	<b>79</b>

## Abbreviations

AC:	Alternating Current
CCS:	Corona Current Signature
CL:	Corona Loss
DC:	Direct Current
EMI:	Electromagnetic interference
FC:	Fire Condition
HVAC:	High Voltage Alternating Current
HVDC:	High Voltage Direct Current
NFC:	No Fire Condition
SD:	Standard Deviation
UKZN:	University of KwaZulu-Natal
UV:	Ultraviolet

## List of figures

Figure 4.1: Corona cage.....	21
Figure 4.2: Circuit of the HVDC generator.....	21
Figure 4.3: Smooth copper conductor with two artificial corona sources.....	22
Figure 4.4: Electric field distributions inside the cage without the burner.....	22
Figure 4.5: Electric field distributions inside the corona cage with the burner in the cage...	23
Figure 4.6: Experimental set up.....	24
Figure 4.7: Background noise of the corona cage.....	25
Figure 4.8: UV image of the corona discharges at 60kV NFC.....	28
Figure 4.9: Measured sample of corona current at 60kV NFC.....	28
Figure 4.10: Individual corona pulse at 60kV NFC.....	29
Figure 4.11: Frequency spectrum of individual corona pulse at 60kV NFC.....	29
Figure 4.12: UV image of corona discharges at 80kV NFC.....	30
Figure 4.13: Measured sample of corona pulse at 80kV NFC.....	31
Figure 4.14: Individual corona pulse at 80kV NFC.....	31
Figure 4.15: Frequency spectrum of individual corona pulse at 80kV NFC.....	32
Figure 4.16: UV of corona discharges at 100kV NFC.....	33
Figure 4.17: Measured sample of corona pulse at 100kV NFC.....	33
Figure 4.18: Individual corona pulse at 100kV NFC.....	34
Figure 4.29: Frequency spectrum of individual corona pulse at 100kV NFC.....	34
Figure 4.20: Frequency distribution of corona pulses time separation at 60kV NFC.....	36
Figure 4.21: Frequency distribution of corona pulses separation at 80kV NFC.....	37

Figure 4.22: Frequency distribution of corona pulses time separation at 100kV NFC.....	38
Figure 4.23: UV image of corona discharges at 60kV FC.....	40
Figure 4.24: Measured sample of corona current at 60kV FC.....	40
Figure 4.25: Individual corona pulse at 60kV FC.....	41
Figure 4.26: Frequency spectrum of individual corona pulse at 60kV FC.....	41
Figure 4.27: UV image of corona discharges at 80kV FC.....	42
Figure 4.28: Measured sample of corona current at 80kV FC.....	43
Figure 4.29: Individual corona pulse at 80kV "FC.....	43
Figure 4.30: Frequency spectrum of individual corona pulse at 80kV FC.....	44
Figure 4.31: UV image of corona discharges at 100kV FC.....	45
Figure 4.32: Measured sample of corona at 100kV FC.....	45
Figure 4.33: Individual corona pulse at 100kV FC.....	46
Figure 4.34: Frequency spectrum of individual corona pulse at 100kV FC.....	46
Figure 4.35: Frequency distribution of corona pulse time separation at 60kV FC.....	48
Figure 4.36: Frequency distribution of corona pulse time separation at 80kV FC.....	49
Figure 4.37: Frequency distribution of corona pulse time separation at 100kV FC.....	50
Figure 4.38: Variation of standard deviation of time with voltage NFC and FC.....	54
Figure 4.39: Variation of mean time of time with voltage NFC and FC.....	55

## List of Tables

Table 1: Dielectric strength at power frequency voltage of 3 m conductor-plane.....	19
Table 2: Average corona current magnitudes of the dominant frequencies at 60kV NFC.....	30
Table 3: Average corona current magnitudes of the dominant frequencies at 80kV NFC.....	32
Table 4: Average corona current magnitudes of the dominant frequencies at 100kV NFC.....	35
Table 5: Comparative table of the averages of corona current magnitude at different voltages NFC.....	35
Table 6: Average and standard deviations of the time period between corona current pulses at 60kV NFC.....	36
Table 7: Average and standard deviations of the time period between corona current pulses at 80kV NFC.....	37
Table 8: Average and standard deviations of the time period between corona current pulses at 100kV NFC.....	38
Table 9: Comparison of average and standard deviations of the time period between corona current pulses for the three applied voltages NFC.....	39
Table 10: Average corona current magnitudes of the dominant frequencies at 60kV FC.....	42
Table 11: Average corona current magnitudes of the dominant frequencies at 80kV FC...	44
Table 12: Average corona current magnitudes of the dominant frequencies at 100kV FC.....	47
Table 13: Comparative table of the averages magnitudes of corona current magnitude at different voltages FC.....	47

Table 14: Average and standard deviation of time period between corona current pulses at 60kV FC.....	48
Table 15: Average and standard deviations of the time period between corona current pulses at 80kV FC.....	49
Table 16: Average and standard deviations of the time period between corona current pulses at 100kV FC.....	50
Table 17: Comparison of average and standard deviations of the time period between corona current pulses for the three applied voltages FC.....	51
Table 18: Average of corona pulse magnitude and average corona time interval at 60 kV NFC and FC.....	51
Table 19: Average of corona pulse magnitude and average corona time interval at 80 kV NFC and FC.....	52
Table 20: Average of corona pulse magnitude and average corona time interval at 100 kV NFC and FC.....	52

## CHAPTER 1

### INTRODUCTION

---

Transmission lines carry electric power over distances from generating stations to load centres, typically at high voltages such as 400 kV and 765 kV. Regional lines may operate at the 132kV level. For domestic loads, supply voltage varies from country to country. For example: 110-120 Volts (North America), 220/380 to 240/415 Volts (South Africa). In distribution networks, 11 kV is normally used so that distribution substations are connected in a network of 11 kV and customers are connected in a low voltage network, supplied through step-down transformers in the distribution substations. In South Africa, electric power transmission systems operate at standard voltages of 132 kV, 220kV, 275kV, 400kV and 765kV; and the approximate total transmission line length is 28,000km long [1].

System studies are conducted from time to time to ascertain the operating state of a network, taking into account load growth projections for the future. Undue stresses on the system or anticipated problems are determined from power flow analysis or during operation and maintenance. Such analysis includes an assessment of the voltage profile, voltage regulation and fluctuations, magnitude of electrical losses, distribution plant loading and utilization, fault analysis, generation stability, the level of harmonics in the system, supply availability and system security. The performance of the transmission system is monitored and analysed to identify the cause of faults that occur on the network. The knowledge of the cause of faults finds its relevance in influencing design and managing line servitudes [1]. South Africa is characterised by two main seasons, namely winter and summer. These weather conditions are a main factor responsible for faults in transmission lines. Birds, lightning, fire and pollution were identified as the four most significant individual causes of faults. These four causes altogether represent about 89% of all faults [1].

HVDC systems present many advantages over HVAC systems over long distances for bulk power transmission. The advantages and disadvantages of both systems can be contrasted [2]:

- HVAC systems are 3-phase 3-wire, while HVDC transmission systems use 2 wires only.
- HVDC systems require additional components, namely: rectifiers and inverters at the beginning and end of the line respectively, while HVAC systems do not.

- HVDC towers require less material, clearance height and reinforcement when compared to equivalent HVAC towers.
- Beyond approximately 400km, the HVDC system has an advantage of lower marginal cost compared to HVAC lines, and this could decrease with better/cheaper power electronic converters (i.e. cost of rectifier/inverter < cost of extra conductor, towers, insulators, etc. for lines exceeding 400km)
- Using power electronic switching devices (FACTS controllers), precise and fast power control in either direction is easier to achieve in HVDC than HVAC systems as dc power is minimally affected by reactance.
- The ease of control of power flow in HVDC lines makes it easy to achieve the maximum power and thermal capacity of transmission lines.

In summary, HVDC transmission lines are cheaper than HVAC transmission lines, but this advantage is redeemed for all but the longest lines by the cost of the AC/DC converter stations. HVDC does offer special technical advantages as outlined. All angular stability problems disappear and even connection of systems at different frequency is feasible. The problems of cable charging current are eliminated and thus cables can readily be used for underwater crossings. It is also simple to control active power transfer at a predetermined level or even to modulate this to improve system damping [2]. HVDC therefore increases the technical and economic feasibility of transmission lines. However, various problems associated with AC and DC transmission lines have been identified and corona discharge is one of these problems.

Corona discharge is one of the undesirable consequences associated with the operation of HVDC transmission lines. Corona is a discharge phenomenon characterized by power loss and environmental effects such as audible noise and radio interference. The environmental effect of corona can be reduced by increasing the conductor diameter or by increasing the number of bundled conductors. The corona discharge parameters are contained in the pulses [3].

## **1.1 Problem Statement**

Fire is a natural phenomenon that can affect the quality of electricity supply. Fire occurring under transmission lines is responsible for a considerable number of power outages. In terms of fires affecting the commercial forest industry and electrical utilities, the frequency of grass fires appears to be higher in South Africa than in countries such as the United States, Brazil and Australia. For approximately 90 000 hectares of South African forest, more than 500 fires were reported in a year however only 36 fires were

recorded in an Australian forest of the same size, for the equivalent period [4]. Sugar cane fires are responsible for several flashovers each year in South Africa. Sugar cane fires are common in the KwaZulu-Natal and the Mpumalanga provinces of South Africa [5]. In 2003 Cecil Richards Evert [6] investigated the detection of fires under high voltage transmission lines and studied the high frequency characteristic of AC corona and electrical discharge generated by fire [6]. Most of his investigations were conducted on an outdoor corona cage. It has been shown that under these conditions, it is nearly impossible to control important variables such pressure, temperature and humidity. These factors are recognised to be important to understand the nature of corona.

The increase in number of operational HVDC schemes has prompted the fundamental need to characterise the electrical environment in the vicinity of these lines so that the environmental impact of HVDC lines may be better understood.

Corona is critical problem in high voltage transmission lines. It is therefore necessary to carry out experimental investigations to obtain an improved understanding of this phenomena under a controlled laboratory environment. To date, there is no literature the author is aware off, discussing a method (and subsequent results) for investigating the influence of fire on DC corona performance. This research investigation therefore provides a procedure and methodology for conducting safe high voltage experiments for fire induced DC corona phenomena under a controlled laboratory environment.

## **1.2 Aims and Objectives**

The primary aim of this study is to determine if fire can increase dc corona current. It investigates dc corona current under different environmental conditions. It covers the following areas and seeks to establish and answer these research questions:

- What is the behaviour of corona pulses under fire conditions?
- What is the relationship between the amplitude of the corona current and the frequency spectrum of the corona current pulses?
- Carry out an assessment and evaluation of the time occurrence of corona pulses under fire condition.
- What is the corona pulse amplitude and the repetition rate of the corona current pulses under fire conditions?

### **1.3 Scope of the dissertation**

#### Chapter 2

This chapter provides a general background on corona phenomena, the mode and the effects of corona on transmission lines and the environment.

#### Chapter 3

The theory and properties of fire is presented in this chapter; such as the reduction in air density; combustion particles and the dielectric strength of air under fire conditions.

#### Chapter 4

This chapter presents the research investigations which were carried out under laboratory conditions. It includes the methodology and the equipment used for the experimental tests. Results of the experiments undertaken on dc corona and fire are also provided in this chapter. Two different measurements were carried out, under two different conditions, namely: "fire condition" and "no fire condition". Lastly, the results of the analysis of recorded data and the discussion of the results are also presented.

#### Chapter 5

This chapter provides a conclusion of the research investigations proposes future studies and gives a few recommendations.

## CHAPTER 2

### CORONA

---

The first investigations on corona were published by F W Peek in 1911 [7]. Ever since, corona has become an important subject for research interest. Considerable research has been undertaken since to better understand this corona phenomena. Different studies have been carried out to determine some of the effects of corona such as: the influence of corona produced on DC lines; the audible noise and the ionisation of air [8]. In many countries, experimental research has been carried out on the electromagnetic environment of HVDC lines, which have produced many empirical formulae for the calculation of corona loss, audible noise and radio interference [8].

Corona may be defined as the creation of ions in air due to the presence of a non-uniform but strong electric field. Corona is the cause of considerable power loss, audible noise and radio-frequency interference. It can also generate toxic compounds such as ozone and oxides of nitrogen; and has been found to initiate arcing.

#### 2.1 Corona Process

Air is composed of nitrogen 78%, oxygen 21%, argon 0.93%, carbon dioxide 0.033%, water vapour and particles (such as dust, and pollen). Ozone is the main by-product of corona [9]. Atmospheric air is almost a perfect insulator under normal conditions but some naturally occurring phenomena such as cosmic radiation or natural ionisation by radioactive substances on earth give rise to charge carriers such as free electrons and ions that make air an imperfect insulator. Under the influence of an electric field, these free electrons and ions start moving and accelerating. If the electric field strength is very high, they will give rise to a sequence of ionisation events in the surrounding air that culminates in the formation of corona.

#### 2.2 Corona Onset Gradient

Corona is a phenomenon that occurs on conductors and line hardware. It is therefore useful to determine the threshold voltage for its' onset on the conductors. When the applied voltage across a conductor is increased, a self-sustained electrical discharge called corona onset occurs. It is possible to determine the conductor surface gradient at which corona onset occurs. A number of experimental studies have been carried out, using a concentric cylindrical setup to determine the corona onset gradient of smooth cylindrical conductors [10]. An empirical formula on smooth cylindrical

conductors where the corona onset gradient is a function of a superficial field, the radius of the conductor and air density was developed by Peek [10]:

$$E_c = mE_0\delta \left[ 1 + \frac{C_1}{\sqrt{\delta r_c}} \right] \quad (2.1)$$

Where:

$E_c$  is the corona onset gradient in kV/cm.

$E_0$  is an empirical constant (superficial field) which is equal to 29.8 kV/cm (peek value) or 21.1 kV/cm (rms value).

$C_1$  is an empirical constant which is equal to  $0.31 \text{ cm}^{1/2}$ .

$r_c$  is the conductor radius in cm.

$m$  is the conductor irregularity factor that takes the surface condition into account.

$m$  is equal to 1 for ideally smooth cylindrical conductor.

For clean stranded conductors  $m$  varies between 0.75 and 0.85, depending on the radii of the outer strand and of the overall conductor. The presence of nicks or scratches can reduce the value of  $m$  to 0.6 and 0.8. The value of  $m$  may also be reduced to the range of 0.3 to 0.6 by the presence of any deposits on the conductor. The relative air density  $\delta$  is defined as [9]:

$$\delta = \frac{273 + t_0}{273 + t} \times \frac{p}{p_0} \quad (2.2)$$

where:

$t$  is the temperature, in ° C.

$p$  is the atmospheric pressure, in mm or bar.

$t_0$  is the reference temperature, usually 25 ° C.

$p_0$  is the reference pressure usually 760 mm or 1.013 bar.

If we take in consideration the two formulae (2.1) and (2.2) we can see that there is an influence of temperature and pressure on the corona onset gradient.

## 2.3 Corona Modes

The physical manifestation of corona may vary depending on the electrode voltage polarity. Thus, there is negative and positive corona.

### 2.3.1 Negative DC Corona

With a high voltage (DC) of negative polarity applied to a conductor, the negative corona can appear in air as Trichel pulses, negative glow, negative or positive streamers, or spark breakdown [11].

- Trichel Pulses

Trichel pulse corona is the first phenomenon that occurs above the corona onset voltage. The pulses appear as a bright spherical discharge of the same amplitude and at short regular intervals of the order of a 100 nanoseconds. The light intensity and length of the Trichel pulse are weaker and shorter compared with the pulses associated with positive polarity corona.

- Negative Glow

By increasing the voltage, the Trichel pulse frequency increases until it reach a critical value. Above a certain voltage level, depending on the gap distance and the line configuration, the intermittent Trichel pulses are replaced by a new mode of continuous corona called “negative glow”. The bright spherical discharges are then followed by a conical positive column [10]. The transition of the two modes is characterised electrically by a steady current of order of 10  $\mu\text{A}$ .

- Negative Streamer

Above a certain voltage level, and depending on the line configuration, the glow corona changes to negative streamer corona. In the case of negative streamer corona, the discharge current consists of pulses super-imposed on a dc component.

### 2.3.2 Positive DC Corona

If a DC voltage of positive polarity is applied to a conductor, the positive corona can appear in different forms, depending on the applied voltage, namely: burst corona,

onset streamers, steady glow (or positive glow) corona, and breakdown streamer corona. Most investigations on corona discharge are made in point-to-plane gaps.

- **Burst Corona**

Burst corona occurs as a light discharge which consists of many filaments near the conductor point when the applied voltage exceeds a certain threshold. This threshold is also influenced by the line configuration. The total duration of the phenomenon is a few hundred nanoseconds, during which the streamer length increases at the velocity of 10 to 100 cm/ $\mu$ s. The build-up time and the total duration of each pulse are much longer when compared with Trichel pulses.

- **Onset Streamer**

The onset streamer (also known as a “plume”) appears when the applied voltage is further increased above the threshold value. To obtain an onset streamer corona, the electric field near point must be sufficiently high and there needs to be non-negligible negative space charge adjacent to the electrode. The voltage interval in which this mode of corona occurs depends on the electrode geometry. For a given geometry, the voltage interval may be ten times larger than that for pulse or burst corona [9]. The onset streamer will stop during an interval of time necessary to clear the space charge. It also resumes as soon as the original field is restored. The onset streamer is pulsative in nature, producing corona current pulse with large amplitudes and lower repetition rates than negative Trichel streamer corona. In practice the onset streamers are the main source of radio interference and audible noise [10].

- **Positive Glow Corona**

The positive glow corona occurs as the discharge progresses from burst corona to a stable glow under a special condition of electrical field distribution near the highly stressed positive electrode. Positive glow is a result of a particular rate combination of creation and removal of positive ions near the electrode. If the voltage applied is further increased, streamers of a more vigorous nature are produced that can eventually lead to breakdown of the conductor-plane gap [11].

### **2.3.3 AC Corona Modes**

When an ac current is applied to a conductor-plane gap, the electric field in the gap varies continuously in intensity and polarity. Different modes of corona can be

observed in the same cycle of the applied voltage [12]. The discharge process under ac voltage differs from that under dc voltage mainly due to the voltage oscillation and the oscillatory movement of space charge developed by the corona. For a short gap, the ion space charge generated in one half-cycle is absorbed by the electrodes in the same half-cycle. We can observe the same modes of corona that develop for dc voltages: negative Trichel streamers, positive onset streamers and burst corona. For long gaps, the ion space charge produced in one half-cycle may not be completely absorbed by the electrodes in the same half cycle, leaving residual space charge in the gap. This residual space charge is drawn back to the region of high field intensity in the following half-cycle and can influence subsequent development of corona. Onset streamers are suppressed in favour of the positive glow discharge [12].

## 2.4 Phenomena of Ionisation in Air

The most common gaseous insulator at atmospheric pressure is air. Air is an excellent insulator at normal temperature and pressure. Various natural phenomena such as cosmic radiation, gamma rays and radioactive substances on earth give rise to natural ionization of air. This ionized air produces charge carriers such as free electrons and ions that inhibit the air ability to be a good insulator. Thus, positive and negative ions are mainly found in atmospheric air as a result of these natural ionisation processes. Air remains almost electrically neutral due to an equal number of positive and negative ions but susceptible to the occurrence of electrical discharge [9]. In the presence of an electric field the positive and negative ions produced by natural ionisation start moving and cause an electric current to flow in the air. The processes primarily responsible for the breakdown of gas are ionization by collision, photo-ionization and secondary ionization. The process of attachment plays an important role in insulating gases [13].

### 2.4.1 Ionization by Collision

Ionisation by collision consists of the release of an electron from an atom or a molecule when the free electron collides with a neutral molecule. This process can be represented by the expression [10]:



Where:

$A$  is the atom,

$e^-$  is the free electron

$A^+$  is a positive ion

### 2.4.2 Photoionization

Photoionization is also called ionisation by radiation. This occurs when the amount of radiation energy absorbed by an atom or molecule exceeds its ionisation energy when an electron is released. The process can be represented by the expression [5]:



Where  $h\nu$  is the photon energy

### 2.4.3 Secondary Ionisation

In the case of secondary ionisation, secondary electrons released from the cathode or gas molecules through collision with positive ions or photons, sustain the discharge after it is established. Secondary ionisation is essential in the streamer breakdown mechanism and corona.

### 2.4.4 Thermal Ionisation

Generally, thermal ionisation occurs at high temperatures. They occur when there is ionisation caused by molecular collisions, radiation and electron collisions. Thermal ionisation is the main source of ionisation in flames. Saha [14] derived an expression for the ionisation  $\beta$  in terms of absolute temperature and gas pressure as follows:

$$\frac{\beta^2}{1 - \beta^2} = \frac{1(2\pi m_e)^{1/2}}{ph} (kT)^{5/2} e^{-W_i/kT} \quad (2.5)$$

$$\frac{\beta^2}{1 - \beta^2} = \frac{2.4 \times 10^{-4}}{p} T^{5/2} e^{-W_i/kT} \quad (2.6)$$

Where:

$p$  is the gas pressure in  $mm$

$W_i$  the ionisation energy of the gas

$k$  is Boltzmann's constant:  $1.3806488 \times 10^{-23} \text{ m}^2\text{kg}\cdot\text{s}^{-2}\text{K}^{-1}$

$T$  is the absolute temperature, in K

$m$  is the mass of the electron

$h$  is the Planck's constant

$\beta$  depends on temperature and it can be shown that thermal ionisation of gas become significant only if the temperature exceeds  $1000^\circ\text{C}$ .

#### 2.4.5 Attachment and Detachment

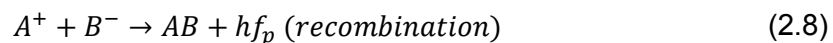
In an electronegative gas, attachment is where the atoms or molecules capture free electrons to form negative ions. The attachment can be represented by the expression:



Detachment is the reverse process where negative ions can lose electrons and revert to their neutral state.

#### 2.4.6 Recombination

Recombination occurs where positive and negative combine to form a neutral atom or molecule that may be in an excited state until it emits a photon. This process may be represented by the expression [15]:



#### 2.4.7 Townsend First Ionisation Coefficient

Townsend [13] studied the variation of gas current as a function of voltage. At first the current increases proportionally as the voltage increases, and then remains constant at a certain value  $I_0$  which corresponds to the saturation current. When the voltage is further increased, the exponential increases in current magnitude above  $I_0$  which is due to ionisation of gas by electron collision. Townsend introduced the first ionisation coefficient  $\alpha$  to explain the exponential rise in current and defined this as the number of electrons produced per unit length of path in the direction of the field. If  $n$  is the number of electrons at the distance  $x$  from the cathode, the increase in electrons  $dn$  in additional distance is  $dx$  is given by [13].

$$dn = \alpha n dx \quad \text{or} \quad \frac{dn}{n} = \alpha dx \quad (2.9)$$

Integrating (2.7)

$$\ln n = \alpha x + C \quad (2.10)$$

$$\text{At } x = 0, n = n_0 \quad (2.11)$$

$$\ln n_0 = C$$

$$\ln n = \alpha x + \ln n_0 \quad (2.12)$$

At  $x = d$ ,

$$n = n_0 e^{\alpha d} \quad (2.13)$$

In terms of current

$$I = I_0 e^{\alpha x}$$

Where  $e^{\alpha x}$ : electron avalanche, and  $I_0$ : current at the cathode

#### 2.4.8 Townsend Second Ionisation Coefficient

In his earlier measurement of current in a parallel plate gap, Townsend observed that the current increased more rapidly at high voltage than can be explained by the first mechanism in equation (2.11). Thus he suggested that the current must be affected by a second mechanism. Townsend postulated that the additional current must be due to the presence of positive ions and the photons. The positive ions may have sufficient energy to liberate the electrons by collision with gas molecules and by bombardment with the cathode. The photons will also release electrons after collision with gas molecules and from the cathode after photon impact [5].

Let:

$\gamma$  - The Townsend second coefficient is defined as the number of electrons released from cathode per incident positive ion.

$n_0$  - Number of electrons released from the cathode by ultraviolet radiation.

$n_+$  - Number of electrons released by the cathode due to the second mechanism.

$n$  - Number of electrons reaching the anode.

Then:

$$n = (n_0 + n_+)e^{\alpha d} \quad (2.14)$$

The number of electrons released from the gas will be given by

$$n_g = n - (n_0 + n_+) \quad (2.15)$$

For,  $n_+ = \gamma n_g$

$$\text{or } n_+ = \gamma[n - (n_0 + n_+)] \quad (2.16)$$

$$n_+(1 + \gamma) = \gamma(n - n_0) \quad \text{or } n_+ = \frac{\gamma(n - n_0)}{(1 + \gamma)} \quad (2.17)$$

Substituting  $n_+$  in (2.12)

$$\begin{aligned} n &= \left[ n_0 + \frac{(n + n_0)}{(1 + \gamma)} \right] e^{\alpha d} \\ &= \frac{(1 + \gamma)n_0 + \gamma n - \gamma n_0}{(1 + \gamma)} e^{\alpha d} \\ &= \frac{n_0 + \gamma n}{1 + \gamma} e^{\alpha d} \end{aligned} \quad (2.18)$$

$$\text{or } (n + \gamma n) = n_0 e^{\alpha d} + \gamma n e^{\alpha d} \quad (2.19)$$

Therefore we have

$$n = \frac{n_0 e^{\alpha d}}{1 - \gamma(e^{\alpha d} - 1)} \quad (2.20)$$

The steady state of current is

$$I = \frac{I_0}{1 - \gamma(e^{\alpha d} - 1)} \quad (2.21)$$

$1 - \gamma(e^{\alpha d} - 1)$  increases as the voltage increases. If  $1 - \gamma(e^{\alpha d} - 1) = 1$  the current becomes infinite. This is possible only theoretically but practically the current is limited by the resistance of the external circuit and partially by the voltage drop in the arc.  $\alpha$

and  $\gamma$  have been determined as functions of electric field and gas pressure [5]. The condition  $e^{\alpha d} = 1$  known as the Townsend breakdown criterion defines the beginning of the spark.

If  $e^{\alpha d} = 1$ , we refer to this as self-sustained discharge. Even if the source producing  $I_0$  is removed the discharge will sustain itself. The discharge comes from the repetition of the avalanche process due to the large number of ion pairs produced in the gap by the electron avalanches. In this case we talk about the threshold sparking condition.

If  $e^{\alpha d} > 1$

The spark discharge grows more rapidly the more  $\gamma e^{\alpha d}$  exceeds unity. In this case ionisation produced by successive avalanches is cumulative.

If  $e^{\alpha d} < 1$

In this case the current ceases to flow on removal of the source of electrons.

## **2.5 Consequences of Corona**

### **2.5.1 Corona Loss (CL)**

When corona is present, energy that is supplied by the power source connected to the transmission line is dissipated in the form of heat and light. This dissipation of energy is called corona power loss. Corona loss is influenced by the conductor's surface roughness and the weather conditions. [15]

### **2.5.2 Radio Interference (RI)**

The impulsive nature of corona is the origin of the electromagnetic interference (EMI). Trichel streamers during the negative half cycle and the onset streamers during the positive half cycle both give rise to transient current pulses with fast rise time and short duration. These transient current pulses and gap discharge generate EMI over a broad range of frequencies [10].

### **2.5.3 Audible Noise (AN)**

The main sources of audible noise are negative Trichel streamers and positive onset streamers [10]. During the formation of the discharge channel, the streamers produce high temperature that creates a corresponding increase in the local pressure

propagating through the surrounding air. This change of local pressure in the surrounding air is the origin of an acoustic wave perfectly audible in the immediate vicinity of the HV lines. Above 500kV the audible noise as well as the radio interference become very relevant and an important parameter in the design of the conductor.

#### 2.5.4 Ozone and NO<sub>x</sub>

During positive and negative corona, complex electrochemical reactions take place. The oxygen molecules may be dissociated into two oxygen atoms due to the ionisation process and this give rise to ozone and nitric oxide [14].

#### 2.5.5 Corona Wind

When an electrical field is applied to a gas, the ions created by any corona discharge are accelerated. In the cases of both negative and positive corona, ions of the respective corona polarity are repelled away from the high field electrode. Due to the collisions and friction with uncharged gas particle, the ions lose some of their kinetic energy to neutral particles. This creates a difference in pressure in the gas and the gas starts moving away from the electrode. This phenomenon is called electrical- or corona wind [11].

### 2.6 Factors Influencing Corona Performance

Corona performance may be influenced by many factors, factors depending on line design such as the operating voltage and system configurations. Other external factors include: ambient weather conditions, ground resistivity and altitude. The influence of temperature is due to conductor heating with a rise in temperature. As the temperature increases the relative air density decreases.

- Conductor surface

As shown in Peek's formula one of the important factors that influences the corona is the radius of the conductor. However the influence of the conductor surface irregularity factor  $m$  is somewhat similar to that of the conductor size. For ideal surfaces such as cylindrical smooth conductors the value of  $m = 1$ . However, in practical transmission lines the conductor surface is far from ideal, because of the stranding, nicks and scratches. Thus the factor  $m$  in practical cases can be defined as the ratio between the measured onset gradient and that calculated for an ideal smooth cylindrical conductor of the same radius. The experimental studies show that the value of  $m$  varies between 0.75 and

0.85 for clean stranded conductors. The presence of nicks and scratches or any deposits on the conductor can reduce the value of  $m$  to 0.6 or less. The conductor surface conditions can be affected by water deposit and pollution. Corona discharges can also cause changes in the surface conditions.

- Weather and atmospheric conditions

Atmospheric condition such as air density, humidity, and wind influence corona generation. An increase in air density and humidity corresponds to the lower levels of corona [10]. Atmospheric conditions also influence the properties of fair-weather sources on the conductor and thus their corona characteristics. The presence of wind increases the positive streamer activity [10].

- Reduced air density

The drop of ambient air pressure causes more ionisation of the air due to the increase in the mean free path of the free electrons. The more the air is ionised the more corona there is. This shows that at high altitudes, conductor corona starts at a lower voltage than at sea level.

## CHAPTER 3

### THEORY OF FIRE

---

Fire reduces the insulating properties of air. Since air is the main insulation of transmission lines, the reduction of the dielectric strength of air can drastically affect the performance of transmission lines. The occurrence of fire has been reported as responsible for power outages in many countries [4]. Sugar cane fires, grass fires, forest fires, oil fires, refuse burning and natural gas fires, are the types of fire that can cause power outage [17].

Annually Eskom records almost 3000 to 6000 fires near transmission lines with a rate of 100 to 150 of fire-induced flashovers per annum [4]. Previous research performed by Eskom has shown that fire under transmission lines produces enough ionised air to cause about 20% of the total number of flashovers [18]. Richard Evert [6] carried out an investigation into the detection of fire under high voltage transmission lines, and studied the high frequency characteristics of corona and electrical discharge generated by fire.

Aaron Sukhnandan [5] conducted a theoretical and experimental investigation into fire induced flashover of High Voltage Transmission Lines, and presented the flame theory conductivity and the effect of fire and flame on the air gap space-charge. It has been shown that the study of fire-induced flashover is dynamic and complex and it is a subject not completely understood.

Three parameters have been identified as the main causes that are responsible for reducing the breakdown strength of air in the presence of fire, namely:

- The thermal ionization caused by the flame.
- The reduced air density caused by the high temperature.
- The particles generated as a result of combustion.

#### **3.1 Thermal Ionization**

The flame is plasma where the air molecules are thermally and chemically ionized. The main source of ions and electrons in the flame are the molecules with a low ionization potential, such as carbon. An increase in temperature increases the rate of ionisation. Thermal ionisation is considered as possible factor contributing to the increase in corona due to fire under a transmission line. [6]

### 3.2 Reduced Air Density

The decrease of the dielectric properties of air is due to the temperature effect. An increase in temperature due to the presence of fire causes a decrease in air density. Temperature and humidity are the two factors that influence the breakdown strength of air. However, the humidity correction factor H is not considerable in the presence of fire, hence the flashover voltage is given by the expression [19]:

$$V_s = V_t \frac{H}{\delta} \quad (3.1)$$

Where

$V_s$  is the flashover voltage under standard conditions

$V_t$  is the flashover voltage under actual conditions

H is the humidity factor

$\delta$  is the relative air density and affects the flashover voltage the most.

$$\delta = \frac{0.392P}{273 + t} \quad (3.2)$$

Where

P is the barometric pressure in mm Hg that is constant

t is the temperature in °C

H is the relative humidity factor and is negligible in fires and can be ignored

Hence

$$V_t = V_s \frac{0.392P}{273 + t} \quad (3.3)$$

Equation (3.3) shows that flashover voltage is directly proportional to the barometric pressure and indirectly proportional to temperature. This theory presumes that a reduction of air density is caused by the heat from fires and results in a reduction in the insulation strength of air. Results from field measurement show that at constant barometric pressure and temperature of ~900°C, the air density can be reduced to 0.25 of its nominal value [20].

### 3.3 Combustion Particles

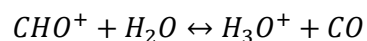
A large number of particles (such as smoke, ashes, soot) are generated within the gap in the presence of fire. The amount of particles generated depends on the source of fire. The amount of particles is greater, for example, in a forest fire or a sugar cane fire than for a gasoline fire or refuse burning. Introducing particles into the flame reduces the air breakdown voltage. The effect of the particles on the dielectric strength is strongly affected by the size and concentration of the particles and can be more significant in smaller gaps [20]. Thermionic emission phenomena can also be considered at high temperatures. However this phenomenon is only more significant under laboratory conditions where the gap space is short [20].

### 3.4 Flame Conductivity

The flame may be conductive because of the thermal ionisation of the air and the presence of ions from fuel oxidation reactions. The fuel oxidation is a complex process with the creation of  $H_3O^+$  ion from the chemical ionisation reactions between a hydrocarbon flame, oxygen and water.



Followed immediately by the charge reaction (3.5)



$H_3O^+$  - the dominant ion in lean fuel such as hydrocarbon flames

$CH_3^+$  - the dominant ion in a very rich flames formed by:



The concentration of ions increase as the temperature increases, and the conductivity increases as the ions concentration increases. Thermal ionisation becomes significant at 1000K [6].

### 3.5 Dielectric Strength

The flashover voltage of air insulation drastically decreases in the presence of fire, when compared to the value at ambient temperature. The flashover voltage at power frequency obtained for a 3m conductor-plane gap configuration under different temperatures and fire sources are shown in Table 2 [16].

Table 1: Dielectric strength at power frequency for a 3 m conductor-plane gap configuration

Gap conditions	Flashover voltage kV rms/cm
Without fire, t = 15 °C	2.5
Without fire, t = 100 °C	1.9
Without fire, t = 120°C	1.7
Fire with gasoline	1.0
Fire with alcohol	0.8
Fire of sugar cane leaves	0.5

Table 2 shows that the flashover voltage depends on the quantity of floating particles within the gap. The significant reduction in the flashover voltage for sugar cane is due to the large amount of combustions.

## CHAPTER 4:

### DC CORONA MEASUREMENTS

---

#### 4.1 Experimental Procedure

The laboratory experiments were designed to:

- Determine and analyse the repetition rate of corona pulses under different applied voltages and different environmental conditions.
- Establish the corona current amplitudes of corona pulses under different applied voltages and different environmental conditions.
- Determine the characteristic frequency of the corona current pulse.

The laboratory experiment was performed using the indoor corona cage facility located at the Eskom Centre of Excellence in HVDC Engineering at the University of KwaZulu-Natal.

##### 4.1.1. Instruments

The investigation was carried out using a DC voltage source and various measuring instruments. The test apparatus for the experiment included: corona cage, flame generator, and a DC high voltage power supply. Measuring instruments used include: oscilloscope, thermocouple and barometer. These were used for the measurement of voltage, corona pulses, temperature, pressure, and humidity respectively.

##### 4.1.1.1 Corona cage

The corona cage is an important tool for studying the effects of corona. High electric field strengths can be obtained at reasonably low conductor voltage [21]. A corona cage is widely used for predicting corona characteristics. The corona cage is typically a single-phase test facility in which smooth or bundled conductors are centred in a grounded meshed cage. The Eskom CoE in HVDC Engineering at the University of KwaZulu-Natal, Durban, South Africa, has an HVDC Research Laboratory which is equipped with a corona cage. This offers the advantage that certain environmental conditions can be varied while others are kept constant. Figure 4.1 shows a general view of the corona cage at the HVDC laboratory. The cross section of the cage is cylindrical with 100cm diameter and 200cm in total length. The two guard sections of the cage are grounded in order to eliminate the electromagnetic interference from the external environment. The central section of the cage was connected to the ground

through two resistors in series of  $1\Omega$  each. The data acquisition system was connected across a resistor.



Figure 4.1: Corona cage

#### 4.1.1.2 HVDC voltage supply

For the high voltage dc supply, a Cockcroft-Walton circuit, which is a half wave voltage multiplier and a half wave voltage doubler circuit, was used.

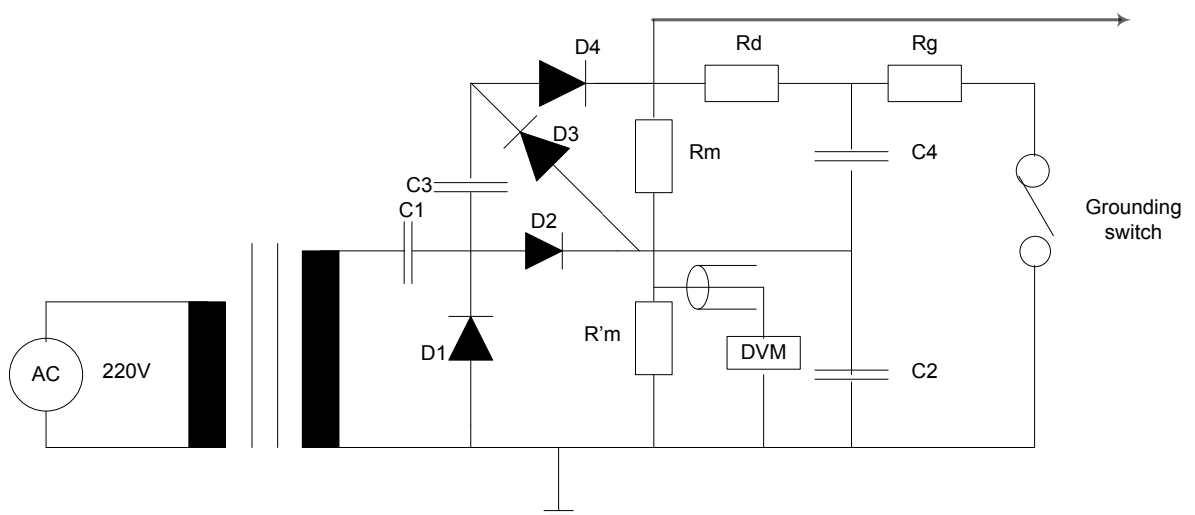


Figure 4.2: Circuit diagram of the high voltage dc generator.

The maximum output of the dc source is  $+500\text{ kV}$ ,  $-540\text{ kV}$ , and  $7.5\text{ mA}$  current capability. For this investigation, the maximum voltage applied was  $100\text{ kV}$  due to the

constraints of the physical clearance height at the HVDC Lab. Only positive dc voltage was investigated due to the dc power supply equipment limitation.

#### 4.1.1.3 Conductor

A single smooth copper conductor of length 260 cm and diameter 2.2 cm was used. Two artificial corona sources (5mm long nails) were added.

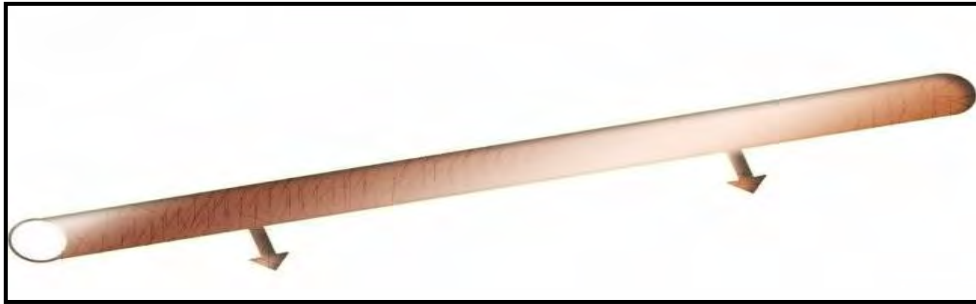


Figure 4.3: Smooth copper conductor with two artificial corona sources

#### 4.1.1.4 Burner

A burner of length 1.09 m, width 30 cm, and height 33 cm was placed in the central section of the corona cage. The burner was connected to a gas cylinder tank. The various measurements were carried out with the burner inside the cage. The presence of the burner in the cage was simulated to show the effect of the burner on the electric field inside the cage.

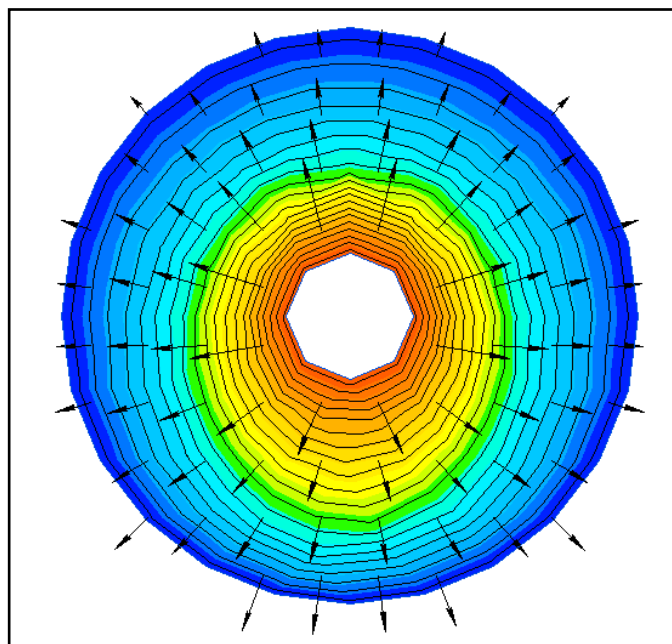


Figure 4.4 Electric field distributions inside the cage without the burner

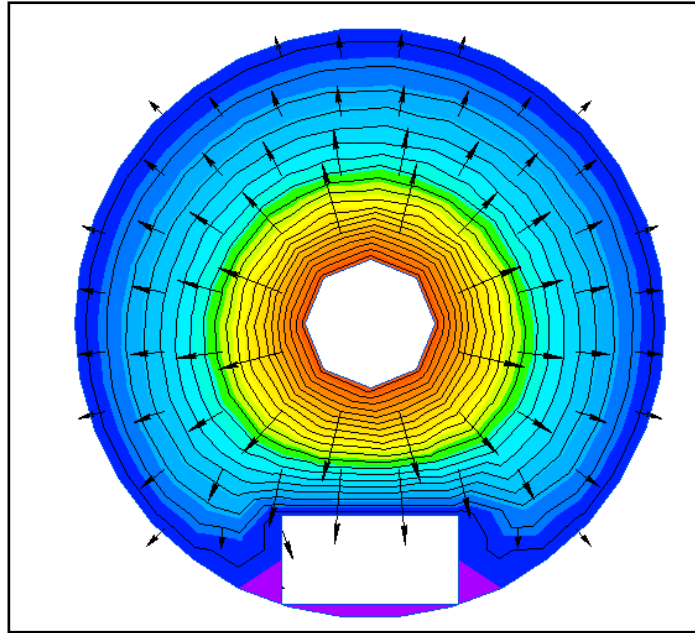


Figure 4:5 Electric field distributions inside the corona cage with the burner in the cage.

Figure 4:4 shows the electric field around the conductor without the burner inside the cage, while Figure 4:5 shows the electric field around the conductor with the burner inside the cage. A comparison of the figures shows that the burner inside the conductor distorts the electric field inside the cage. However, the distortion is not significant around the conductor.

#### **4.1.2. Apparatus**

##### **4.1.2.1. Picoscope**

A picoscope 5000 was used for corona current pulse and voltage measurement.

##### **4.1.2.2. Camera**

Two different cameras were used for temperature measurement, namely: a CoroCam for visual corona, and an infrared camera for temperature measurement.

## 4.2 Test measurements

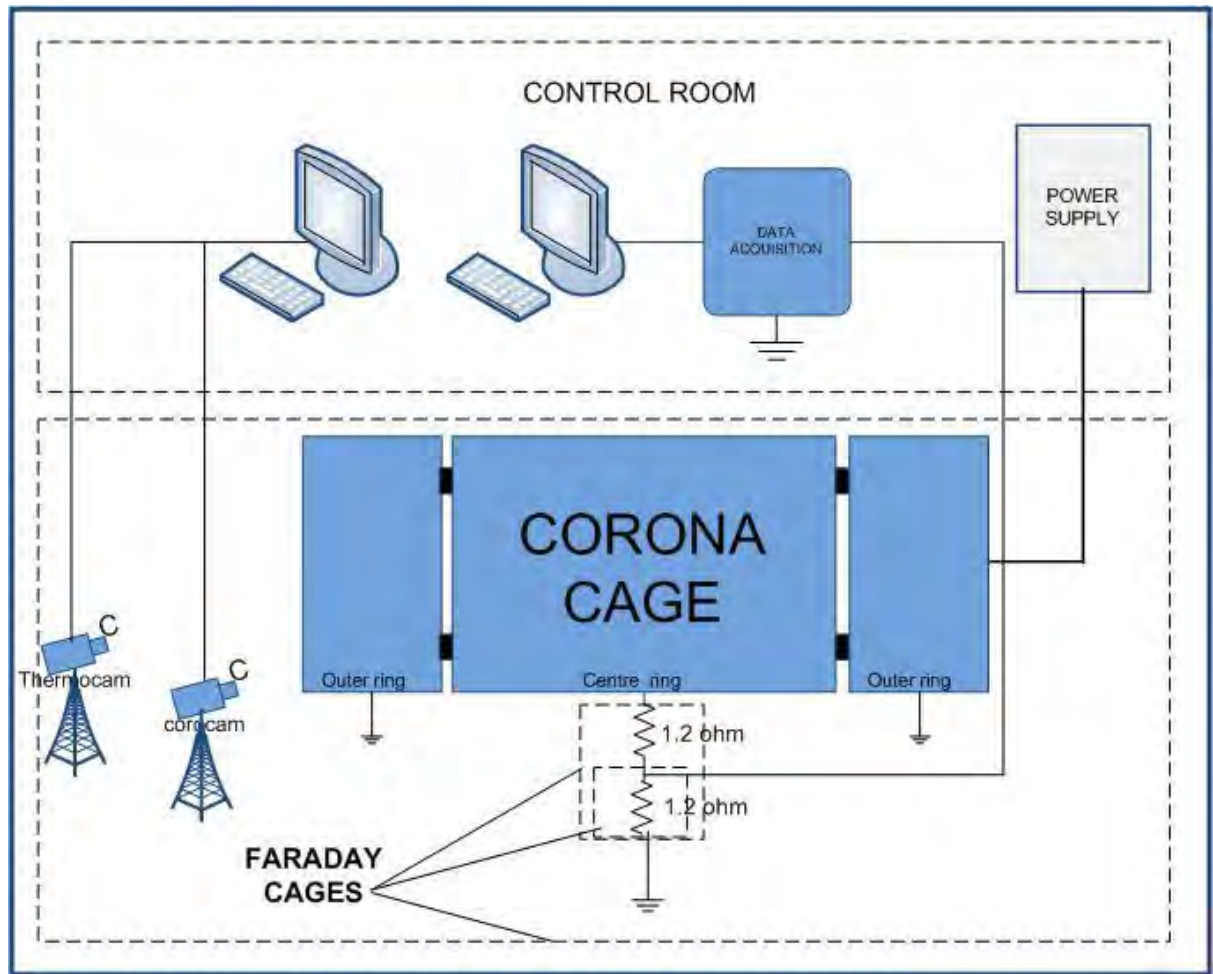


Figure 4.6: Experimental set-up

Figure 4.6 shows the electrical set-up of the corona cage which was used for the experimental tests. A resistive sensor and a high-speed data acquisition system were used for the corona current measurement system. To minimize errors due to the noise arising from the applied voltage to the resistive sensor, and to protect the current measurement system from electromagnetic interference, the experimental set-up was contained in a triple Faraday cage.

Two different conditions were considered for the experiments, namely: “No Fire condition (NFC)” and “Fire Condition (FC)”. In the NFC, the tests were performed on the conductor under standard laboratory conditions without fire beneath the conductor, and this served as a baseline. Under the FC, tests were performed with fire underneath the conductor, which is the main focus of this research investigation. Both experiments were performed using the same electrical set-up configuration of measurement, and similar atmospheric conditions. The temperature during the test was recorded and kept

in the range of 23°C and 25°. The relative humidity and the air pressure were kept stable at approximately 55% and 738 mmHg respectively. The effect of wind speed was neglected given that the experiment was performed in an indoor cage. To ensure accuracy of the results, the experiment was repeated three times for the two different conditions.

#### 4.2.1 Background Noise

Before carrying the tests, it is necessary to ensure that the measurements are shielded against background noise. The frequency spectrum of the corona cage without any applied voltage was measured at different frequencies in order to determine the noise level of the corona cage.

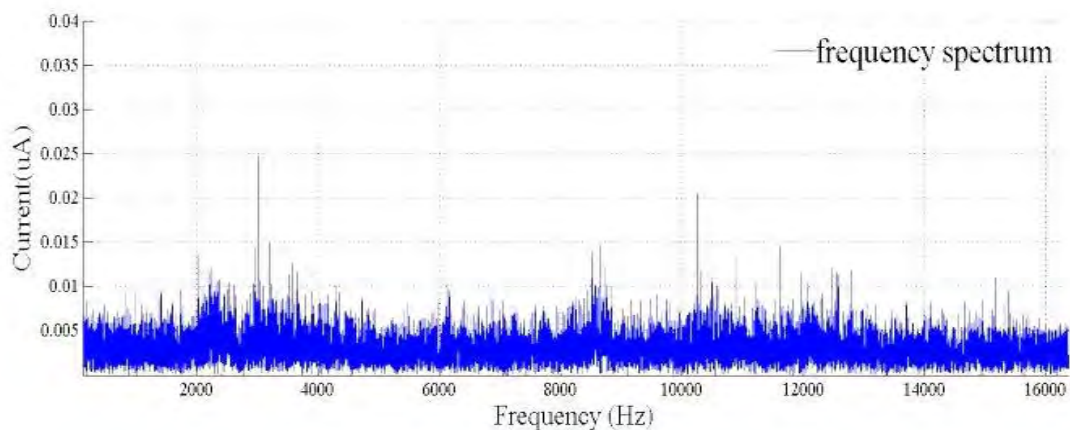


Figure 4.7: Background noise of the corona cage

Figure 4.7 shows the results obtained, which indicate that the outer surface of the cage provides reasonable shielding to the lower frequency of background noise.

#### 4.2.2 Experiment 1 - No Fire Condition (NFC)

This first set of experiments was to determine the time interval between different corona pulses and to measure the corona current. The corona current was determined through the voltage measurement across the shunt resistors. The corona current pulses were recorded using picoscopes. A voltage was applied to the conductor in the cage and increased up to the onset of the visual corona as indicated by the corocam. This value was considered to be the corona onset voltage and therefore recorded. The image of the visual corona was captured. Upon recording the onset voltage, the voltage was increased in steps of 20 kV up to 100 kV. The corona pulses were recorded on the picoscope at each applied voltage level. To ascertain consistency and

accuracy of the measurements, the experimental procedure was repeated three times so as to evaluate reliability of the experimental procedure and samples of these experimental results. Before performing each experiment, the influence of the space charge was taken into account. The extractor and industrial fans at the HVDC laboratory were used to disperse the air in order to remove all the ions in the cage.

#### **4.2.3 Experiment 2 - Fire Condition (FC)**

The second set of experiments was to determine the corona current and to assess the time interval between the corona pulses under fire conditions. These experiments were performed under similar laboratory atmospheric conditions as the NFC experiment, namely: temperature, pressure and humidity. The same experimental set up as the “No Fire Condition” was used. However, fire arising from flaring the gas was used for this experiment. All safety measures and precautions were implemented in order to avoid any risk of a fire hazard to personnel, laboratory or surroundings. The gas tank was placed outside the laboratory. The fire was initiated and controlled remotely by the operator. This allowed for effective control of the height and intensity of the flame. It is useful to mention that because of the different parameters influencing a flame such as convection due to the heat generated in the flame, the distribution of the flame temperature was non-uniform under the conductor.

Using the thermocam, the temperature was measured and the height of the flame determined. To prevent the conductor from melting, the temperature had to be controlled by keeping the height of the flame constant. Every effort was made to avoid flashovers while the applied voltage was steadily increased. This ensures adequate protection of the power supply and the measuring instruments. A Flir thermo camera was also used to capture the visual image of the flame beneath the conductor. The procedure involved placing the fire beneath the conductor; ensuring the gap distance between the flame and the conductor was recorded and kept at approximately 35cm while the voltage was applied to the conductor. Lastly, the applied voltage was increased until visual corona appeared. Having obtained the visual corona, the applied voltage was further increased steadily until streamers were observed. The procedure was repeated three times for each experiment. An extractor and fan were used to remove ions from the cage before each experiment was carried out or repeated.

### **4.3 Results**

This experiment produced valuable results and observations made on the influence of fire on the dc corona. The study focused on determining the characteristic frequencies of positive pulsating corona or corona pulses under the fire (FC) and no-fire condition (NFC). The positive or negative pulsating corona are built up by a corresponding series of successive generation of electron avalanches which take place in the ionisation area of the electrode [22]. The positive pulsating streamers occur near the onset voltage as an onset streamer and as pre-breakdown streamers when the voltage is increased much higher [23].

A new technique called the “corona current signature” (CCS) was introduced to investigate the corona effect under different conditions [24]. The corona current signature was used as a technique to evaluate the corona performance under various environment conditions. The CCS uses a combination of the corona cage and a high frequency corona current measuring system. The analysis method based on the CCS technique was developed for “no fire condition” and “fire condition”. A picoscope was used for capturing data digitally and the frequency domain was then evaluated with the aid of the Fast Fourier Transformation function using Matlab.

#### **4.3.1 No Fire Condition (NFC)**

This experiment was carried out at three different applied voltages, namely: 60 kV, 80 kV and 100 kV respectively. For each applied voltage two different operations were considered. First, a 100  $\mu$ s/div time base and a sample rate of 1 GS/s were used for recording individual corona pulses in order to determine the corona current amplitude and the magnitude of the frequency spectrum. The next step involved increasing the voltage until the appearance of the visual corona on the corocam. Once the visual corona was confirmed, the voltage was recorded, which is the corona onset voltage. From our investigations, the corona onset voltage was found to be 60kV. This was then taken as our baseline operating voltage. Subsequently, the voltage was increased in steps of 20 kV until 100 kV.

#### 4.3.1.1 Measurements at 60 kV

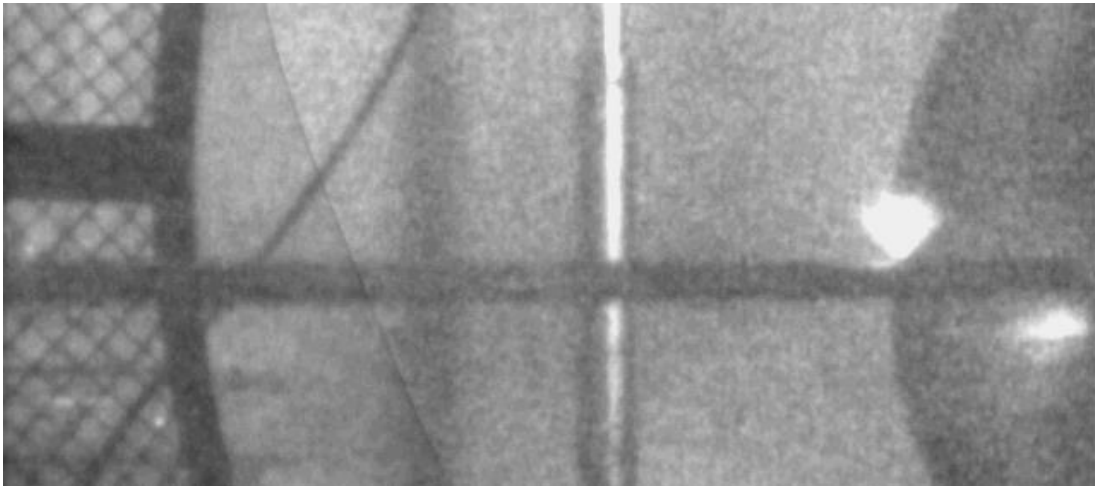


Figure 4.8: UV image of Corona discharges at 60 kV NFC

The image of the visual corona at 60 kV is illustrated in Figure 4.8. The UV image shows a capture of the first visual corona at the onset streamer corona voltage. The streamer corona is the cause of pulsative corona that produced the corona pulses. A random sample of corona current pulses was measured for a time period of 1 ms. An isolated or individual pulse was considered for each measured sample in order to determine the dominant frequencies of the corona current pulse.

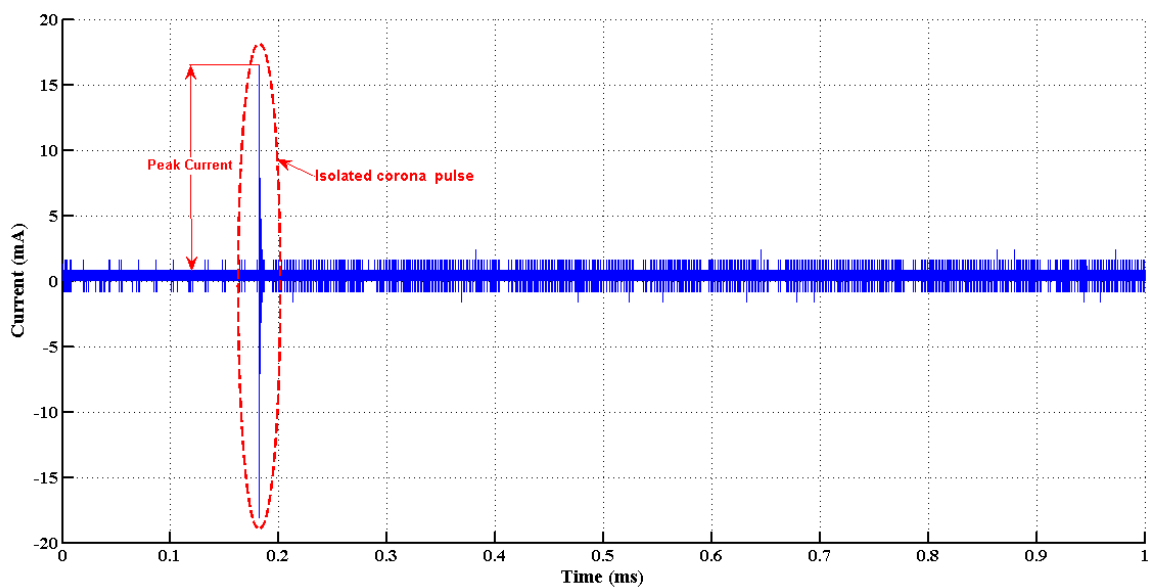


Figure 4.9: Measured sample of corona current at 60 kV NFC

The measured sample of the corona current pulse at 60 kV is presented in Figure 4.9. An individual corona current pulse is also shown in same figure. Data from each the corona pulse was used to determine the maximum or the peak corona current (amplitude) and the current magnitude of the dominant frequencies of the corona pulse. The average of the peak corona current at 60 kV was 149.6 mA. The Fourier analysis was performed on the individual corona pulse to determine the characteristic frequencies of the corona pulses.

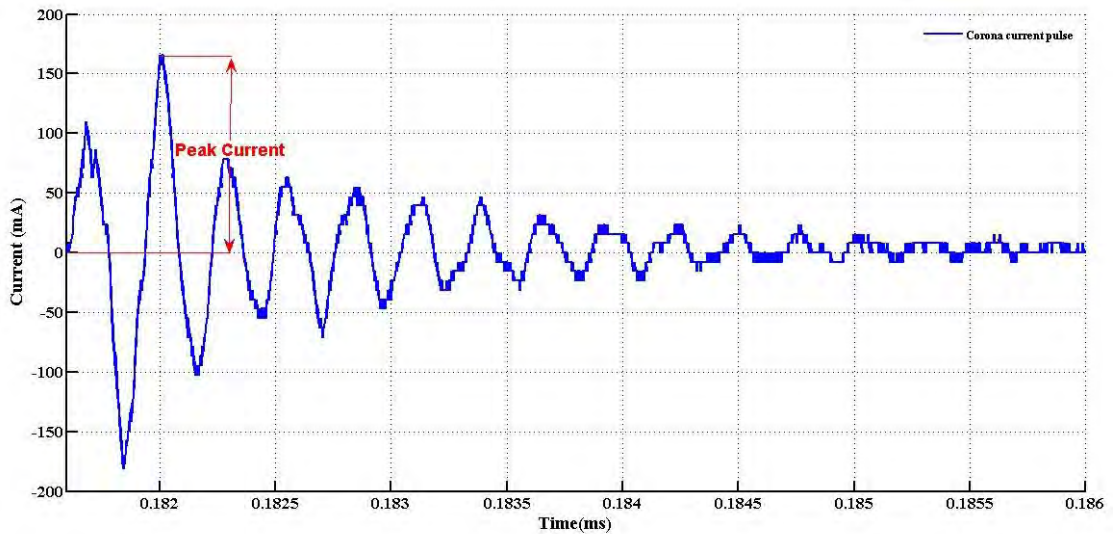


Figure 4.10: Individual corona pulse at 60 kV NFC

A zoomed view of the individual corona pulse of Figure 4.9 is presented in Figure 4.10.

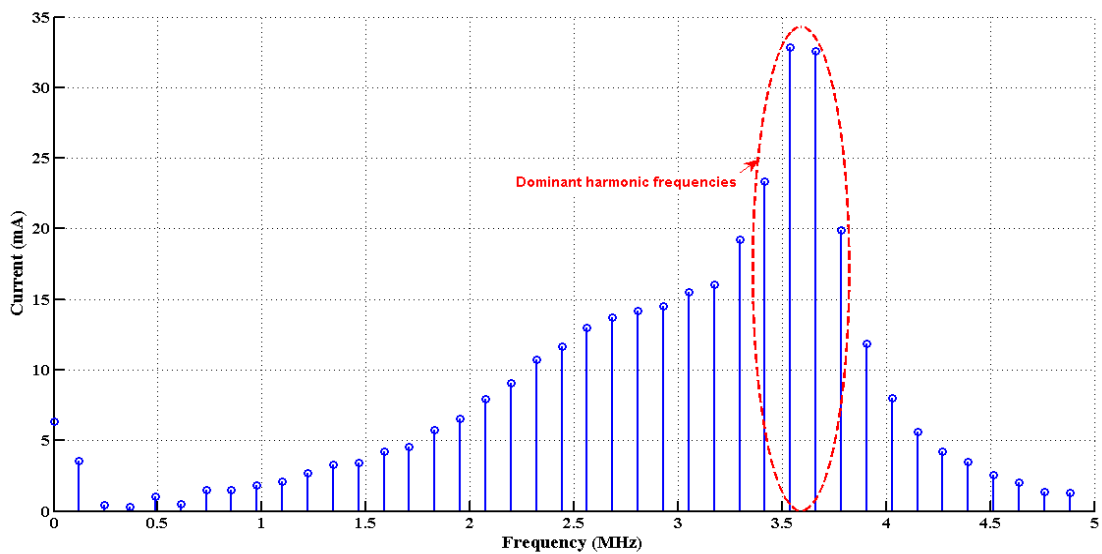


Figure 4.11: Frequency spectrum of individual corona pulse at 60 kV NFC

The spectrum signal of the individual corona pulse at 60 kV is represented in Figure 4.11. It has been observed that the spectrum signal of the background noise is different from the frequency spectrum of the individual corona current pulse. From Figure 4.11, four different frequencies were considered to be dominant frequencies and taken as the characteristic frequencies of the CCS technique. The mean or average magnitudes of the dominant frequencies represent a part of the CCS.

**Table 2:** Average corona current magnitude of the dominant frequencies at 60 kV NFC

Frequency(MHz)	3.42	3.54	3.66	3.78
Test 1	23.36 mA	32.82 mA	32.59 mA	19.87 mA
Test 2	18.81 mA	26.76 mA	27.12 mA	16.74 mA
Test 3	19.10 mA	26.54 mA	27.02 mA	16.73 mA
Average	20.42 mA	28.70 mA	28.97 mA	17.78 mA

The four values of the dominant frequencies are shown in Table 2. These have the respective values of 3.42MHz, 3.54MHz, 3.66MHz and 3.78MHz. A statistical analysis was carried out to determine the average magnitude and the values of the dominant frequencies. The average magnitudes of the frequencies are presented in Table 2. Similar experiments were carried out at 80kV and 100kV respectively. The magnitudes of the corona current for the dominant frequencies of the three tests are shown in Table 2.

#### 4.3.1.2 Measurements at 80 kV

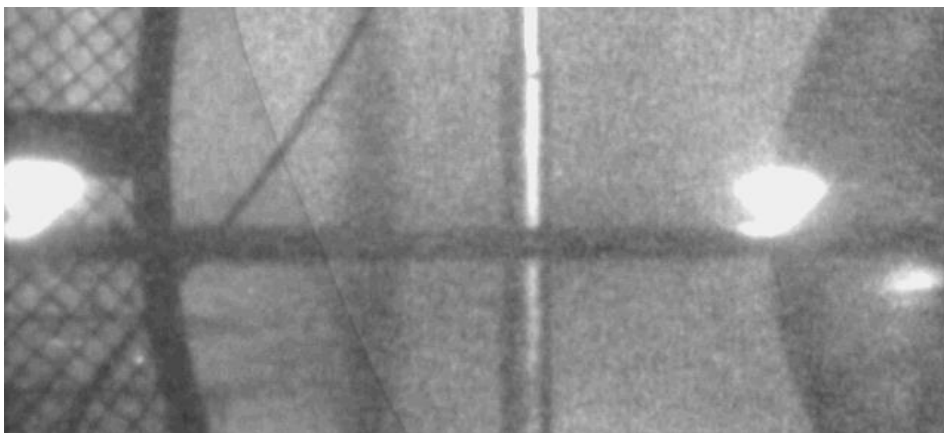


Figure 4.12: UV image of Corona discharges at 80 kV NFC

Figure 4.12 shows the visual corona at 80kV. It is observed that the visual corona in the figure is larger than the visual corona at 60 kV. This suggests that corona becomes more visible as the voltage increases.

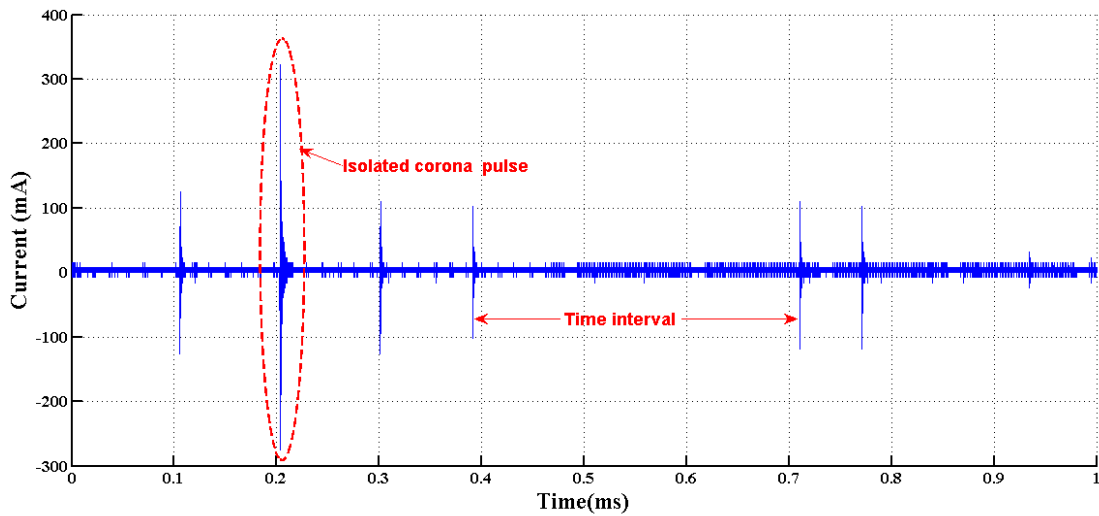


Figure 4.13: Measured sample of corona pulse at 80 kV NFC

The random measured sample of corona pulses at 80 kV is shown in Figure 4.13. The measurement of the corona pulses and the visual corona were taken after an interval time of 1 ms. The isolated pulse and the time interval between corona pulses are shown in Figure 4.13. A zoomed view of the corona pulse was also considered for 80kV in order to determine the characteristic frequencies of the pulses.

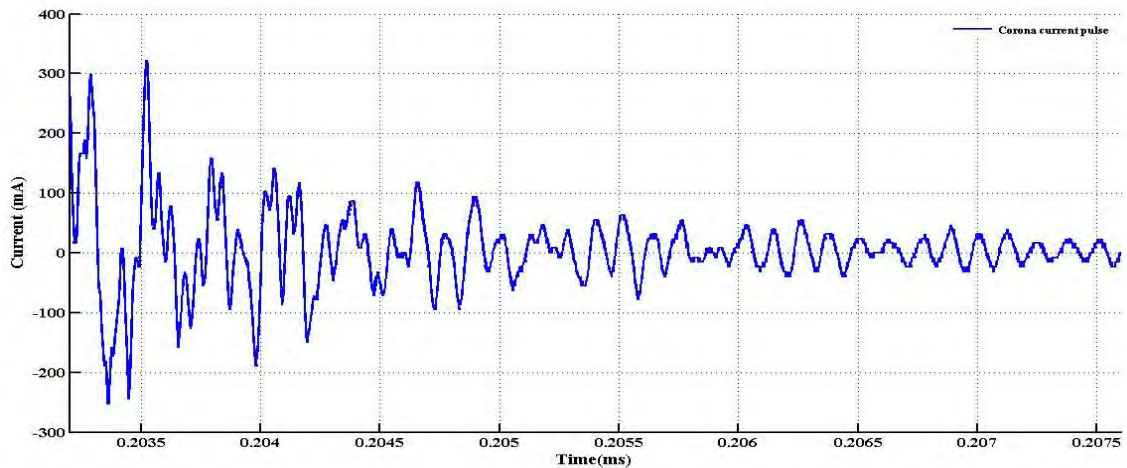


Figure 4.14: Individual corona pulse at 80 kV NFC

Figure 4.14 shows a zoomed view of the individual corona pulse at 80 kV. The average value of the peak corona current at 80 kV was found to be 204.9 mA.

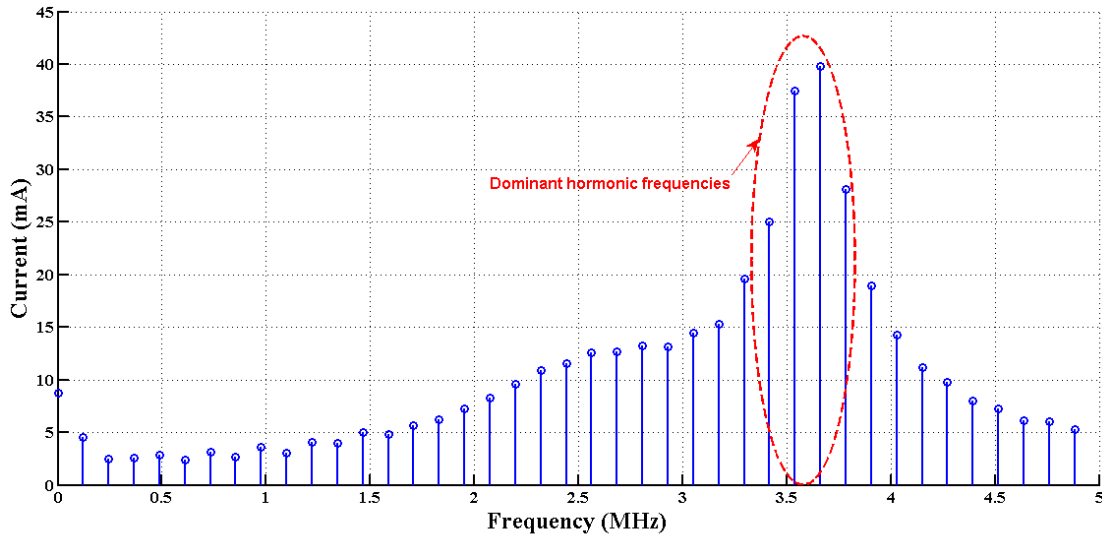


Figure 4.15: Frequency spectrum of individual corona pulse at 80 kV NFC

The spectrum signal of an isolated pulse at 80 kV is shown in Figure 4.15. The average corona current magnitudes and the dominant frequencies at 80 kV are presented in Table 3.

**Table 3:** Average corona current magnitude of the dominant frequencies at 80kV NFC

Frequency(MHz)	3.42	3.54	3.66	3.78
Test 1	25.06 mA	37.48 mA	39.81 mA	28.15 mA
Test 2	23.51 mA	35.04 mA	36.91 mA	23.95 mA
Test 3	21.40 mA	35.09 mA	34.99 mA	24.94 mA
Average	23.32 mA	35.87 mA	37.23 mA	25.68 mA

**4.3.1.3 Measurements at 100 kV**

The voltage was increased to 100 kV; the ultraviolet (UV) image of the visual corona was recorded at 100 kV. The UV image of the visual corona at 100 kV is shown in Figure 4.16. Compared to the UV images of visual corona in Figures 4.8 and 4.12, the UV image in Figure 4.16 appears larger than in the other two figures. That shows that corona discharge becomes more visible as the voltage increases.

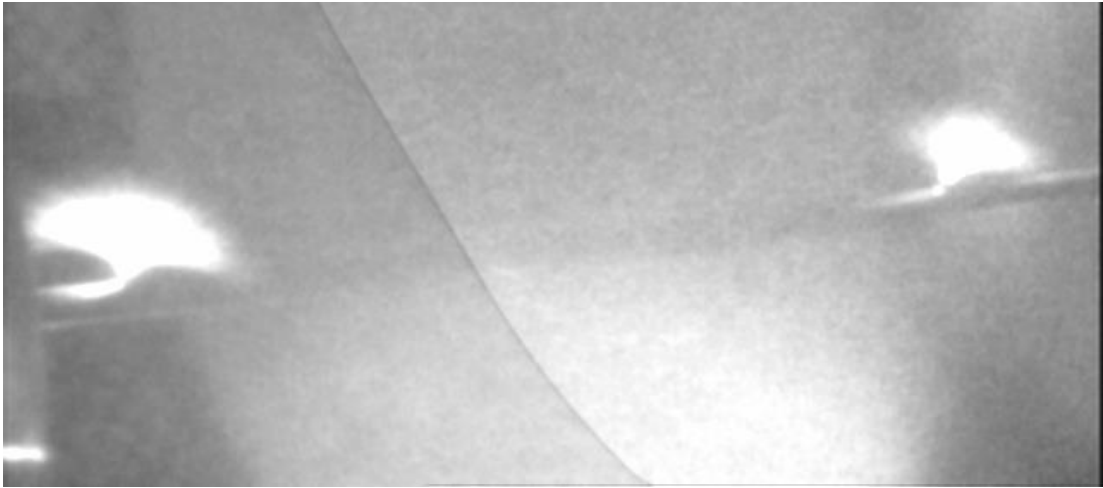


Figure 4.16: UV image of Corona discharges at 100 kV NFC

A measured sample of corona pulse was recorded at an interval time of 1 ms. Figure 4.17 shows the measured sample of the corona pulse at 100 kV related to the UV image in Figure 4.16. An isolated pulse was considered for determining the frequency signal of the corona current pulse. The average value of the maximum amplitude of the corona pulse was 352.6 mA.

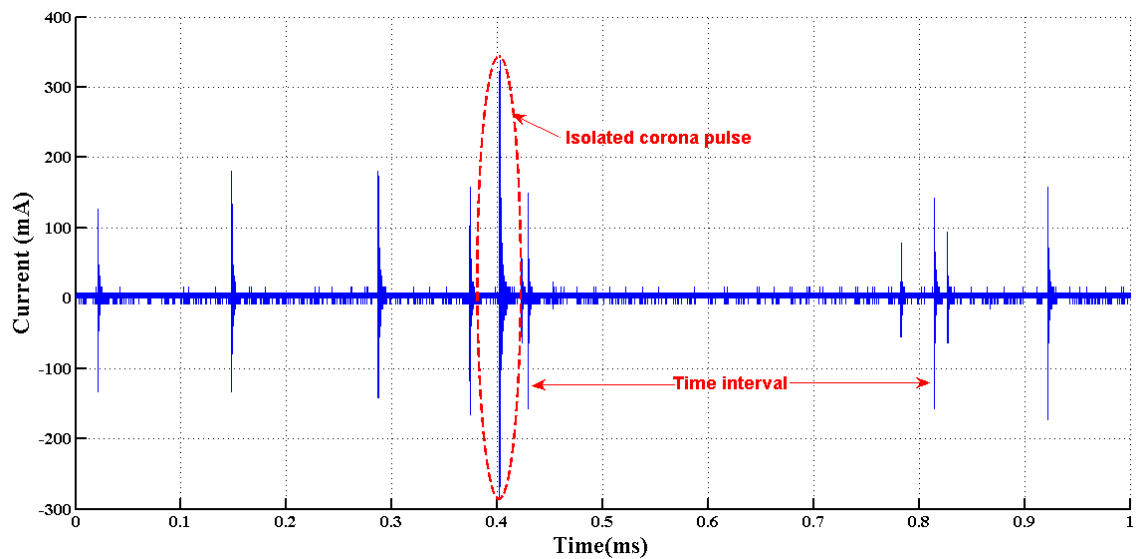


Figure 4.17: Measured sample of corona pulse at 100 kV NFC

A zoomed view of the individual pulse inside the indicated ellipse on Figure 4.17 is shown in Figure 4.18.

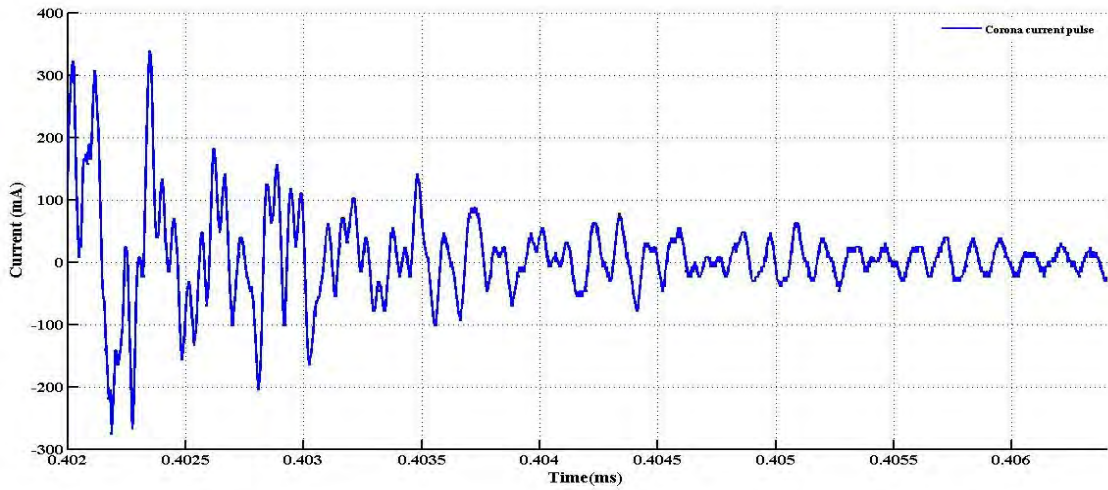


Figure 4.18: Individual corona pulse at 100 kV NFC

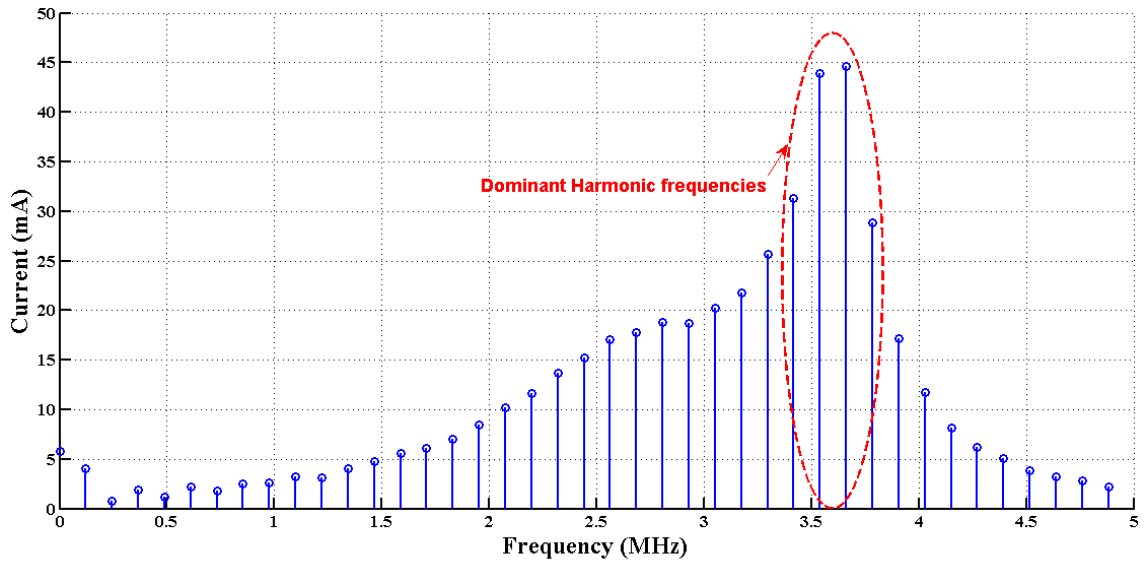


Figure 4.19: Frequency spectrum of individual corona pulse at 100 kV NFC

The frequency spectrum at 100 kV is shown in Figure 4.19. It was observed that the dominant frequencies remain the same for the three applied voltages. The average magnitude/values of the dominant frequencies at 100 kV are shown in Table 4.

**Table 4:** Average corona current magnitude for dominant frequencies at 100 kV NFC

Frequency(MHz)	3.42	3.54	3.66	3.78
Test 1	28.79 mA	44.66 mA	43.91 mA	31.31 mA
Test 2	32.2 mA	46.47 mA	47.96 mA	29.86 mA
Test 3	27.91 mA	41.1 mA	43.53 mA	28.45 mA
Average	29.63 mA	44.07 mA	45.13 mA	29.87 mA

It was observed that there was no significant change in the values of the dominant frequencies for the three applied voltages. The magnitudes of the dominant frequencies appear to increase with the applied voltage. Table 5 shows the comparison between the averages values of the four dominant frequencies at different applied voltages.

**Table 5:** Comparison of average corona current magnitude at different voltages NFC

Frequency(MHz)	3.42	3.54	3.66	3.78
60 kV	20.42 mA	28.7 mA	28.97 mA	17.78 mA
80 kV	23.32 mA	35.87 mA	37.23 mA	25.68 mA
100 kV	29.63 mA	44.07 mA	45.13 mA	29.87 mA

The experiments were repeated three times in order to validate results of the dominant frequencies. Results for the repeated experiments are presented in the appendix. The results of the experiments have shown that there is a variance in the corona pulses. A statistical analysis was performed to quantify the variance and reliability of the corona current pulses. A time window of 10 ms and a sampling rate of 200 MS/s were used in order to estimate the corona pulses distributions, time interval between corona pulses and the corona current pulse amplitude distribution. The corona time interval is defined as a time between two successive corona pulses and the corona pulse amplitude is defined as the peak of the corona current pulse. As presented in Figures 4.9, 4.10 and 4.12. The amplitude of the individual corona pulse defines the DC corona current. Because of the longer time window used for time separation, the amplitude of the

corona pulses used for the current distribution were not exactly the same as for the individual corona pulse. Two kinds of pulses were observed: the burst corona pulses and the streamer corona pulses. The streamer corona pulse was high and variable. The focus of this research investigation is on the streamer corona pulses.

#### 4.3.1.4 Time Distribution at 60 kV

Figure 4.20 shows a histogram of the statistical analysis of the time separation of corona pulses at 60 kV.

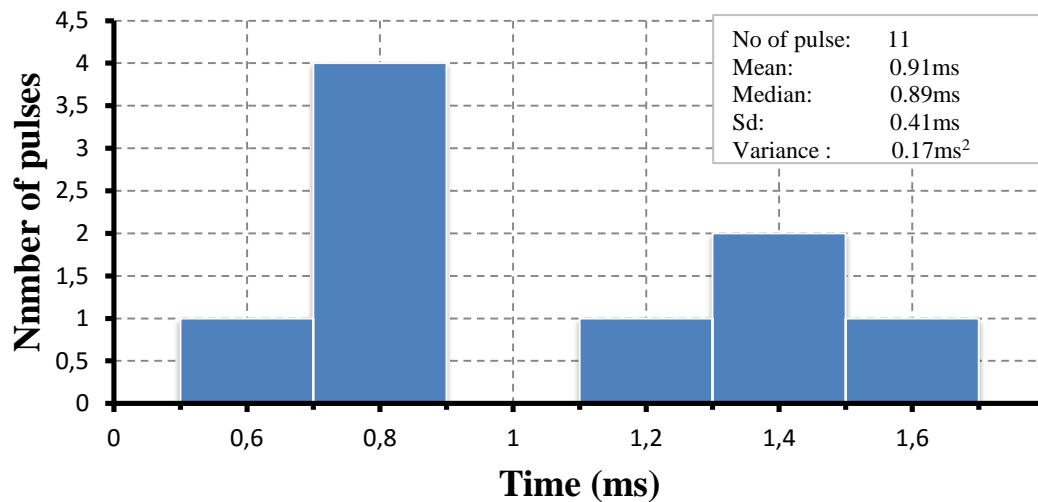


Figure 4.20: Frequency distribution of corona pulses time separation at 60 kV NFC

Table 6 shows the mean values of standard deviation (SD) of the three experimental tests and their average values at 60 kV.

**Table 6:** Average and SD of the time period between corona current pulses: 60 kV  
NFC

60kV	Mean	Standard Deviation (SD)
Test 1	0.91 ms	0.41 ms
Test 2	0.89 ms	0.26 ms
Test 3	0.80 ms	0.49 ms
Average	0.86 ms	0.38 ms

The average of the mean values and the SDs of the time interval between the corona pulses were 0.38 ms and 0.86 ms.

#### 4.3.1.5 Time Distribution at 80kV

The results of a statistical analysis of the corona pulse time separation at 80kV are presented in Figure 4.21.

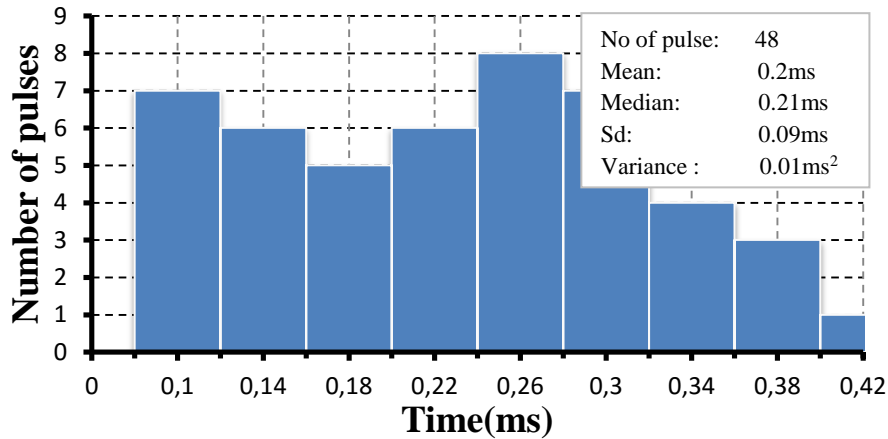


Figure 4.21: Frequency distribution of corona pulses time separation at 80 kV NFC

The average values of the time interval and SD for three sets of experiments are shown in Table 7.

**Table 7:** Average and SD of the time period between corona current pulses: 80 kV NFC

80kV	Mean	Standard Deviation (SD)
Test 1	0.2 ms	0.09 ms
Test 2	0.21 ms	0.16 ms
Test 3	0.22 ms	0.14 ms
Average	0.21 ms	0.13 ms

The average value of the time interval between corona pulses at 80 kV was 0.21 ms with a standard deviation of 0.13 ms.

#### 4.3.1.6 Time Distribution at 100 kV

Figure 4.22 shows a histogram of the time distribution of the corona pulses at 100 kV for one set of experiments.

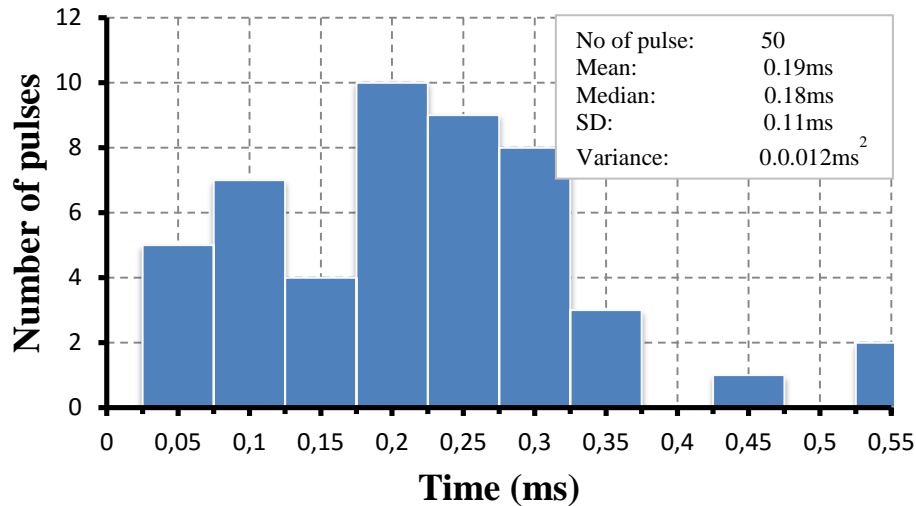


Figure 4.22: Frequency distribution of corona pulses time separation at 100 kV NFC

The results of corona pulses time distribution for the three different runs are shown in Table 8. The average value of the mean of time intervals and the standard deviations for the three runs of the experiments at 100 kV were found to be 0.2 ms and 0.12 ms.

**Table 8:** Average and SD of the time period between corona current pulse: 100 kV NFC

100kV	Mean	Standard Deviation (SD)
Test 1	0.21 ms	0.14 ms
Test 2	0.20 ms	0.11 ms
Test 3	0.19 ms	0.11 ms
Average	0.20 ms	0.12 ms

Table 9 shows the average time separation of corona pulses. The average time separation between corona pulses form part of the corona current signature. The results presented in Table 9 show that in normal condition or NFC, the time interval

between corona pulses decreases as the voltage increases. The decrease in the time interval indicates that the corona pulses occur quickly when the voltage increases.

**Table 9:** Comparison of average and SD of the time period between corona current pulses for the three applied voltages NFC

Voltages	Mean	Standard Deviation (SD)
60 kV	0.86 ms	0.38 ms
80 kV	0.21 ms	0.13 ms
100 kV	0.20 ms	0.12 ms

The results obtained at 80 kV and 100 kV show no considerable difference. That may be explained by memory effects caused by residual ions in the space charge. It has been reported that near the onset voltage, the experiments near the onset voltage are free of residual ions space charge and metastable species while experiments above the onset voltage are more influenced [25].

#### 4.3.2 Fire Condition (FC)

The experimental procedure was the same as for the “No fire condition (NFC)” in term of measurement of samples. The individual corona current pulse was measured using 100  $\mu$ s/div time base and 1 GS/s sampling rate. The images of visual corona at different voltages were recorded using the corocam. A Flir thermocam was used to record image and temperature of fire underneath the conductor. The images of fire underneath the conductor are presented in the appendix. The temperatures of the flame were measured and varied respectively between 360 and 400° C.

##### 4.3.2.1 Measurements at 60 kV

Figure 4.23 shows the photographic image of visual corona pulse at 60 kV FC. Corona could be observed on the two artificial sources of corona. When compared to the “no fire condition” at the same applies voltage, there was no corona on the two sources. The glow corona was of a smaller magnitude than obtained under “no fire condition”.

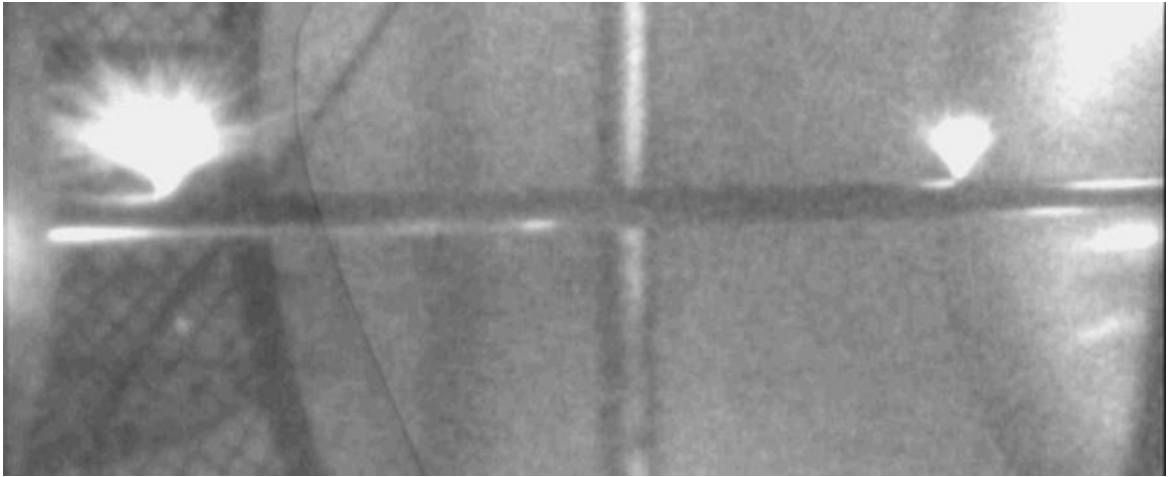


Figure 4.23: UV image of Corona discharges at 60 kV FC

A random sample of corona current pulses was measured. Figure 4.24 shows the corona pulse at 60 kV under “Fire Condition”.

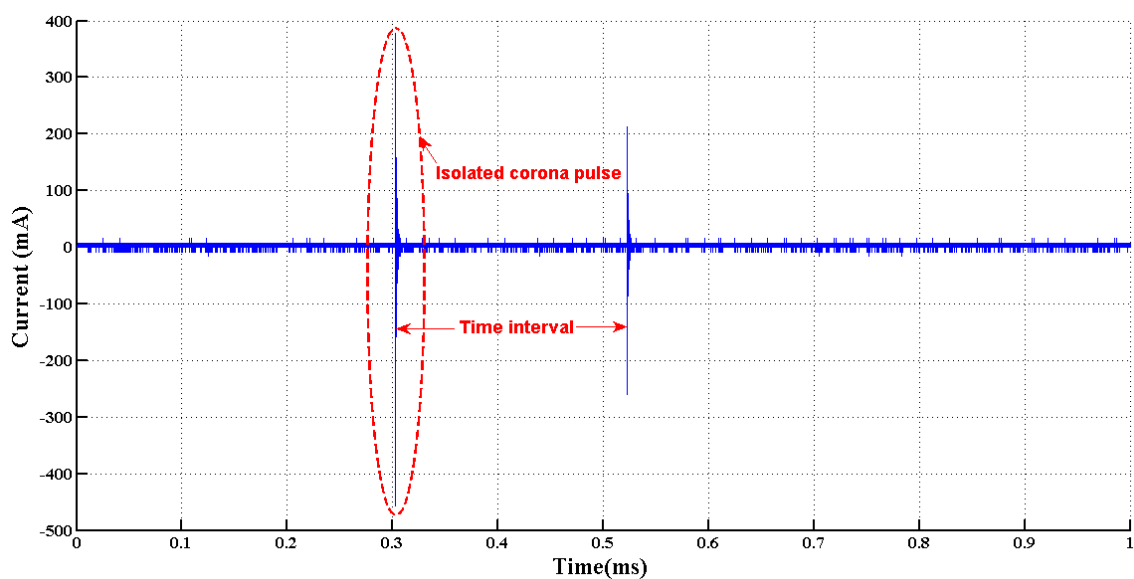


Figure 4.24: Measured sample of corona current at 60kV FC

A time base of  $100 \mu\text{s}/\text{div}$  and a sampling rate of  $1 \text{ GS}/\text{s}$  were used to record the corona pulse under “fire condition. The maximum corona current was measured and recorded. The average of the maximum corona current was found to be  $448.8 \text{ mA}$ .

The Fourier analysis was performed on the individual corona pulse to determine the dominant frequencies of the corona current pulse. A zoomed view of the isolated corona pulse at 60 kV FC is shown in Figure 4.25.

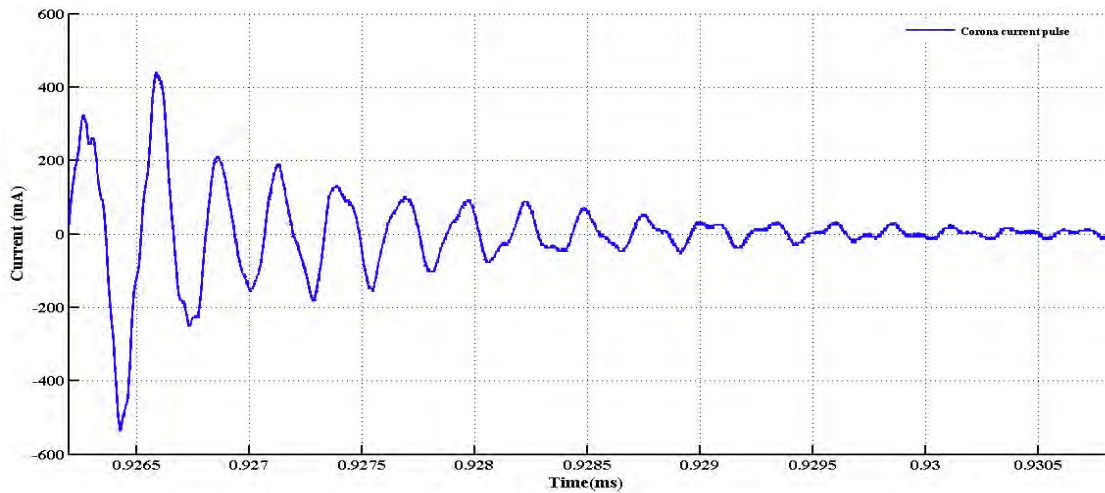


Figure 4.25: Individual corona pulse at 60 kV FC

The dominant frequencies of the corona current at 60 kV for “fire conditions are illustrated in Figure 4.26.

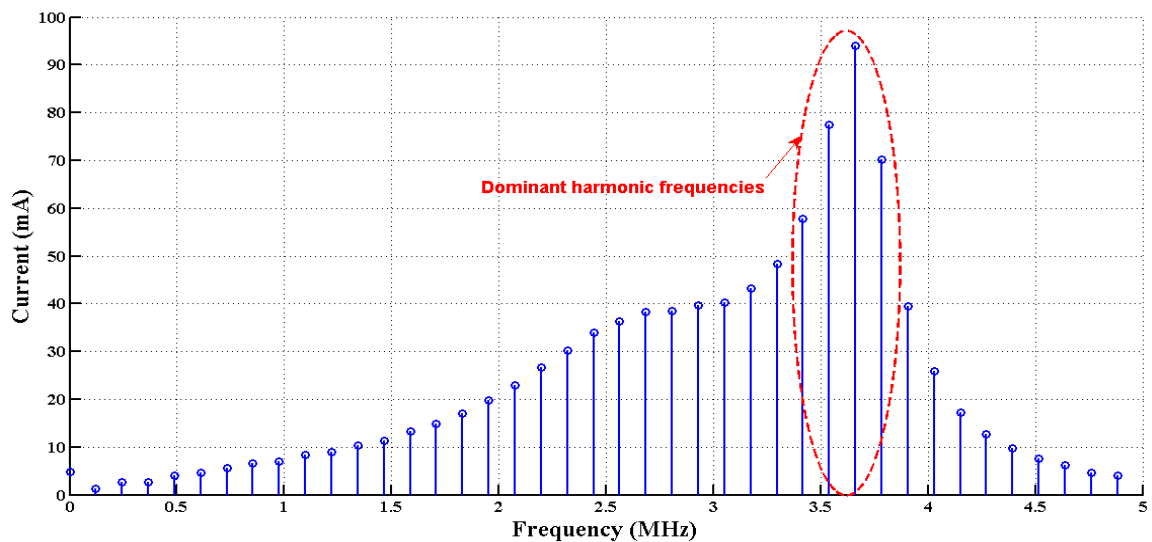


Figure 4.26: Frequency spectrum of individual corona pulse at 60 kV FC

Figure 4.26 shows that there are four dominant frequencies, namely 3.42 MHz, 3.54 MHz, 3.66 MHz and 3.78 MHz. These dominant frequencies are considered to be the characteristic frequencies of the corona current magnitudes for FC at 60 KV. The corona current magnitudes of the characteristic frequencies are shown in Table 10.

**Table 10:** Average corona current magnitudes for dominant frequencies at 60 kV FC

Frequency(MHz)	<b>3.42</b>	<b>3.54</b>	<b>3.66</b>	<b>3.78</b>
Test 1	71.4 mA	97.12 mA	117.74 mA	89.35 mA
Test 2	57.71 mA	77.55 mA	93.93 mA	70.12 mA
Test 3	53.06 mA	73.17 mA	89.82 mA	69.24 mA
Average	60.72 mA	82.61 mA	100.49 mA	76.23 mA

Table 10 results show that the dominant frequencies for “fire condition” are the same as for “no fire condition” for the same applied voltage. For the FC measurements were taken for 80kV and 100kV. The results are presented and discussed.

#### 4.3.2.2 Measurements at 80kV

The visual corona at 80kV “Fire Condition” is shown in Figure 4.27. Compared to Figure 4.10, the visual corona on the two corona sources is larger in the FC than in the NFC. We can also observe the visual corona on the surface of the conductor.

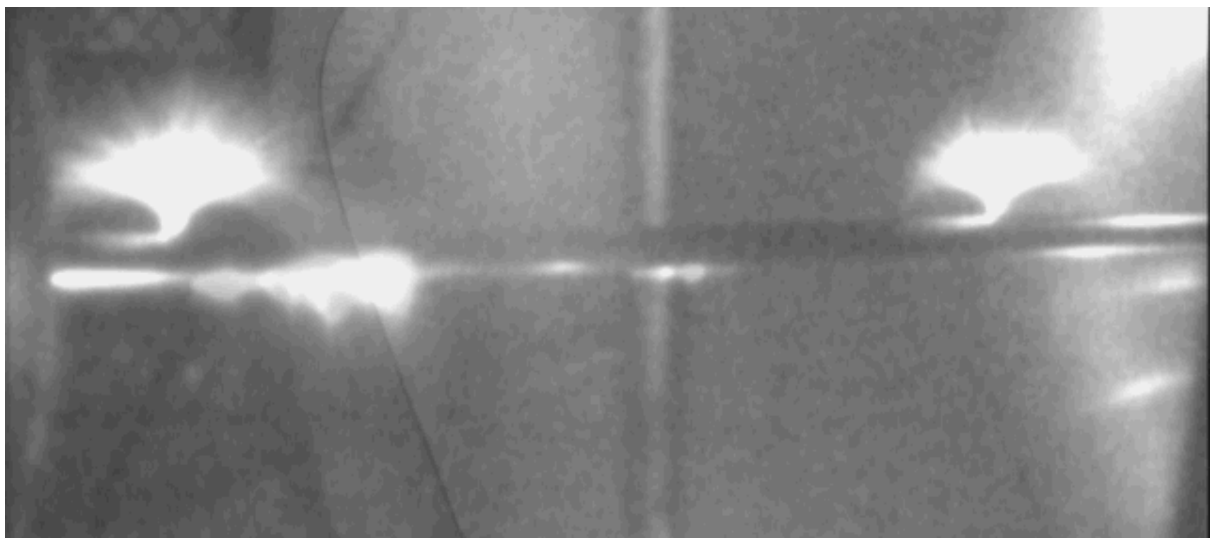


Figure 4.27: UV image of corona discharge at 80 kV FC

After capturing the visual corona, a sample of corona current pulse was measured at 80 kV under fire condition. The measured sample of corona pulse under FC is shown in Figure 4.28.

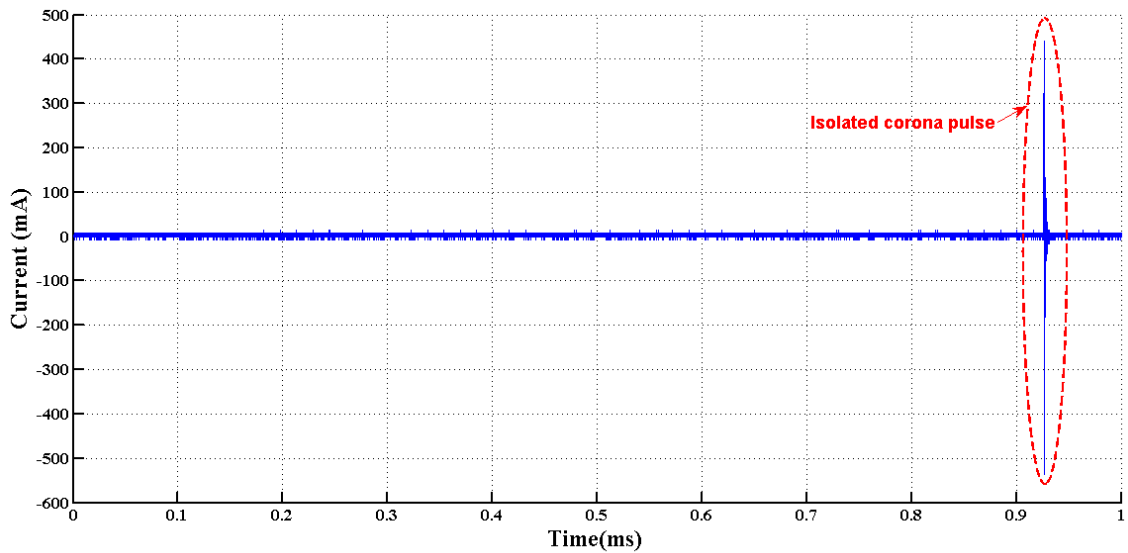


Figure 4.28: Measured sample of corona current at 80 kV FC

The maximum corona current at 80 kV for the individual corona pulse was determined to be 766.4 mA.

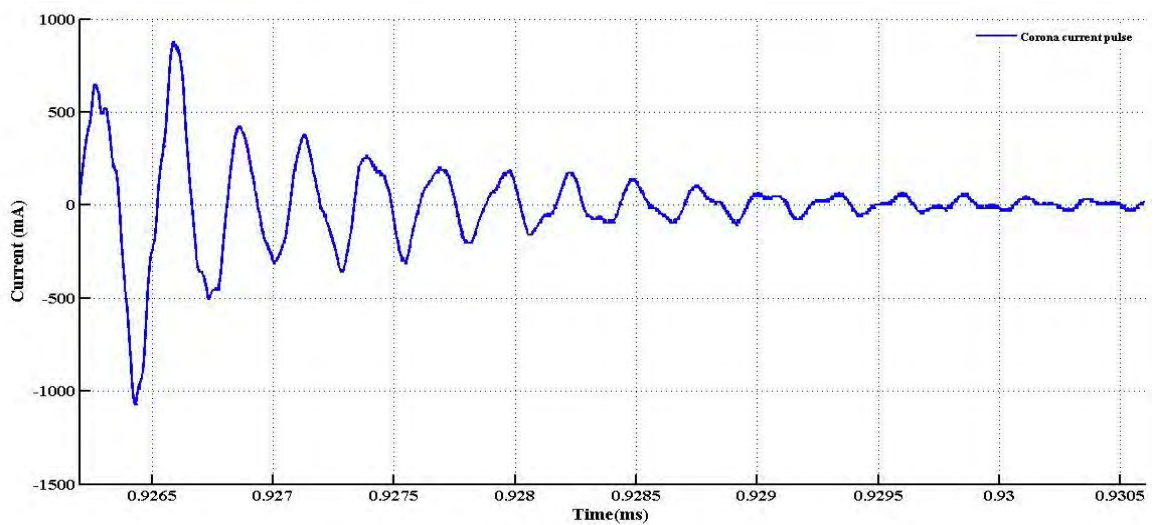


Figure 4.29: Individual corona pulse at 80 kV FC

A zoom in view of the individual corona pulse at 80 kV under FC is illustrated in Figure 4.29.

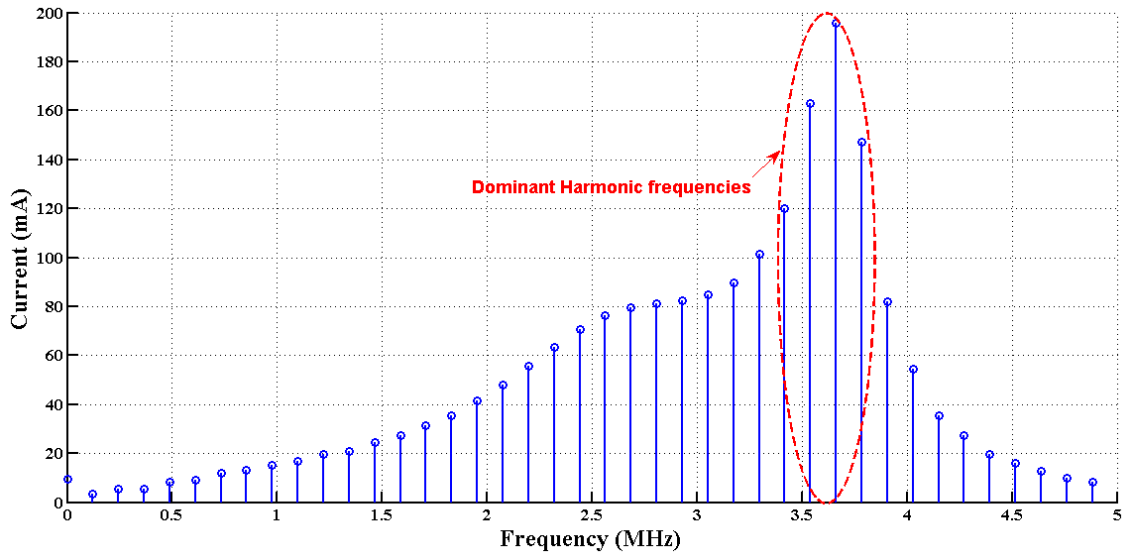


Figure 4.30: Frequency spectrum of individual corona pulse at 80 kV FC

The spectrum signal of the individual pulse at 80 kV FC is presented in Figure 4.30. It is observed that the dominant frequencies are the same for 80kV FC and 80kV NFC in Figure 4.15.

The results of the magnitude of the characteristic frequencies of the corona pulse at 80 kV FC are shown in Table 11.

**Table 11:** Average corona current magnitudes of the dominant frequencies: 80 kV FC

Frequency(MHz)	3.42	3.54	3.66	3.78
Test 1	119.94 mA	162.85 mA	195.72 mA	147.13 mA
Test 2	109.58 mA	148.60 mA	177.20 mA	132.52 mA
Test 3	85.37 mA	116.69 mA	141.72 mA	110.09 mA
Average	104.96 mA	142.71 mA	171.55 mA	129.91 mA

### 4.3.2.3 Measurements at 100 kV



Figure 4.31: UV image of Corona discharges at 100 kV FC

Figure 4.31 shows a photograph of visual corona at 100kV FC. The visual corona at 100 kV was much larger with streamers moving along the whole surface of the conductor. The observed streamer is the breakdown streamer. A major streamer was observed at 95 kV. A flashover occurred at approximately 100 kV and was observed in the corona cage. A picture of the fire induced flashover is shown in Appendix C.

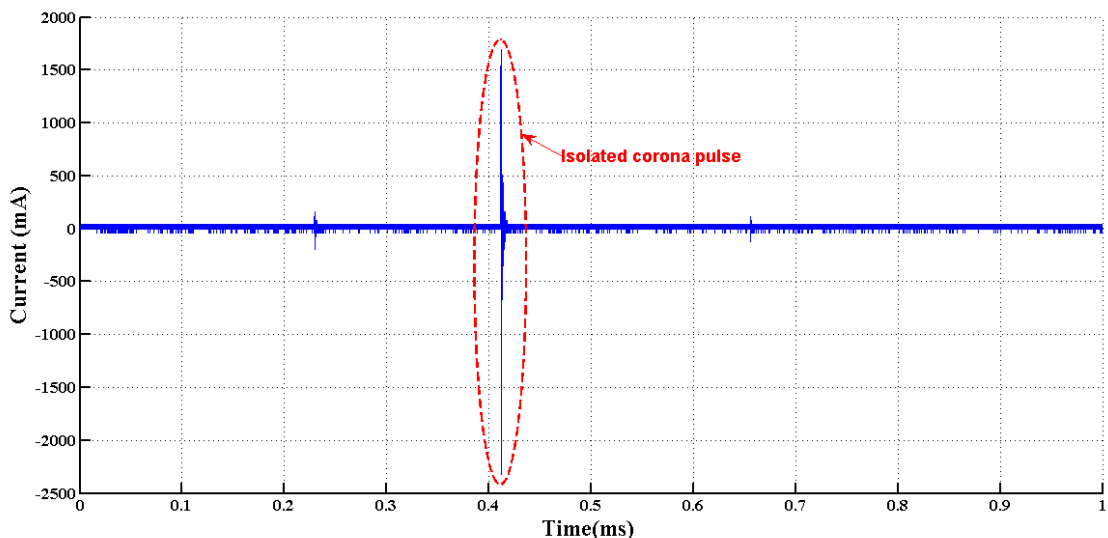


Figure 4.32: Measured sample of corona current at 100 kV FC

The measured sample of the corona pulse at 100 kV FC is shown on Figure 4.30. The average of the maximum corona current amplitude at 100 kV FC was 1755.66 mA.

Figure 4.33 shows a zoomed in view of the individual corona pulse at 100 kV.

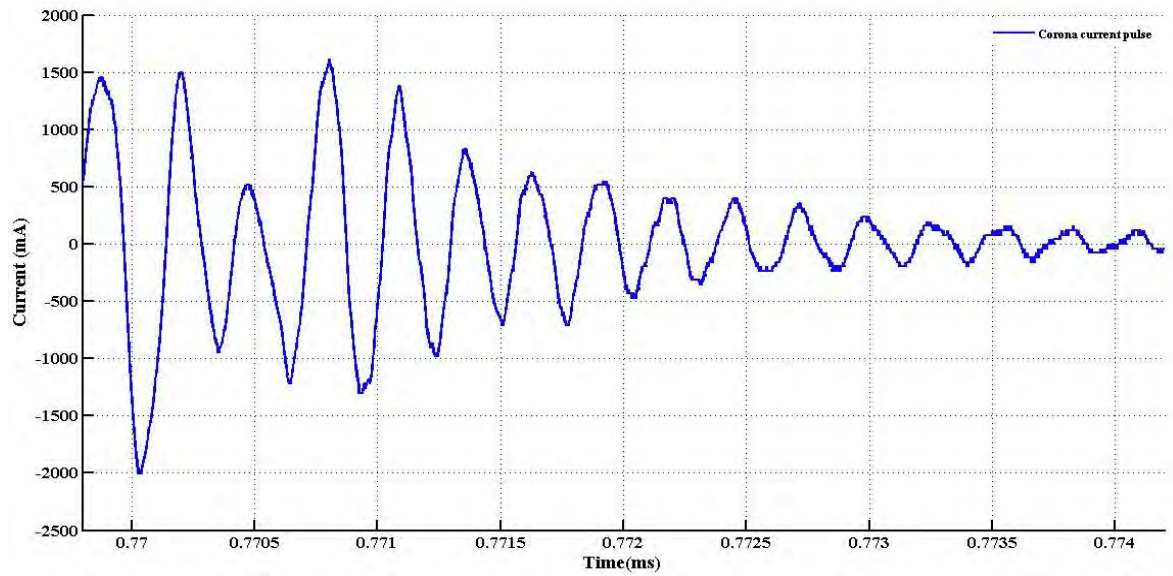


Figure 4.33: Individual corona pulse at 100 kV FC

The spectrum signal of the individual corona pulse is shown on Figure 4.34.

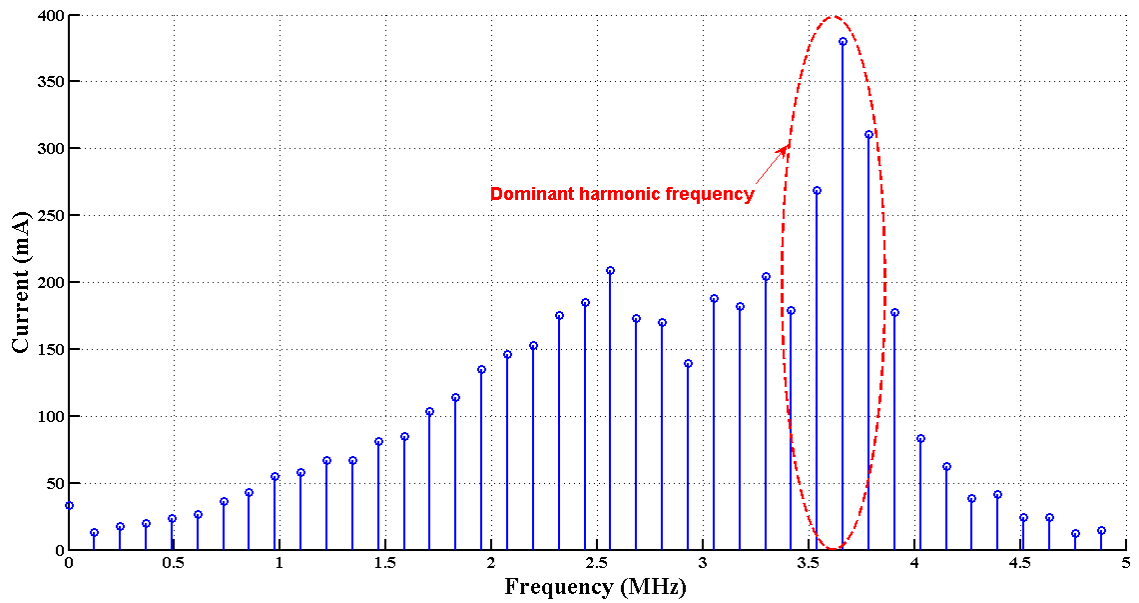


Figure 4.34: Frequency spectrum of individual corona pulse at 100 kV FC

**Table 12:** Average of corona current magnitude of the dominant frequencies:100 kV  
FC

Frequency(MHz)	<b>3.42</b>	<b>3.54</b>	<b>3.66</b>	<b>3.78</b>
Test 1	311.41 mA	352.91 mA	393.75 mA	325.19 mA
Test 2	179.00 mA	263.85 mA	381.19 mA	310.86 mA
Test 3	445.57 mA	509.13 mA	410.96 mA	160.62 mA
Average	311.99 mA	375.29 mA	395.96 mA	265.55 mA

The results of the magnitudes of the characteristic frequencies for the three sets of measurements at 100 kV are shown in Table 12.

**Table 13** Comparison of the average value of corona current magnitude at different voltages FC

Frequency(MHz)	<b>3.42</b>	<b>3.54</b>	<b>3.66</b>	<b>3.78</b>
60 kV	60.72 mA	82.61 mA	100.49 mA	76.23 mA
80 kV	104.96 mA	142.71 mA	171.55 mA	129.91 mA
100 kV	311.99 mA	375.29 mA	395.96 mA	265.55 mA

The results in Table 13 show that the magnitude of the corona current increases as the applied voltage increases under fire condition. It has been observed that the presence of fire did not affect the dominant frequencies of the corona pulses. This shows that the frequency response of the corona pulse depends on the configuration geometry arrangement [26], [27]. The average values of the current form a part of our corona current signature under fire condition.

For the “no fire condition” the time distribution and the current distribution were assessed. A time window of 10 ms with 200 MS/s sampling rate was used in order to estimate the corona pulse distributions and time interval between corona pulses. To avoid any damage of the measurement equipment and the power supply, the voltage was increased cautiously with careful attention paid to the experiment under FC.

#### 4.3.2.4 Time Distributions at 60 kV

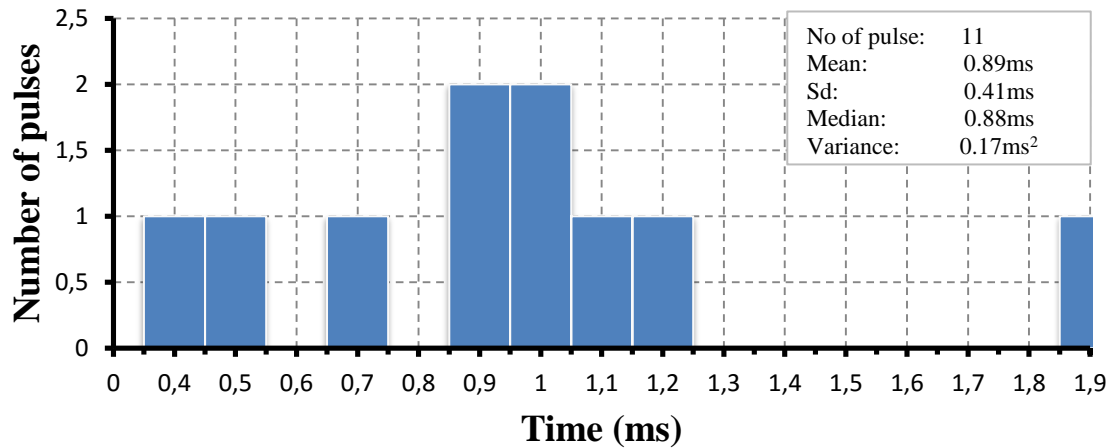


Figure 4.35: Frequency distribution of corona pulses time separation at 60 kV FC

Figure 4.35 shows the histogram of the time distribution of the corona pulses at 60 kV FC. The results of the mean time interval and standard deviation for the three runs of the experiment at 60 kV FC are illustrated in Table 14 below.

**Table 14:** Average and SD of the time period between corona current pulses: 60kV FC

60kV	Means	Standard Deviation (SD)
Test 1	0.89 ms	0.41 ms
Test 2	0.47 ms	0.32 ms
Test 3	0.62 ms	0.26 ms
Average	0.66 ms	0.33 ms

The average values of the mean time interval at 60 kV for the three runs were 0.66 ms and a standard deviation of 0.33 ms.

#### 4.3.2.5 Time Distribution at 80 kV

The statistical analysis of the corona pulses at 80kV FC for one set of measurements is shown in Figure 4.36.

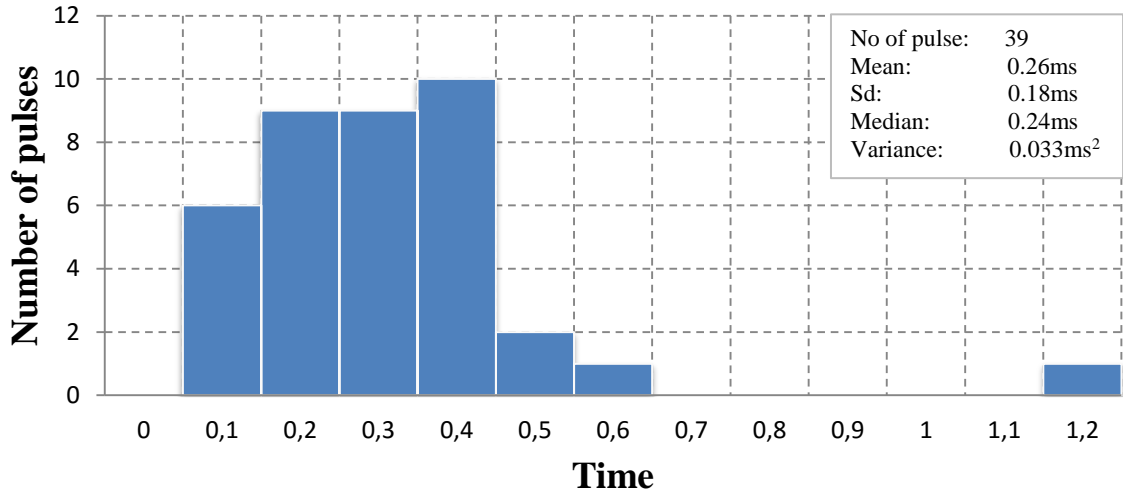


Figure 4.36: Frequency distribution of corona pulses time separation at 80 kV FC

The average values of the mean time interval and standard deviation at 80 kV FC are presented in Table 15.

**Table 15:** Average and SD of the time period between corona current pulses: 80 kV FC

80kV	Mean	Standard Deviation
Test 1	0.22 ms	0.15 ms
Test 2	0.27 ms	0.14 ms
Test 3	0.26 ms	0.18 ms
Average	0.25 ms	0.16 ms

#### 4.3.2.6 Time Distribution at 100 kV

Figure 4.37 shows the statistical analysis of the time distribution of the corona pulses at 100 kV for one set of experiments. The results and the average values of the time interval and the standard deviation for the three set of experiments are as shown in table 16.

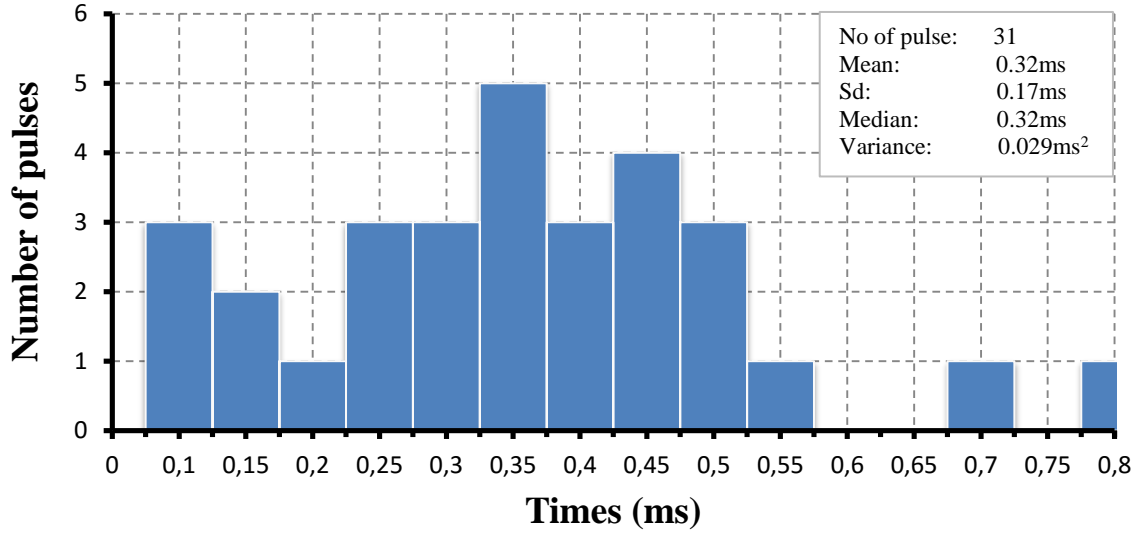


Figure 4.37: Frequency distribution of corona pulses time separation at 100 kV FC

**Table 16:** Average and SD of the time period between corona current pulses: 100 kV FC

100kV	Mean	Standard Deviation
Test 1	0.26ms	0.11ms
Test 2	0.32ms	0.17ms
Test 3	0.31ms	0.13ms
Average	0.30ms	0.14ms

The results of the average values of the mean time interval and the standard deviation for the three different voltages under fire condition are shown in table 17. The results show that the mean time interval at 60 kV is larger than the mean time interval at 80 kV and 100kV. That implies that the repetition rate of corona pulses is lower at 60 kV than it is at 80 kV and 100 kV.

**Table 17:** Comparison of average and SD of the time period between corona current pulses for the three applied voltages FC

Voltages	Means	Standard deviation
60kV	0.66ms	0.33ms
80kV	0.25ms	0.16ms
100kV	0.30ms	0.14ms

### 4.3.3 Influence of Fire on Corona Current

As mentioned at the beginning of this investigation, this study uses an analysis tool called the corona current signature (CSS) technique. This technique is a combination of the current magnitude of the dominant frequencies of the corona pulse and the repetition rate of corona pulses.

#### 4.3.3.1. Corona Current Signature at 60 kV

Table 18 shows the results of measurements with 60kV applied to the conductor.

**Table 18:** Average of corona pulse magnitude and average corona time interval at 60 kV NFC and FC

Frequency(MHz)	Magnitude (mA)				Time (ms)	
	3.42	3.54	3.66	3.78	Mean	SD
No fire condition	20.42	28.7	28.97	17.78	0.86	0.38
Fire condition	60.72	82.61	100.49	76.23	0.66	0.33

The average corona current magnitudes of the dominant frequencies are much higher for the “fire condition” than for the “no fire condition”. However, there is a decline or decrease in the average time interval and the standard deviation of corona pulses. The increase in the average value of the corona current magnitudes suggests that fire beneath the conductor appears to increase corona current. The decrease in the time interval between corona pulses shows that the frequency of occurrence of corona pulses is higher under fire conditions. This may be attributed to additional ions created when there is fire beneath the conductor.

#### 4.3.3.2. Corona Current Signature at 80 kV

Table 19 shows the results of measurements for the corona current signature at 80 kV.

**Table 19:** Average of corona pulse magnitude and average corona time interval at 80kV NFC and FC

	Magnitudes (mA)				Time (ms)	
	3.42	3.54	3.66	3.78	Means	SD
Frequency(MHz)						
No fire condition	23.32	35.87	37.23	25.68	0.21	0.13
Fire condition	104.96	142.71	171.55	129.91	0.25	0.16

The results show that the average magnitudes of the dominant frequencies increased in the FC case, where there was fire beneath the conductor at 80 kV. It has been found that in comparison to the result obtained at 60 kV, the mean time and the standard deviation between corona pulses increased with fire beneath the conductor. The increase in time may be due the increase in the pulse amplitude that created a build-up of the space charge. Thus, the repetition rate of pulses is less under fire condition.

#### 4.3.3.3. Corona Current Signature at 100 kV

The corona current signatures at 100 kV “for no fire” and “fire condition” are presented in Table 20.

**Table 20:** Average of corona pulses magnitude and average corona time interval at 100 kV NFC and FC

	Magnitudes (mA)				Time (ms)	
	3.42	3.54	3.66	3.78	Means	SD
Frequency(MHz)						
No fire condition	29.63	44.07	45.13	29.87	0.2	0.12
Fire condition	311.99	375.29	395.96	265.55	0.3	0.14

The experimental results indicate that the corona current magnitudes increased with fire beneath the conductor at 100 kV. The time interval and standard deviation between corona pulses also increased with the presence of fire.

Considering the corona current signatures presented in tables 18-20, the results show that the corona current magnitudes increased with fire beneath the conductor. This interpretation of the results in tables 18-20 can be attributed to the proposed theory of the physics of fire [5]. Fire as a plasma contains air molecules that are chemically and thermally ionized. The increase in corona current magnitude is due to thermal ionization caused by temperature. The increase in temperature increases the rate of ionization. An increase of 100 K in temperature can increase the ion generation rate to 2 to 4 times [6]. As the temperature increases, the air density reduces, hence the electrical strength of air decreases. The presence of additional ions caused by fire and the ions produced by corona discharge, collectively enhance corona activities that can produce large corona streamers. As the streamer becomes larger, the amplitude of the corona current pulses increases and consequently the corona current magnitudes of the dominant frequencies also increase. The occurrences of corona pulses are mutually inter-dependent. When the amplitude of the pulse is higher, the ion space charge is larger; therefore an increase in the time interval is required for the ions space charge to evacuate before the occurrence of the next corona pulse. This may explain why the time interval between corona pulses is larger with the presence of fire.

It was observed that at 60 kV the corona current magnitudes under “fire condition” were about 3 to 4 times larger than the corresponding corona current magnitude for “no fire condition. At 80 kV the increase in current was 3 to 4.6 times larger under fire condition. When 100 kV was applied to the cage the increase in corona current magnitudes was 9 to 10.5 times larger. These results suggest that when there is fire beneath a conductor, the corona current magnitude increases significantly with an increase in the applied voltage. However, as one approaches the corona onset voltage, the rate of increase in current magnitude is lower than when it is above the onset voltage. That may be attributed to the memory effect in space charge. Corona pulses appear to be free from the memory effect close to the onset voltage. However, when the voltage is much high the memory effect is considerable and produces a build-up of a larger space charge.

The results of time interval for corona current signature at the three applied voltages indicates that when the conductor is under the influence of fire, the time interval decreases at the onset voltage and increases as the voltage increases. Fire as plasma creates additional ions in the gap between the flame and the conductor. The presence of the additional ions accelerates the repetition rate of corona pulses on the onset voltage.

It is observed that corona pulse amplitudes increased as the voltage increased. Therefore the repetition rate of corona pulse decreases. The corona pulses occur less frequently as the applied voltage increases. It has been shown that corona pulse amplitudes and corona pulse repetition rate are dependent random variables [23]. The occurrences of corona pulses are dependent on each other. When the amplitude of the pulse is higher, the ions space charge is larger, hence it requires some time for the ions space charge to be evacuated before the rise of the next pulses. It can also be inferred from the results that the amplitudes of corona pulse are much high under fire condition. It would then seem that fire makes the corona pulses appear less frequently.

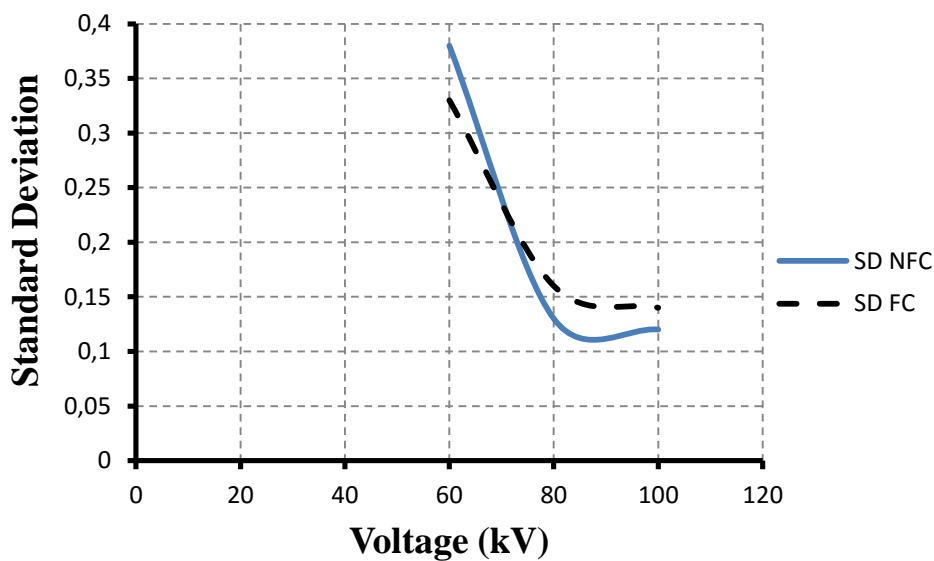


Figure 4.38: Variation of standard deviation of time interval with voltage NFC and FC

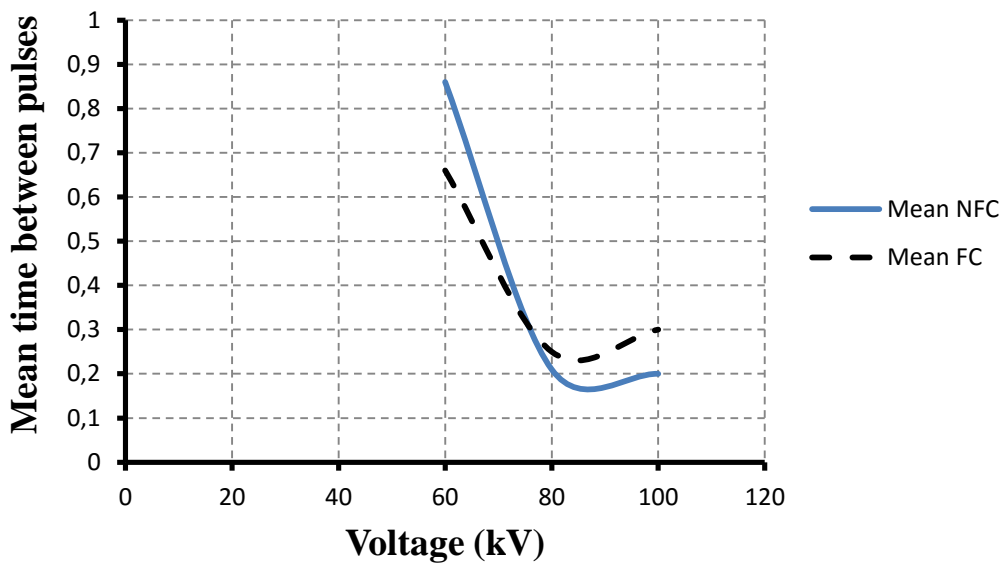


Figure 4.39: Variation of Mean time between pulses with voltage NFC and FC

The mean value of the time interval and the standard deviation are plotted against the voltage in Figures 4.38 and 4.39. The mean and the standard deviation of the time interval decreases while the voltage increases in both the NFC and FC case. However it is observed that the mean and standard deviation decrease for FC near the inception voltage, while it increases as the applied voltage is increased.

#### **4.3.4 Discussion**

The results obtained from the measurement of the fire induced dc corona current were similar to those obtained by Evert for ac corona current [6]. Evert performed the experiment on fire and rain induced ac corona noise. He found that the major differences seen in the time domain measurements were related to the pulses observed and thereby related to the physical occurrence of the streamers at the conductors. The two most significant differences in the fire-induced corona noise pulses and the rain-induced corona noise pulses were the amplitude and the time between pulses. The fire induced corona noise pulses were much larger and the time between pulses was more irregular [6].

The results obtained in this research investigation for dc corona current corroborate those obtained for ac corona. It has been shown that the amplitude of the corona current pulses was much high for fire condition than the amplitude of the corona current pulses for normal condition. The occurrence of corona current pulses was more regular for no fire than for fire condition. This shows that, similar result can be obtained by performing experiment for dc corona using different environment conditions.

## CHAPTER 5

### CONCLUSION

---

#### 5.1 Corona current tests

A high voltage engineering research investigation on fire induced DC corona currents has been successfully conducted in the HVDC laboratory at the University of KwaZulu-Natal, under standard conditions of a safe, regulated and controlled environment.

A new technique, the “corona current signature (CCS)”, was used to measure the corona current under different conditions.

The influence of fire on DC corona current was investigated using the “CCS” experimental method and tests were conducted using the indoor corona cage test facility.

Visual corona was observed at different applied voltages and different environmental conditions. Corona current signature was performed at three different voltages for two different conditions, namely: “no fire condition (NFC)” and “fire condition (FC)”. The experimental investigation, mathematical analysis and statistical evaluation focussed on determining the characteristic frequencies and magnitudes of the corona pulses.

It was observed that for both NFC and FC, all the corona pulses measured using the technique presented in this work had four dominant frequencies. The magnitudes of the corona current at these frequencies for a conductor, form part of the corona current signature. Furthermore, the time period between corona pulses is important and also forms part of the corona current signature.

The results obtained show that the magnitude of the dominant frequencies of the corona current increases as the applied voltage increases. It was also observed that for the same applied voltage, the magnitude of the corona pulses was higher under the fire condition than in the no-fire condition.

The time interval between corona pulses was also assessed. It was observed that a difference exists in the behaviour of the repetition rate of the corona pulses near the onset voltage and the voltages above the onset voltage. The repetition rate of corona pulse is lower near the onset voltage and higher as the applied voltage is increased.

The presence of fire generates additional ions, due to the increase in temperature, and this produces a reduction in the air density. The corona streamers were observed to be 3 to 10 times larger under fire condition than under a normal condition or no fire condition. We can therefore deduce that, when the corona streamers are larger, the amplitudes of the corona pulse are also higher; hence the current magnitudes of the corona pulses are bigger. It may be conclusively stated that when there is fire under a high voltage dc transmission line, dc corona current increases.

## **5.2 Future work**

The following is suggested as feasible investigations that will add value to the design and operation of high voltage transmission systems.

- Determine the corona current signature for negative corona current under no fire and fire condition.
- Design and conduct experiments under laboratory conditions on HVDC lines subjected to different types of fires; gaseous partial discharge (PD); the effect of CO<sub>2</sub> concentration and different particles on discharge characteristics; the influence of dilute CO<sub>2</sub> concentration on AC/DC spark-over in atmospheric air; characteristics of DC spark-over; gas temperature of steady glow and streamer discharges in atmospheric air gap (at sea level); and to establish the influence of CO<sub>2</sub> Levels and fire quality on streamers.
- Performance analysis of the corona current signature in the operation of high voltage transmission lines.
- Modelling and simulation of the electrical field before and after the occurrence of corona discharge. Establish a correlation with the electric field on a typical transmission line and corona inspection level under fire condition. Compare the results obtained by simulation results with the experimental measurements.
- Provide measures and design parameters or modifications necessary for improved line design, by reducing the impact of fire on corona discharge in high voltage DC transmission lines.

## **5.3 Recommendations**

The research on fire as plasma should be extended and continued, to provide the engineering community with a better understanding of how to reduce corona losses and gap discharge for partial discharges.

## References

- [1]. Minnaar U J, Gaunt C T and Nicolls F, "Characterisation of Power System Events on South Africa Transmission Power Lines", *Electrical Power Systems Research* 88, 25-32. 2012..
- [2]. Yang Y, "A Calculation Method for the Electric Field under Double-Circuit HVDC Transmission Lines". *IEEE Transaction on power delivery*, Vol. 23, No 4 October 2008.
- [3]. Nema R S and Fathima Z, "Study of Corona Pulses in Air-solid Interface", *IEEE International Symposium of Electrical Insulation*, Vol. 2, pp. 407-410, June 1998.
- [4]. Frost P and Vosloo H, "Providing Satellite-based Early Warning of Fires to Reduce Fire Flashovers on South Africa's Transmission Lines", *Bushfire Conference, Brisbane, Australia, 6-9 June 2006*.
- [5]. Sukhnandan A, "A Theoretical and Experimental Investigation into Fire Induced Flashover of High Voltage Transmission Lines", *Master of Science in Electrical Engineering, University of KwaZulu-Natal, June 2004*.
- [6]. Evert C R, "The High Frequency Characteristics of Corona and Electrical Discharge Generated by Fire Phenomenon", *Master of Science in Electrical Engineering, University of KwaZulu-Natal, July 2003*.
- [7]. Hamel M, "Influence de la Variation de la Température Ambiante sur les Vibrations Induites par Effet de Couronne", (Influence of the Change in Ambient Temperature on Corona Induced vibration) *Maîtrise en Ressources et Systèmes, Université de Québec, 1991*.
- [8]. Fortin S, Zhao H and Ma J, "A New Approach to Calculate the Ionized Field of HVDC Transmission Line in the Space and Earth Surface", *International Conference on Power System Technology, Chongqing, China October 2006*.
- [9]. Panicker P K, "Ionisation of Air by Corona", *Master of Science in Aerospace Engineering, University of Texas at Arlington, August 2003*.
- [10]. EPRI, "AC Transmission Line Reference Book - 200kV and Above", 3<sup>rd</sup> Edition. Palo Alto, California 2005.
- [11]. Pank T, "Positive Corona at Combined Voltage", *University of Tartu, Dissertation for Doctor of Philosophy in Physics. November 2001*.
- [12]. Leonard L G, "Electric Power Generation, Transmission and Distribution", 2<sup>nd</sup> Edition, CRC Press, New York, 2006.

- [13]. Kamaraj N V, "High voltage Engineering, 2<sup>nd</sup> Edition", McGraw-Hill Companies, New York, 1995.
- [14]. Mokwape J L, "A study of HVDC Transmission Line Audible Noise and Corona Loss in an Indoor Corona Cage, Master of Science in Electrical Engineering, University of Kwazulu Natal, 2007.
- [15]. Kothari D P. and Nagrath I J., "Power System Engineering", 2<sup>nd</sup> Edition McGraw-Hill Companies, New York.
- [16]. Abhijit C. and Sunita H., "Power System Analysis, Operation and Control", 3<sup>rd</sup> Edition, PHI Learning Private limited, New Delhi, February 2010.
- [17]. Working Group 7, Guidelines for the Evaluation of the Dielectric Strength of External Insulation, Dielectric Strength of External insulation under Transient Voltage of Study Comity 33, Overvoltage and Insulation Coordination, Cigre, Paris 1992.
- [18]. Vosloo H F, Britten A C, and Burger A A, "Susceptibility of 400 kV Transmission Lines to Bird Streamers and Bush Fires", Transmission and Distribution, Energize, pp. 25, December 2011.
- [19]. Frost P E, "Development of a Fire-Induced Flashover Probability index (FIFPI) for Eskom Transmission Line", Master of Science in Geography, University of Johannesburg, November 2010.
- [20]. Colin C, "Three Dimensional Flame Reconstruction Towards the Study of Fire-Induced Transmission Line Flashovers", Master of Science in Engineering, University of KwaZulu-Natal, March 2007.
- [21]. Fang-Cheng L, Shao-Hua Y., Yun-Peng L., Qi-Fa W., and Zhi-Bin Z, "AC Conductors' Corona-Loss Calculation and Analysis in Corona Cage". IEEE TPD, Vol. 27, No. 2, 2012, pp. 877-885.
- [22]. Khalifa M, Kamal A, Zeitoun A, Radwan R and El-Bedwaihy S, "Correlation of Radio Noise and Quasi-Peak Measurements to Corona Pulse Randomness", IEEE Transactions on Power Apparatus and Systems, Volume: PAS-88, Issue: 10, pp.1512 – 1521, October 1969.
- [23]. Soliman E and Mohammad K, "Calculating the Corona Pulse Characteristics and its Radio Interference", IEEE Transactions on Power Apparatus and Systems, Vol. PAS-90, No. 1, January/February 1971.
- [24]. Chetty L, Ijumba N, Chetty N, Singh Y, Ilunga K G, "Evaluating the Effect of Paint Coatings on the Corona Performance of Conductor Surfaces", 18<sup>th</sup> International Symposium on High Voltage Engineering, Seoul, Korea, august 2006

- [25]. Jonson E S, "Influence of Voltage and Load Current on dc Bipolar Corona Pulses", IEEE Transactions on Dielectrics and Electrical Insulation, Vol. 1, No 2. April 1994.
- [26]. Khalifa M and Abdel-Salaam M. "Improved Calculation of Corona Pulse Characteristics" IEEE Transactions on Power Apparatus and Systems Vol. PAS-93, Issue: 5. September 1974.
- [27]. Clevis T T J, Nijdam S, and van Deursen A P J, "Electrical Diagnostics in a HV Corona Streamer Discharge Setup: Improved Current Measurement through Electromagnetic Frequency Response Analysis", IEEE EMC EUROPE pp. 1-4, September 2012.
- [28]. Al-Arainy A A, Malik N H, and Al-Bahoul M K, "Statistical variation of AC corona pulse amplitudes in point to plane air gaps", IEEE Transaction on Electrical Insulation, Vol. 24, No 4, August 1989.

# APPENDIX A

## No fire condition (NFC)

### Test 2

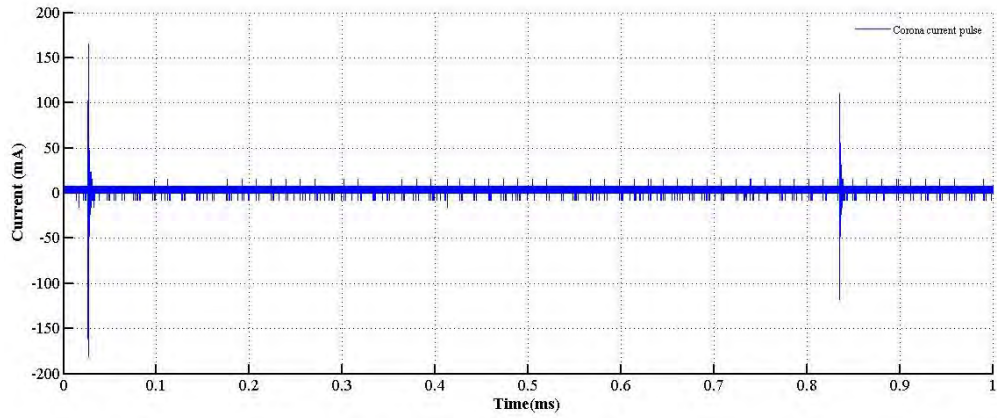


Figure A1: Measured sample of corona current at 60kV NFC

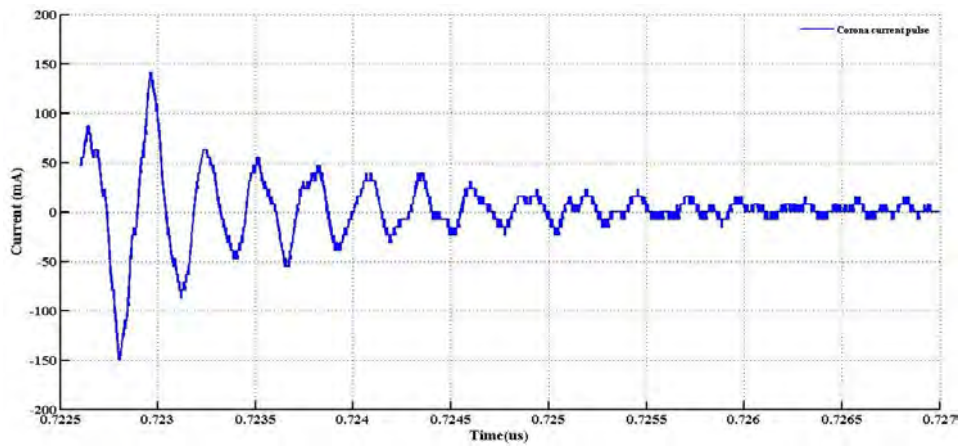


Figure A2: Individual corona pulse at 60kV NFC

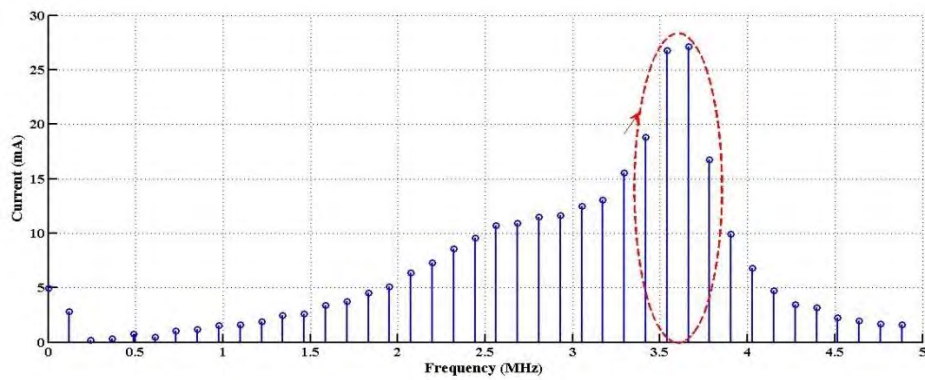


Figure A3: Frequency spectrum of individual corona pulse at 60 kV NFC

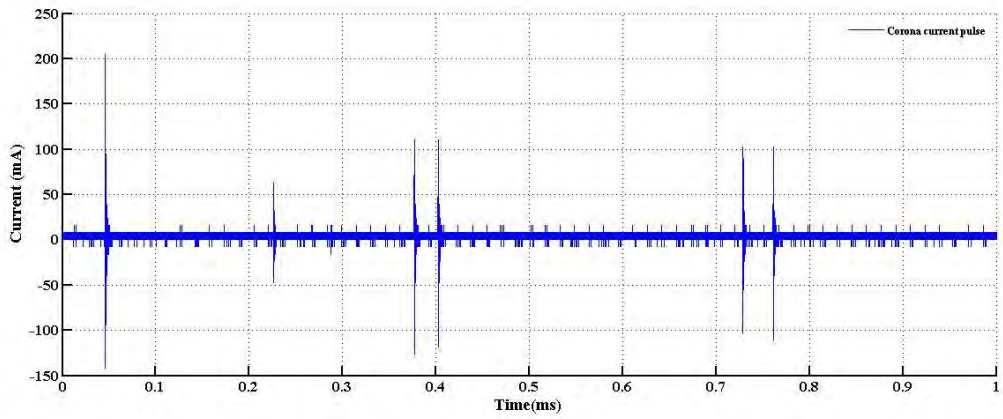


Figure A4: Measured sample of corona current at 80kV NFC

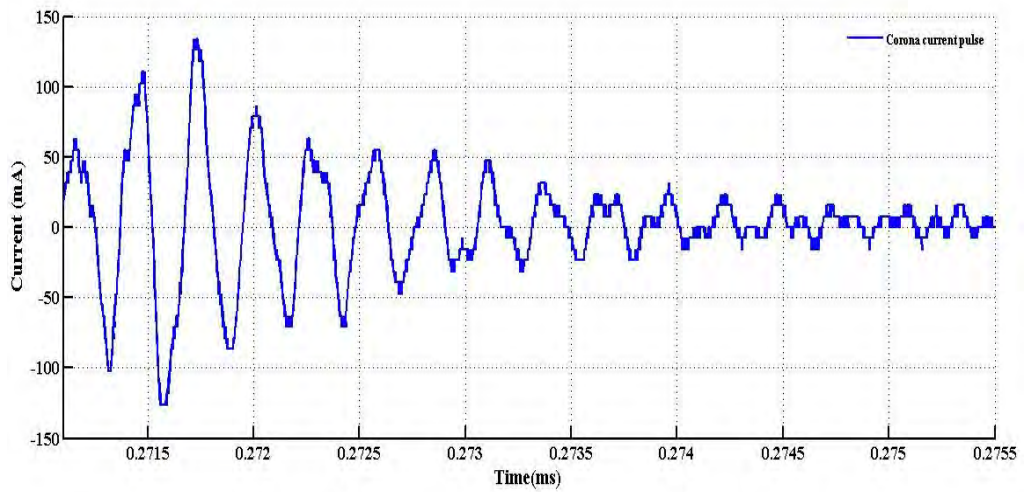


Figure A5: Individual corona pulse at 80KV NFC.

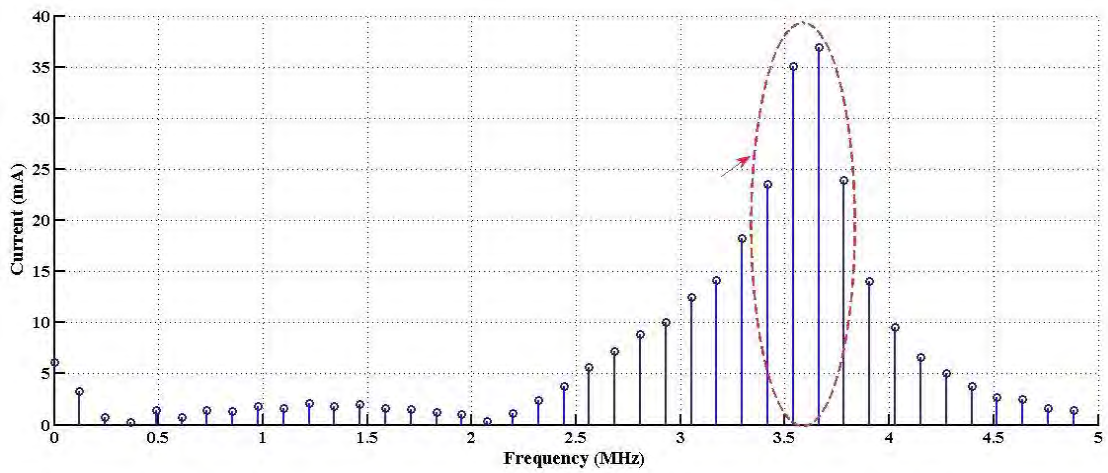


Figure A6: Frequency spectrum of individual corona pulse at 80 KV NFC

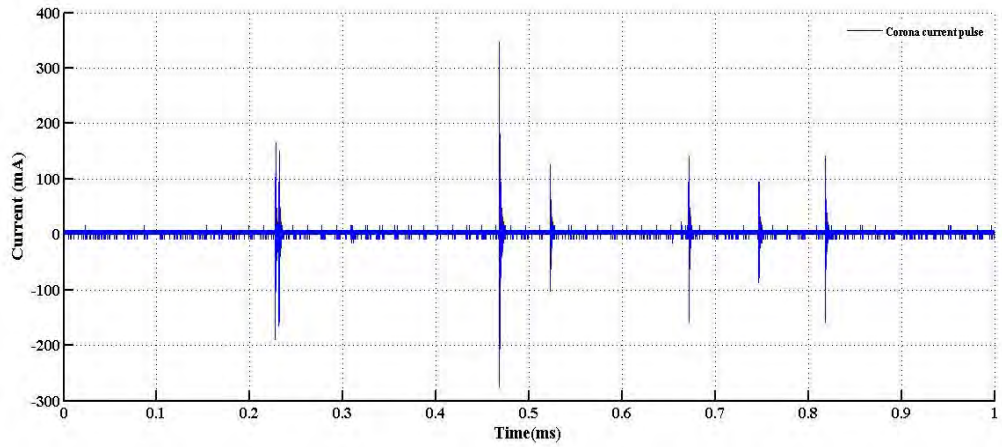


Figure A7: Measured sample of corona current at 100kV NFC

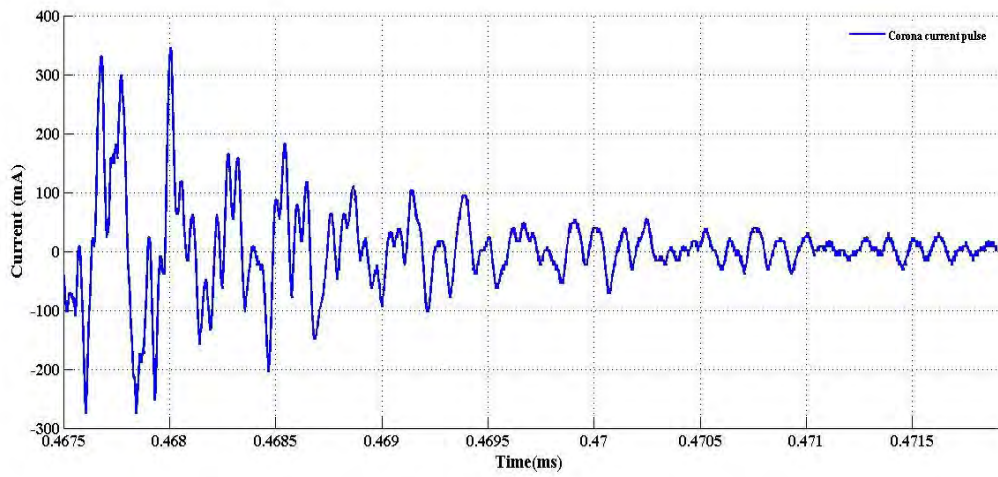


Figure A8: Individual corona pulse at 100kV NFC.

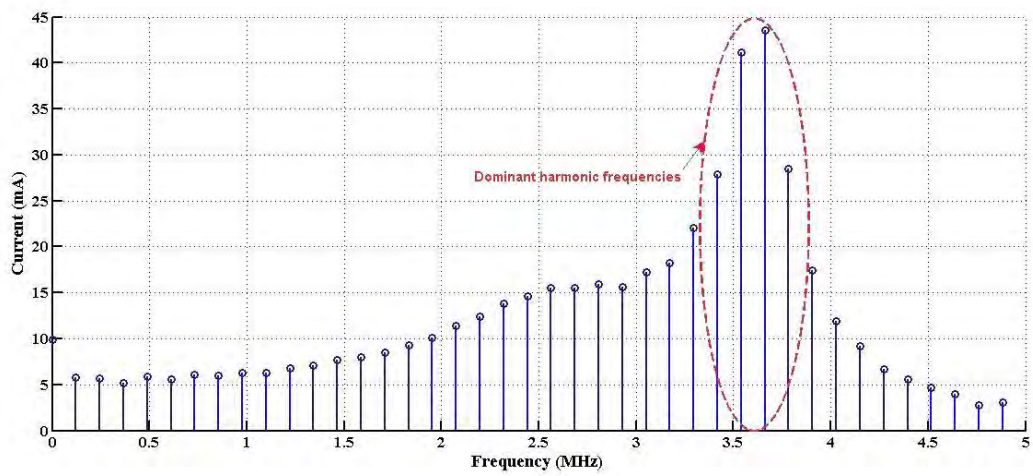


Figure A9: Frequency spectrum of individual corona pulse at 100kV NFC

Test 3 NFC

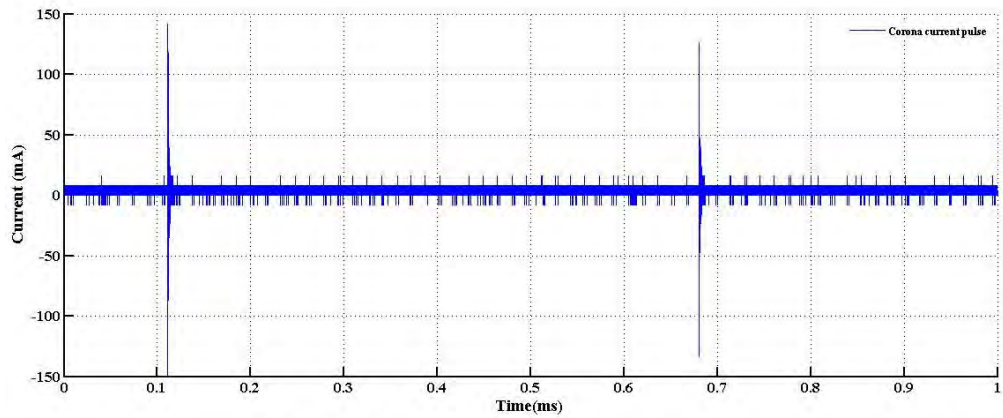


Figure A10: Measured sample of corona current at 60kV NFC

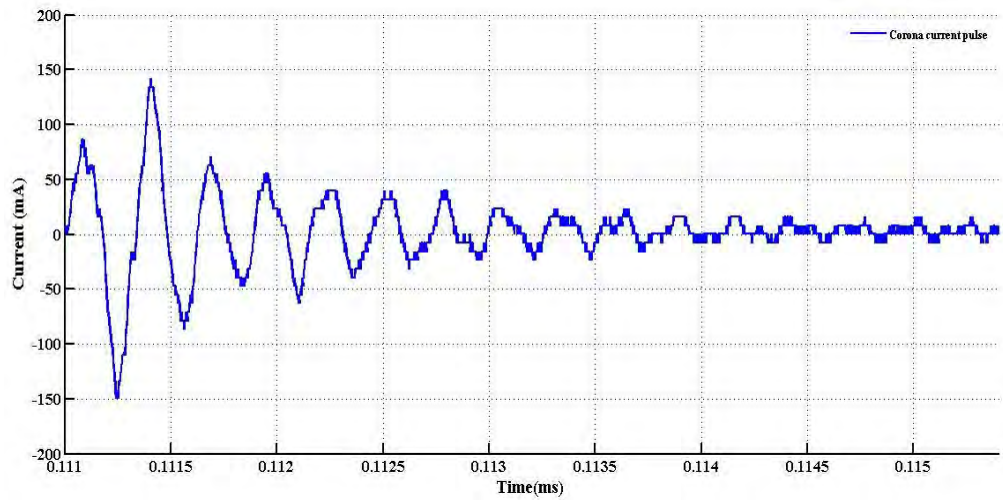


Figure A11: Individual corona pulse at 60kV NFC.

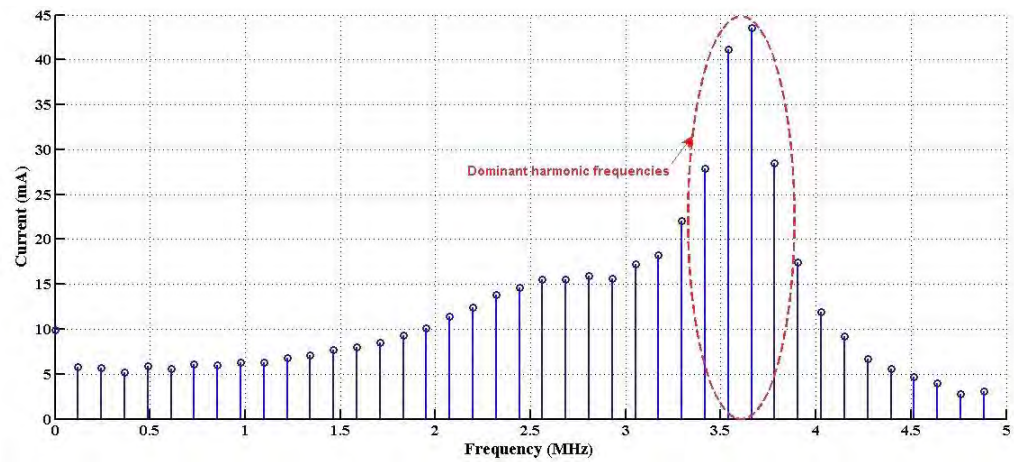


Figure A12: Frequency spectrum of individual corona pulse at 60 KV NFC

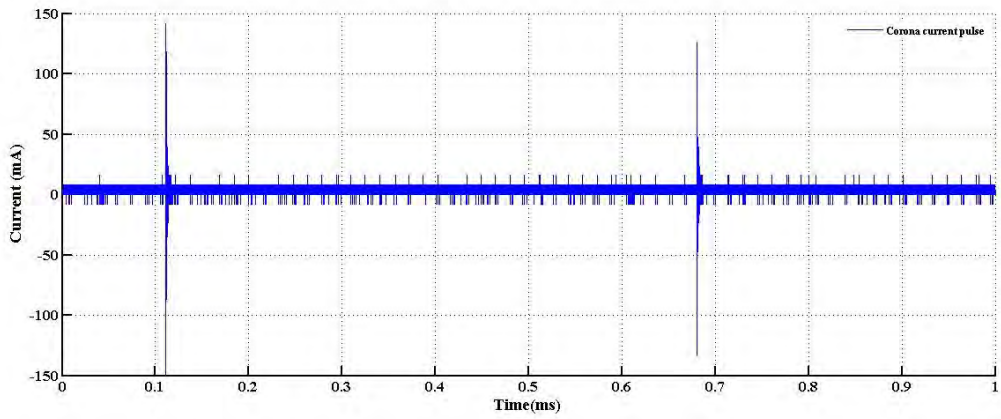


Figure A13: Measured sample of corona current at 80kV NFC

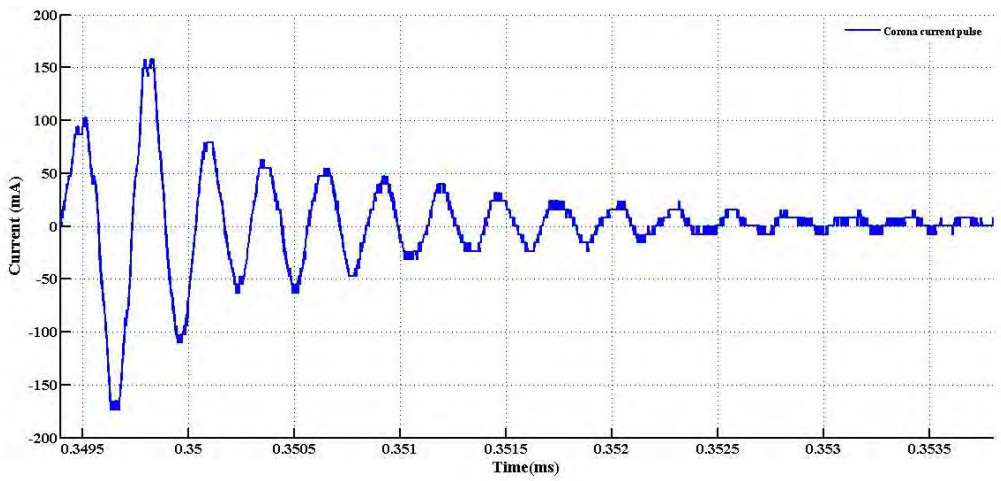


Figure A14: Individual corona pulse at 80kV NFC

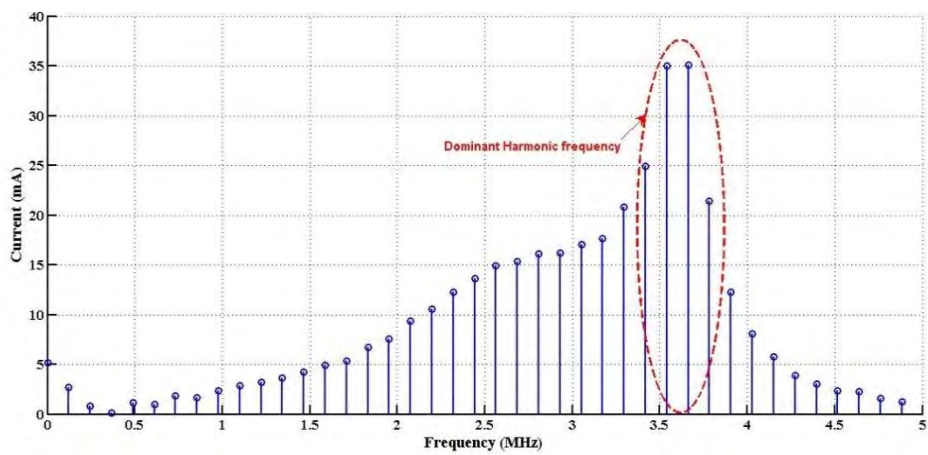


Figure A15: Frequency spectrum of individual corona pulse at 80 kV NFC

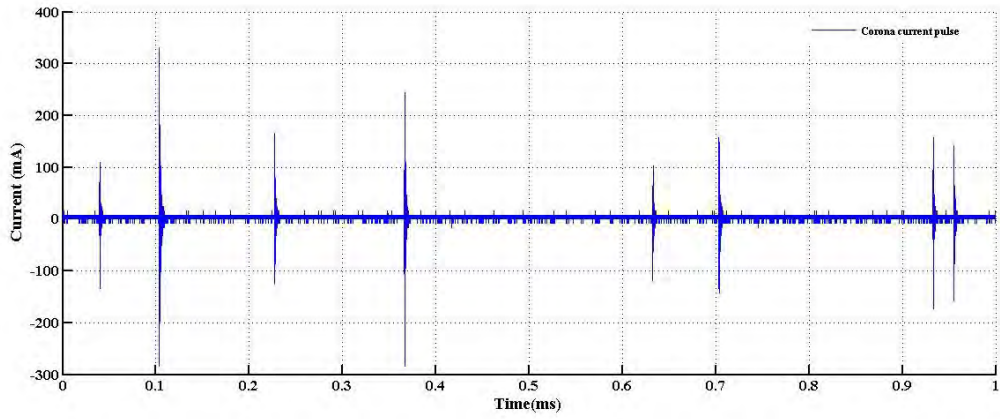


Figure A16: Measured sample of corona current at 80 kV NFC

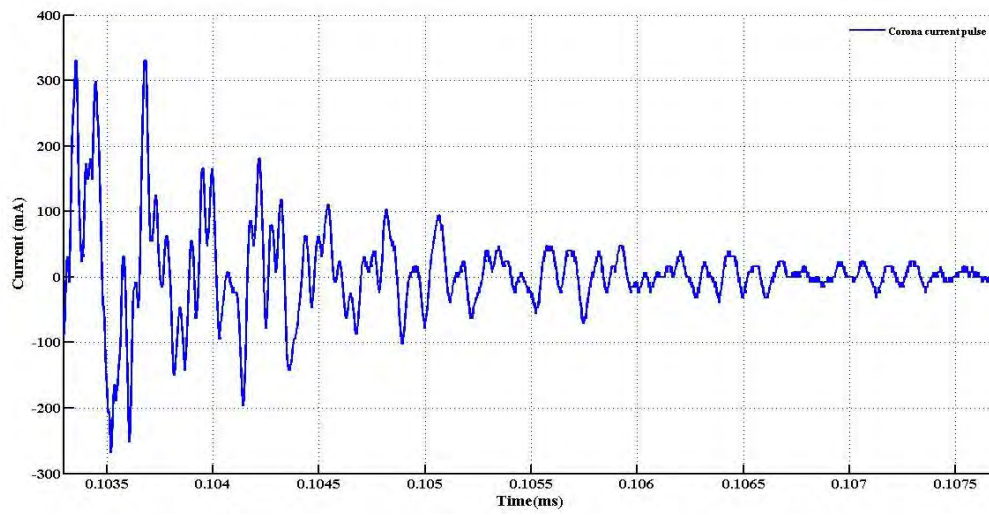


Figure A17: Individual corona pulse at 100 kV NFC

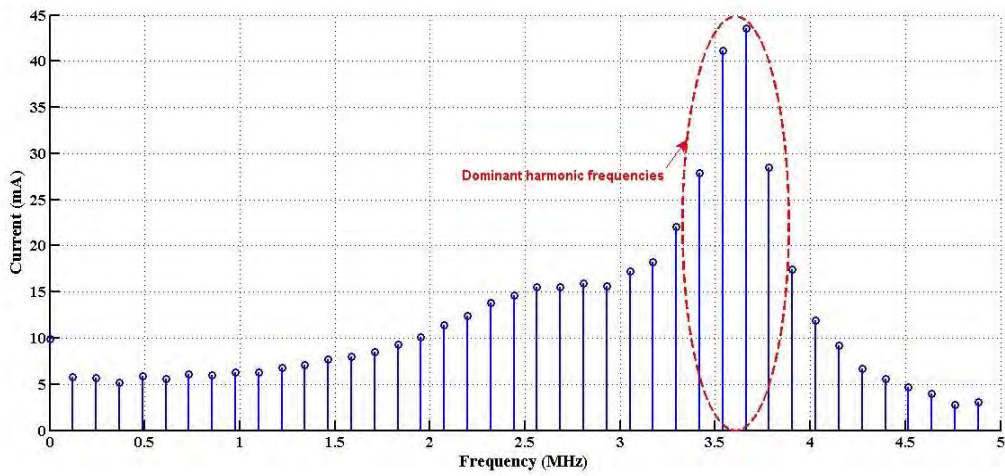


Figure A18: Frequency spectrum of individual corona pulse at 100 kV NFC

# Fire condition FC individual corona pulse

Test 2 FC

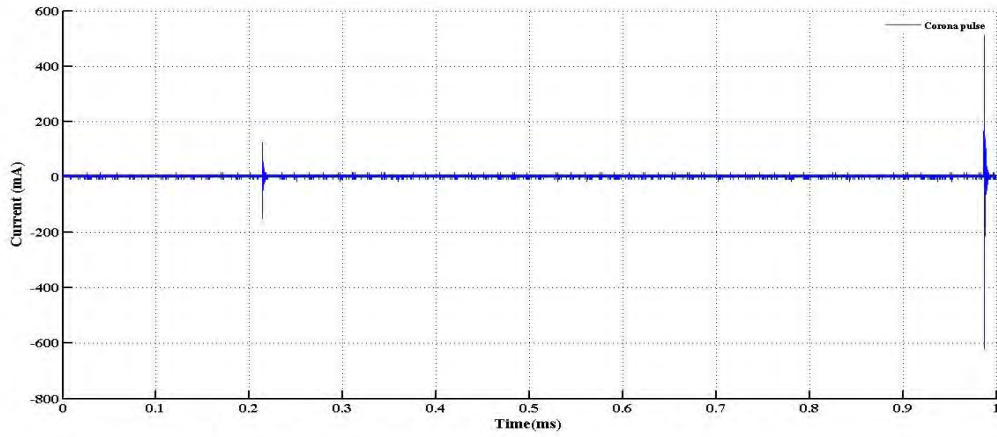


Figure A19: Measured sample of corona current at 60 kV FC

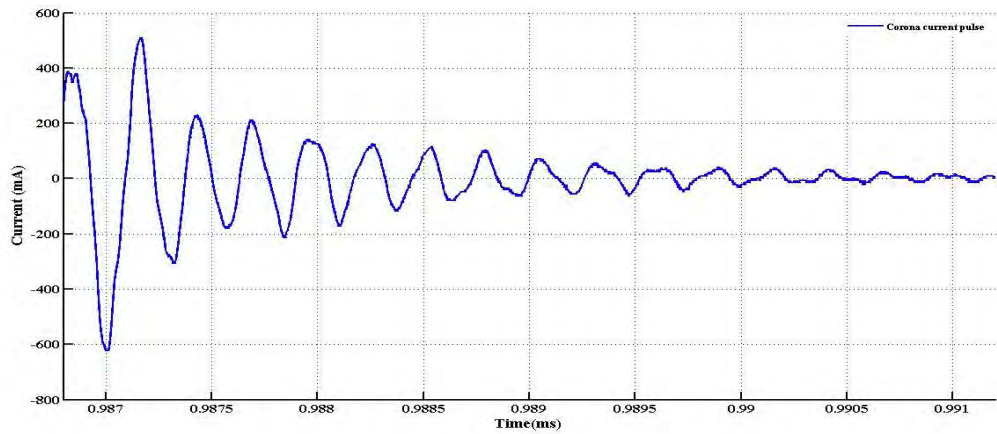


Figure A20: Individual corona pulse at 60 kV FC

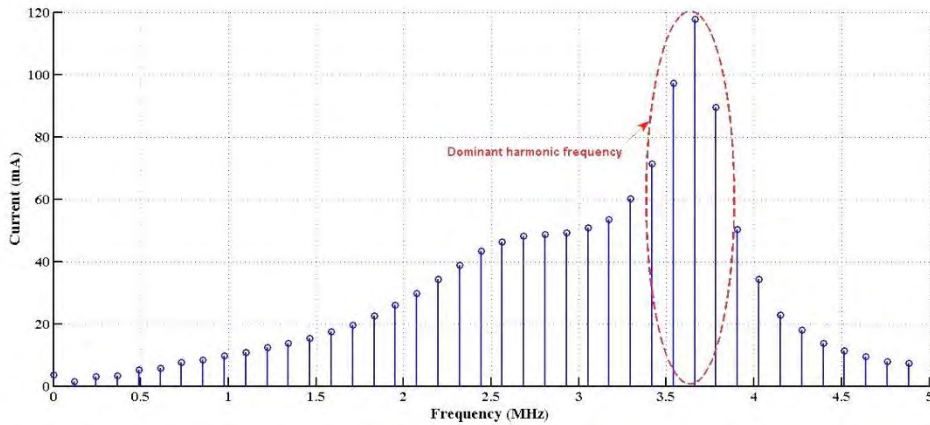


Figure A21: Frequency spectrum of individual corona pulse at 60 kV FC

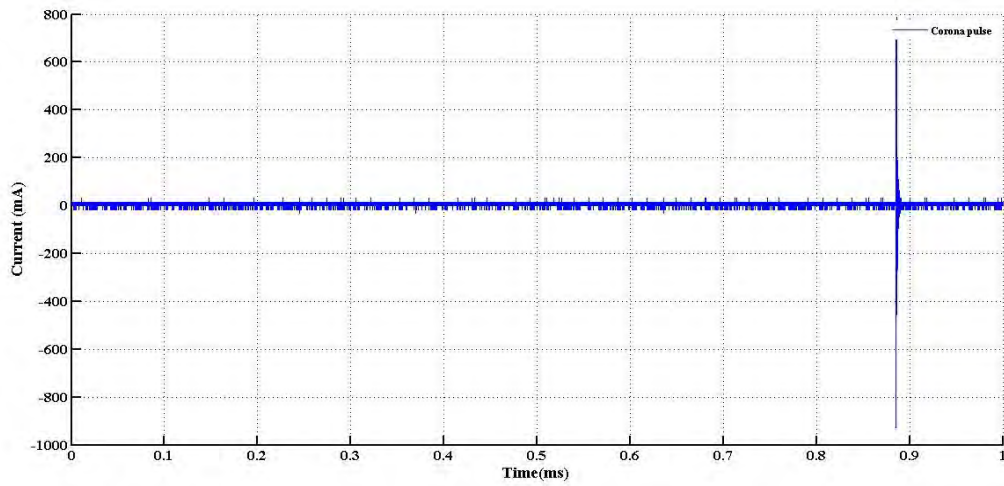


Figure A22: Measured sample of corona current at 80 kV FC

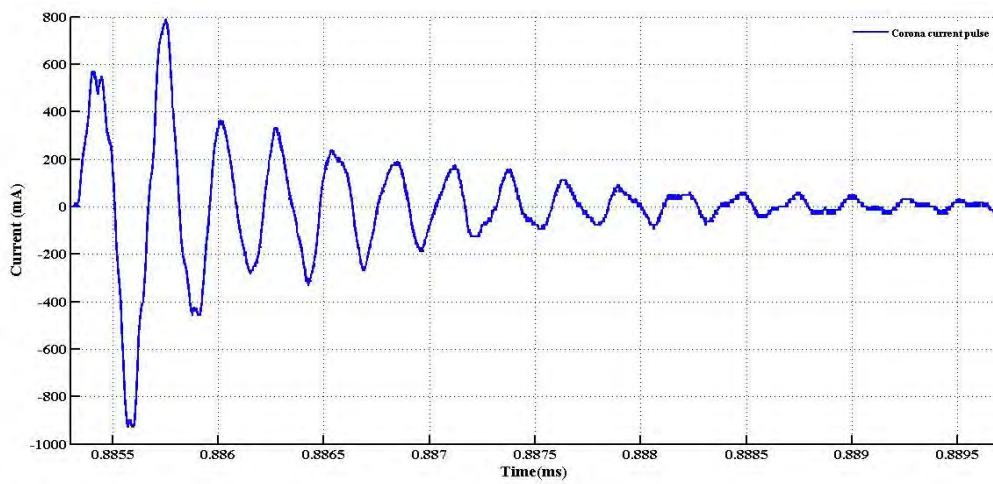


Figure A23: Individual corona pulse at 80 kV FC

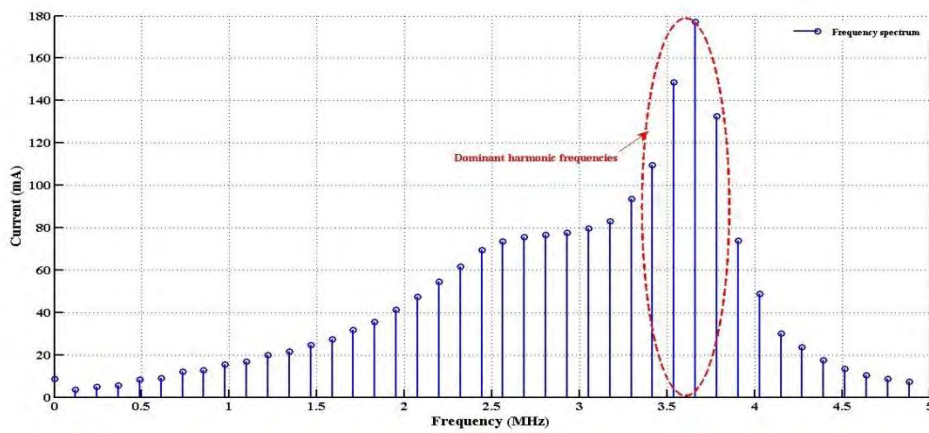


Figure A24: Frequency spectrum of individual corona pulse at 80 kV FC

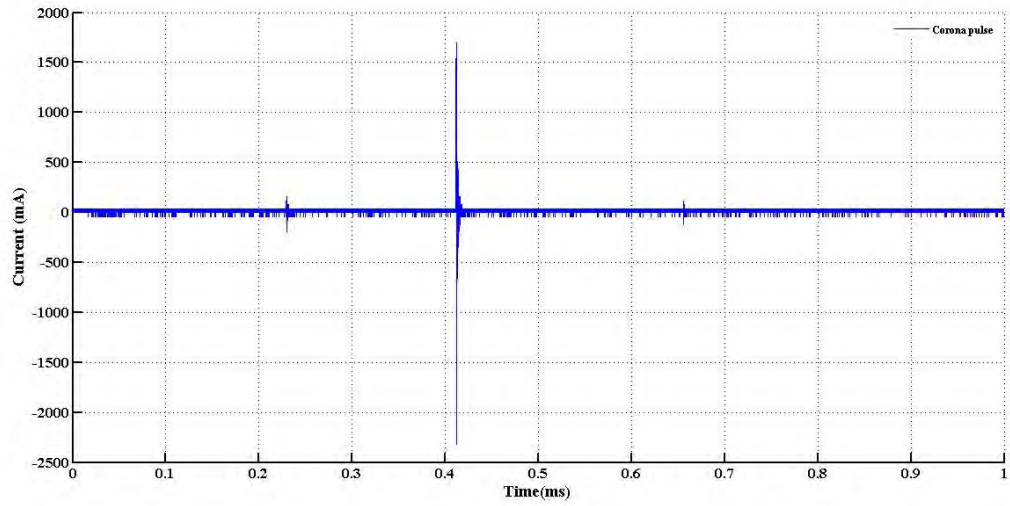


Figure A25: Measured sample of corona current at 100 kV FC

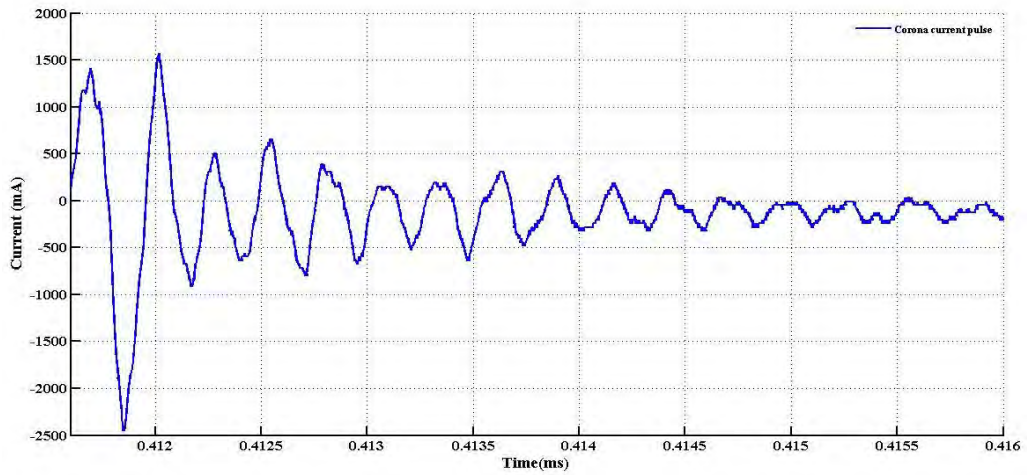


Figure A26: Individual corona pulse at 100 kV FC

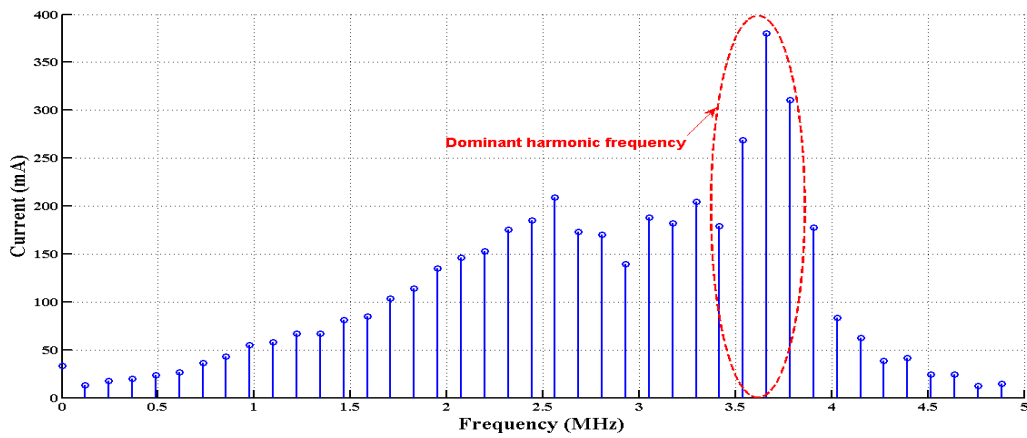


Figure A27: Frequency spectrum of individual corona pulse at 100 kV FC

Test 3

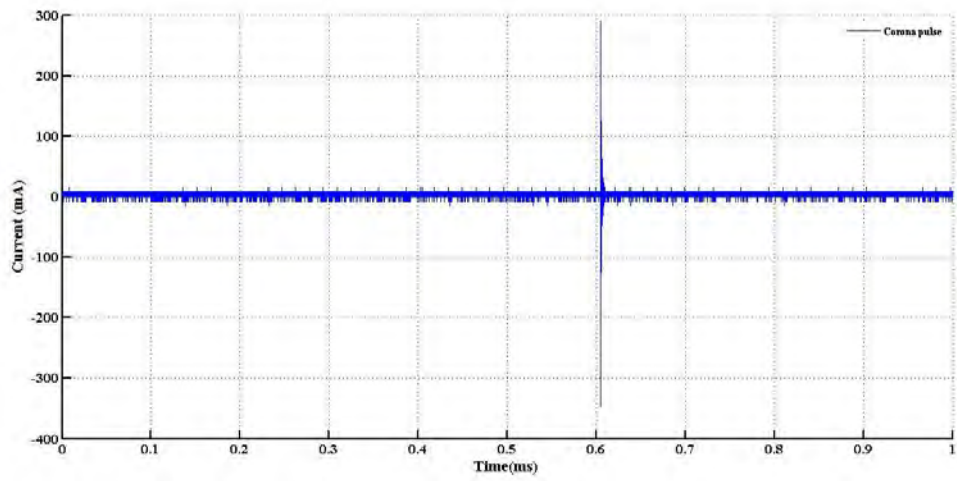


Figure A28: Measured sample of corona current at 60 kV FC

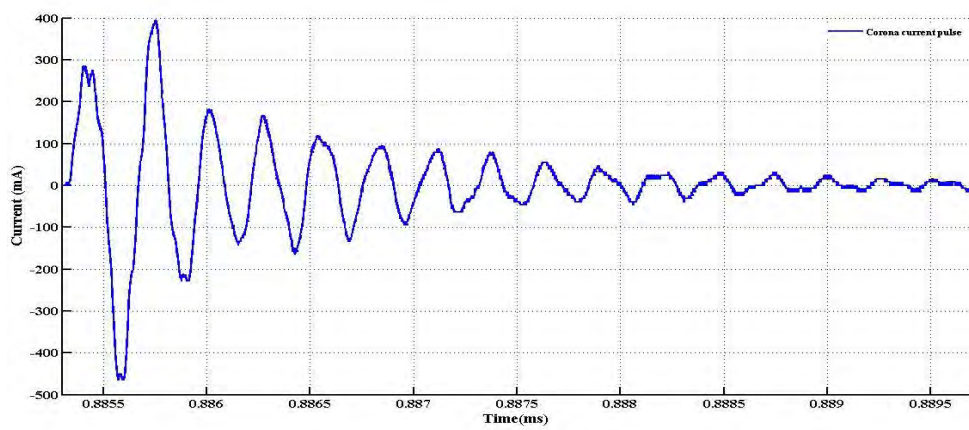


Figure A29: Individual corona pulse at 60 kV FC

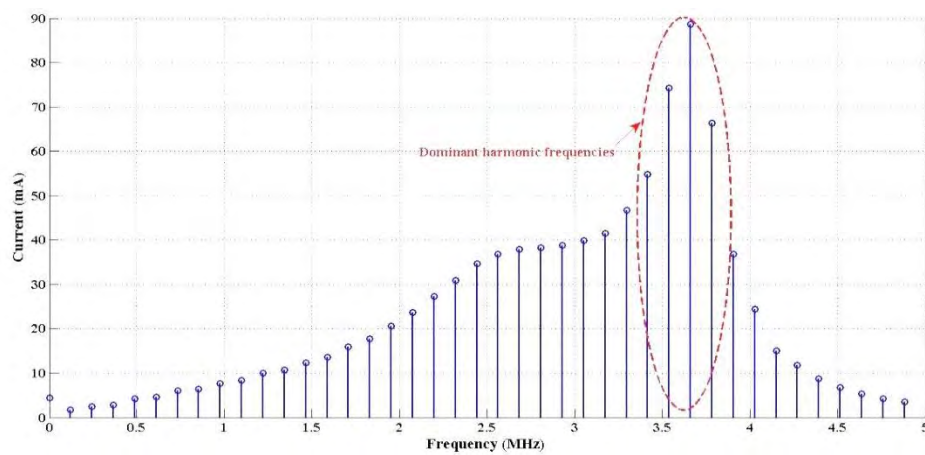


Figure A30: Frequency spectrum of individual corona pulse at 60 kV FC

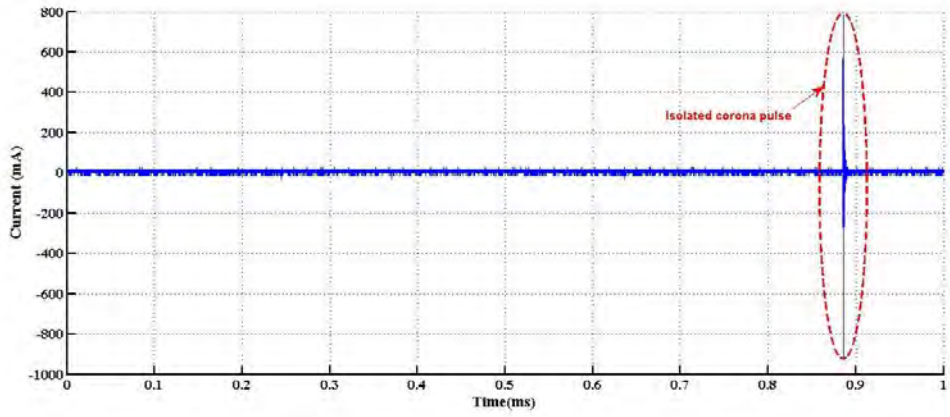


Figure A 31: Measured sample of corona current at 80 kV FC

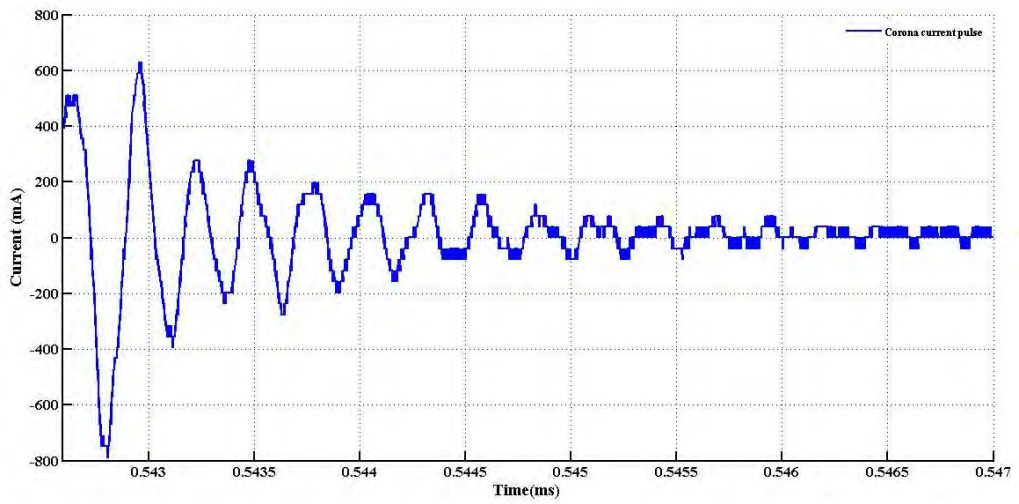


Figure A32: Individual corona pulse at 80 kV FC

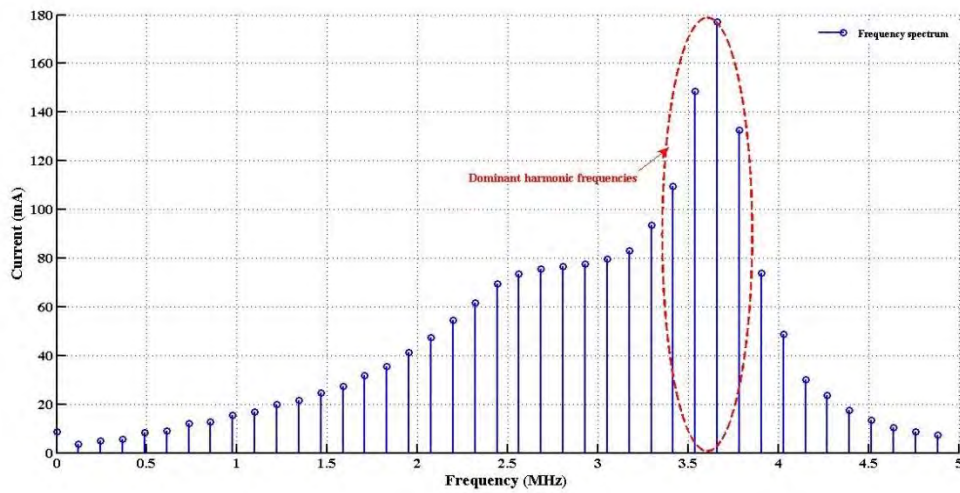


Figure A33: Frequency spectrum of individual corona pulse at 80 kV FC

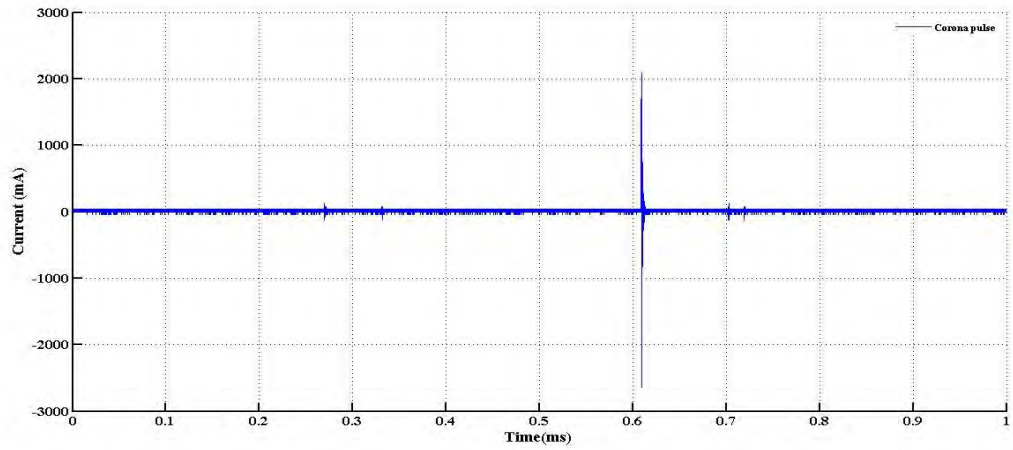


Figure A34: Measured sample of corona current at 100 KV FC

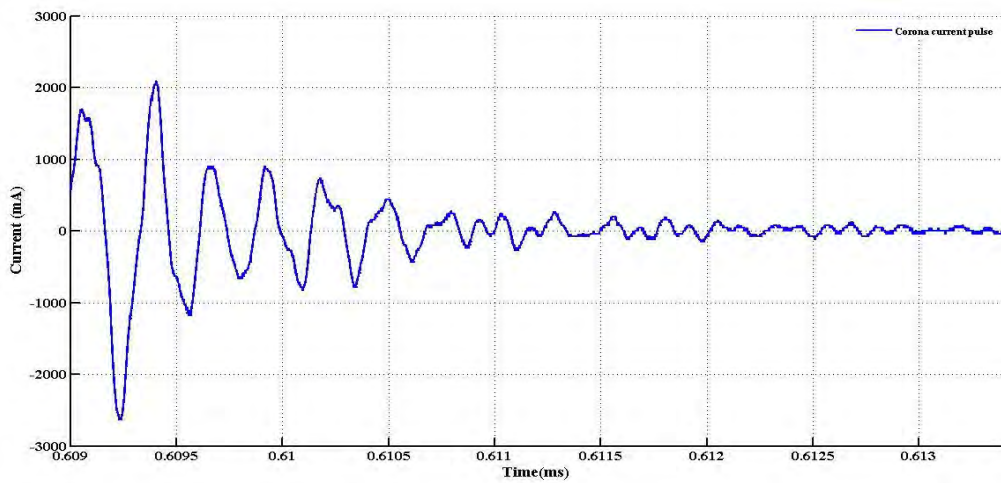


Figure A35: Individual corona pulse at 100 kV FC

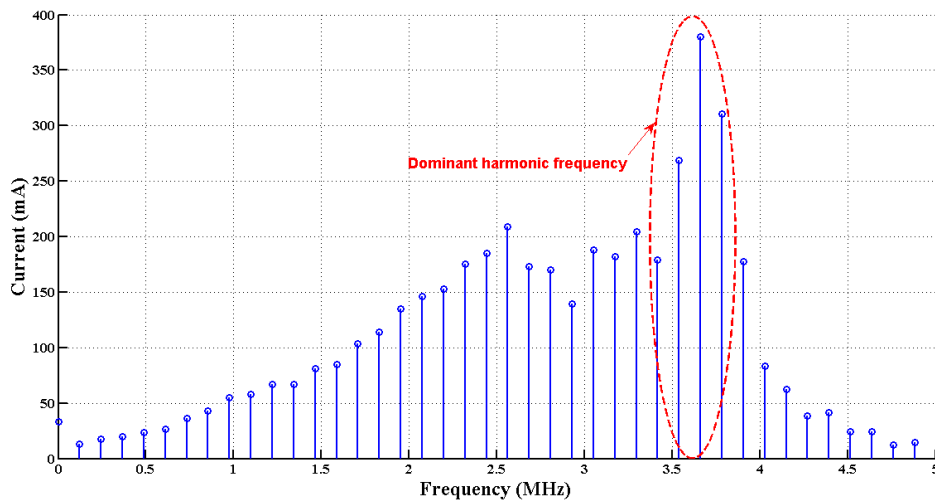


Figure A36: Frequency spectrum of individual corona pulse at 100 KV FC

## APPENDIX B

### Test 2 time distribution NFC

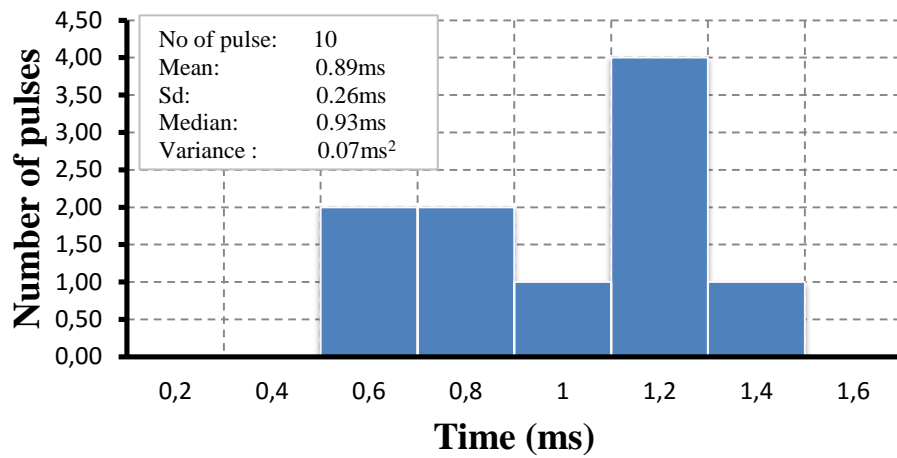


Figure B1: Frequency distribution of corona pulses time separation at 60 kV NFC

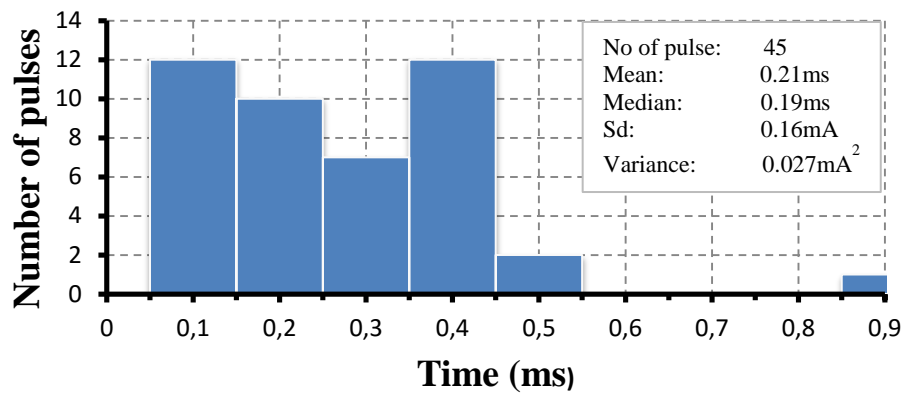


Figure B2: Frequency distribution of corona pulses time separation at 80 kV NFC

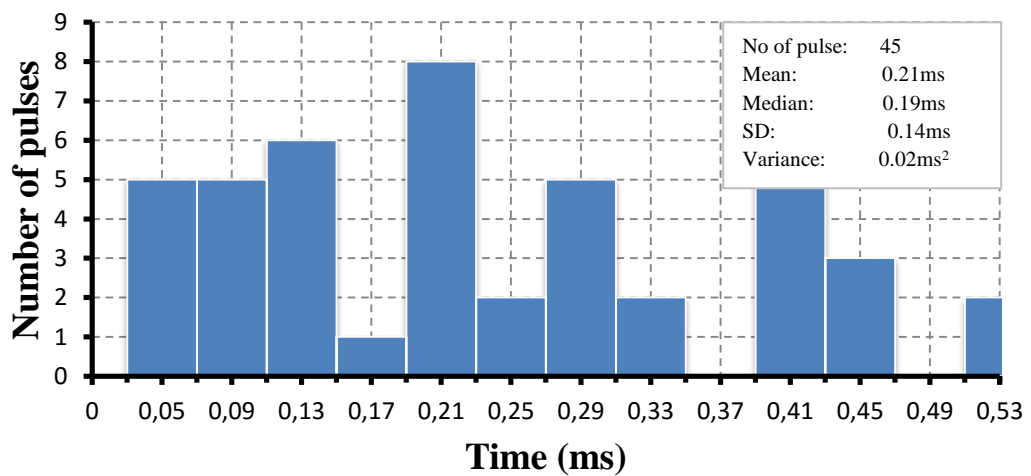


Figure B3: Frequency distribution of corona pulses time separation at 100 kV NFC

## Test 3 time distribution NFC

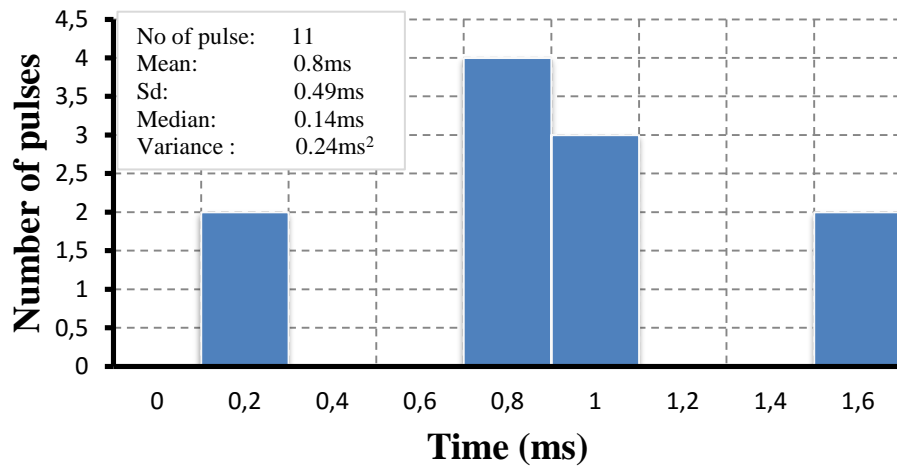


Figure B4: Frequency distribution of corona pulses time separation at 60 kV NFC

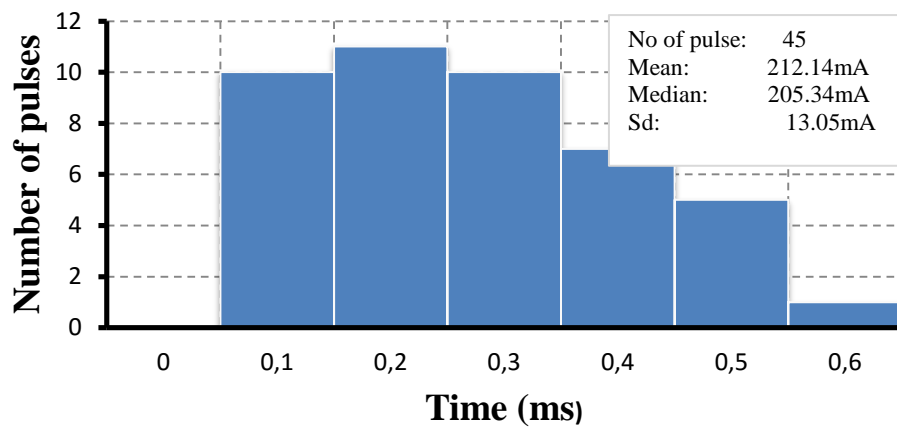


Figure B5: Frequency distribution of corona pulses time separation at 80 kV NFC

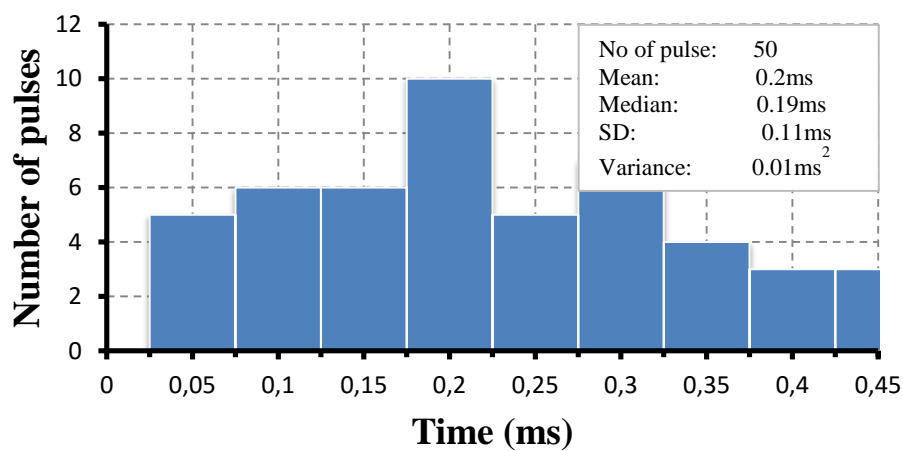


Figure B6: Frequency distribution of corona pulses time separation at 100 kV NFC

Test 2 time distribution FC

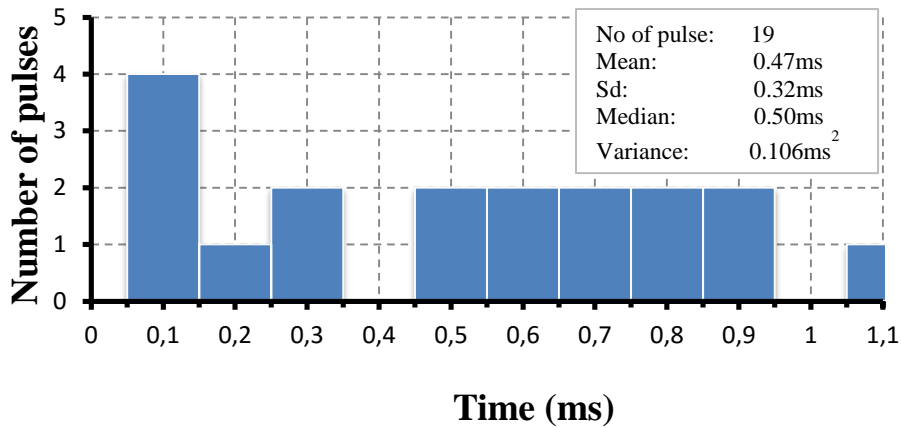


Figure B7: Frequency distribution of corona pulses time separation at 60 kV FC

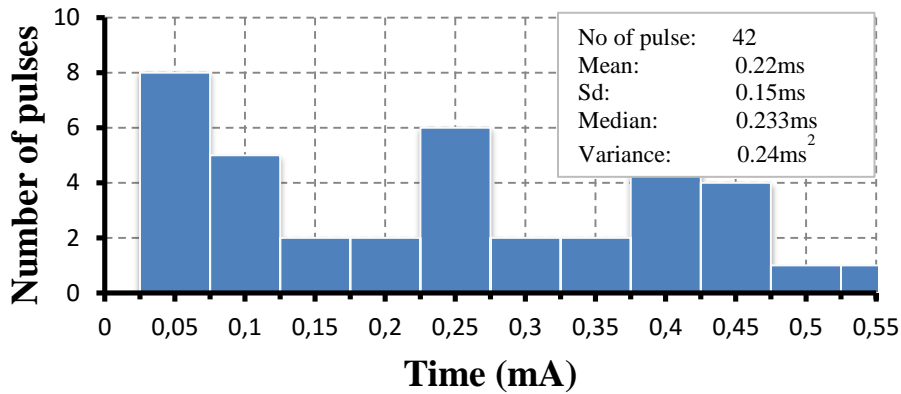


Figure B8: Frequency distribution of corona pulses time separation at 80 kV FC

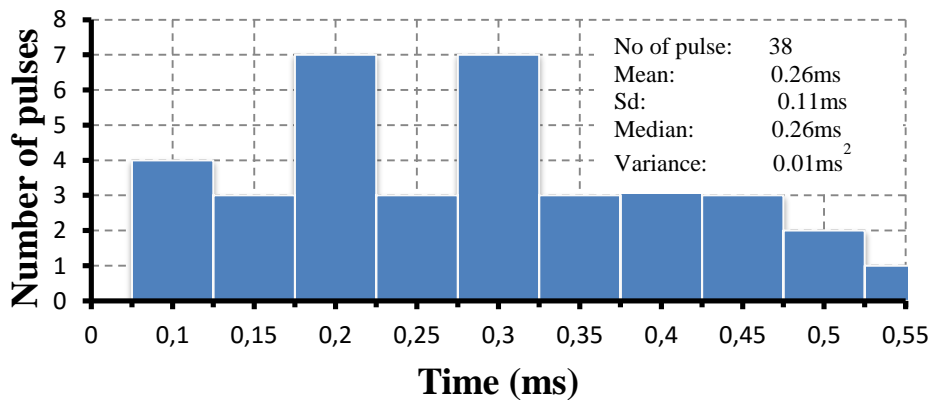


Figure B9: Frequency distribution of corona pulses time separation at 100 kV FC

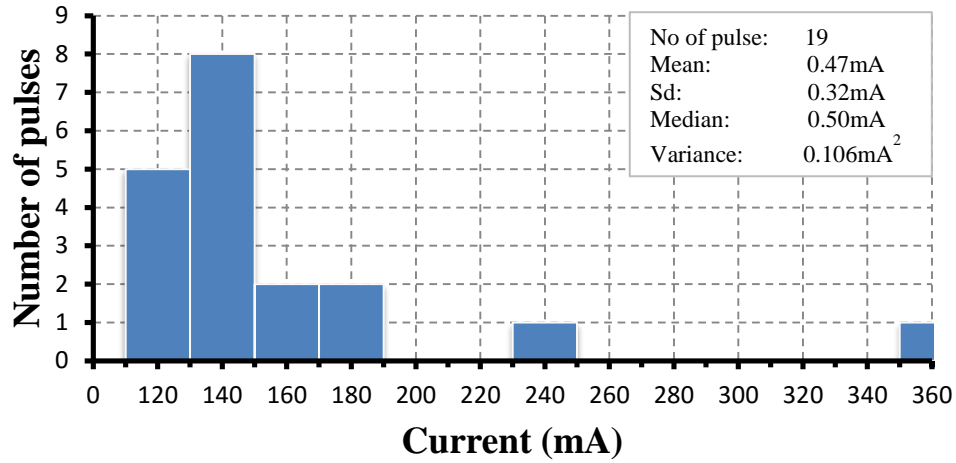


Figure B10: Frequency distribution of corona pulses magnitudes at 60 kV FC

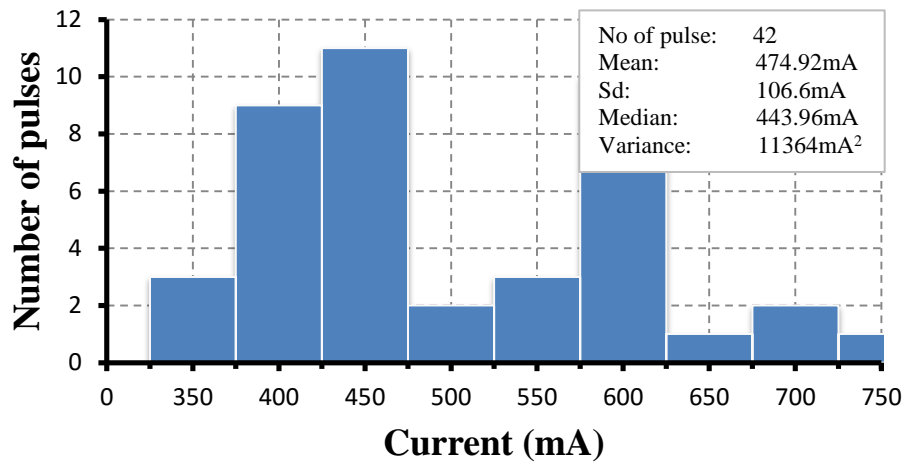


Figure B11: Frequency distribution of corona pulses magnitudes at 80 kV FC

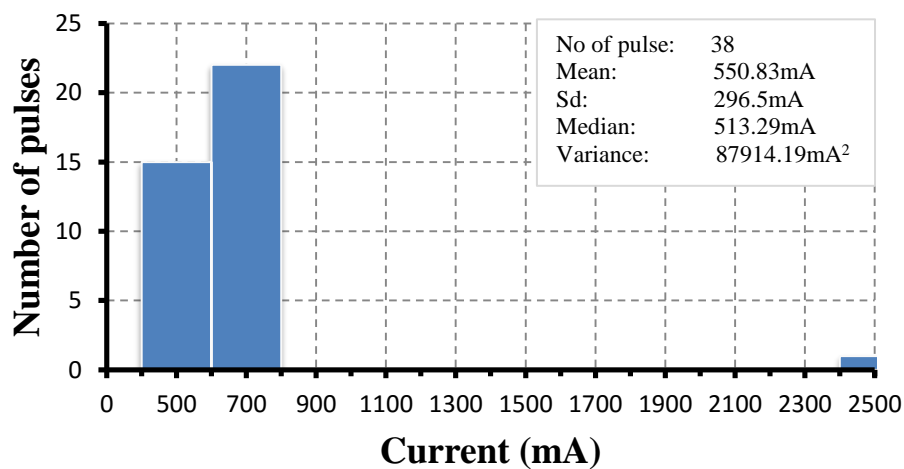


Figure B12: Frequency distribution of corona pulses magnitudes at 100 kV FC

Test 3 Time distribution

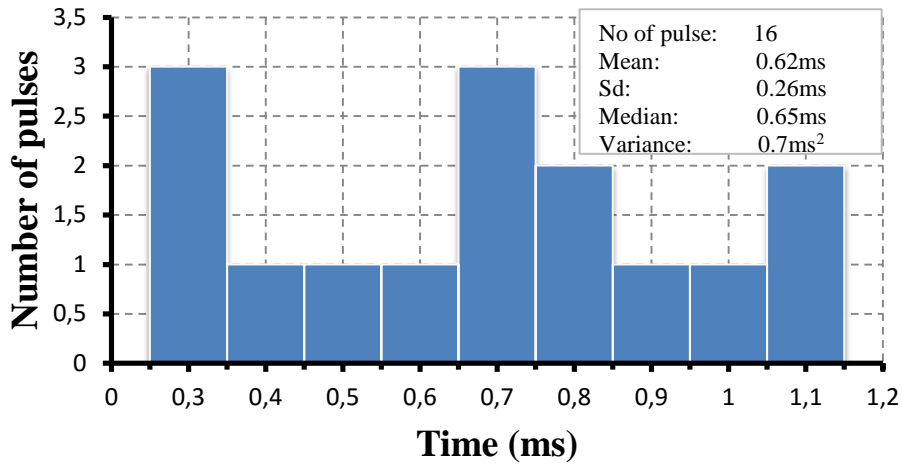


Figure B13: Frequency distribution of corona pulses time separation at 60 kV FC

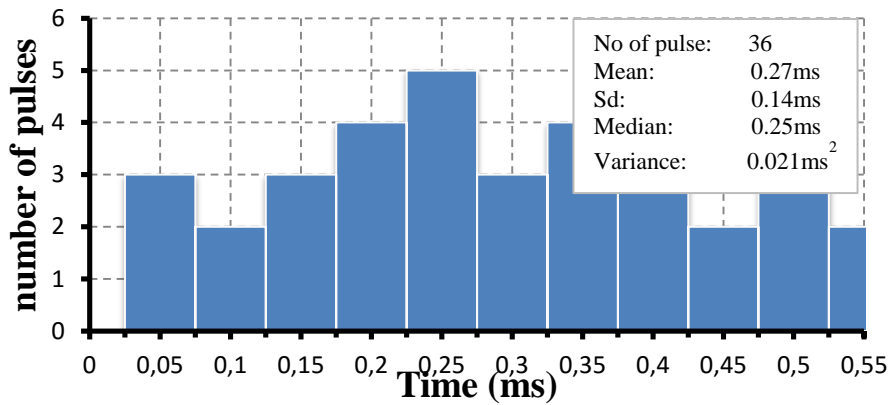


Figure B14: Frequency distribution of corona pulses time separation at 80 kV FC

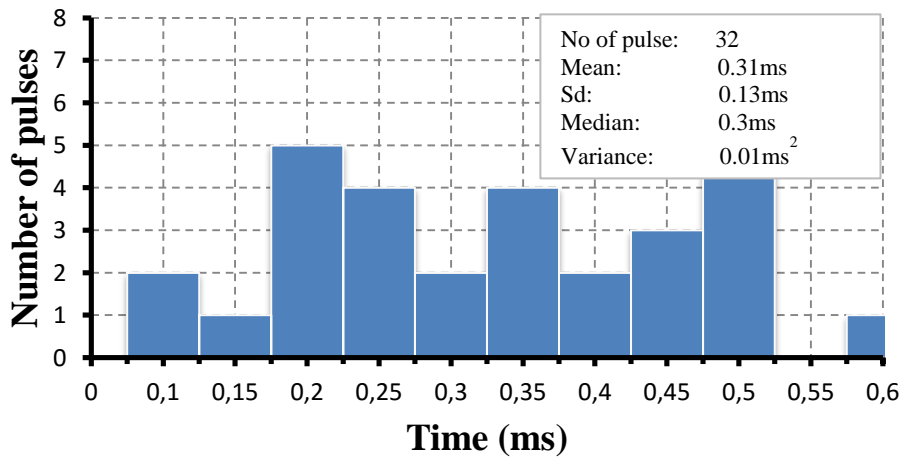


Figure B15: Frequency distribution of corona pulses time separation at 100 kV FC

APPENDIX C

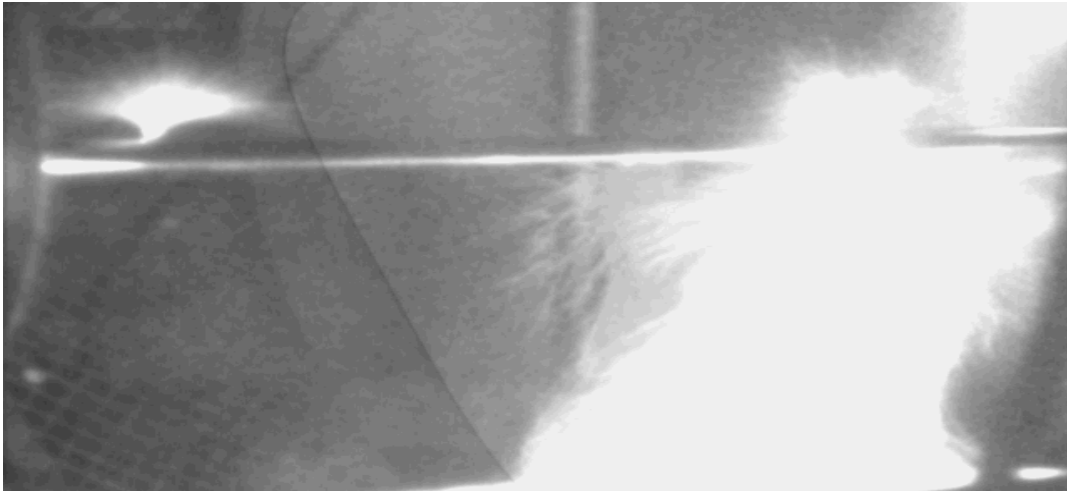


Figure C1: flashover at 100 kV

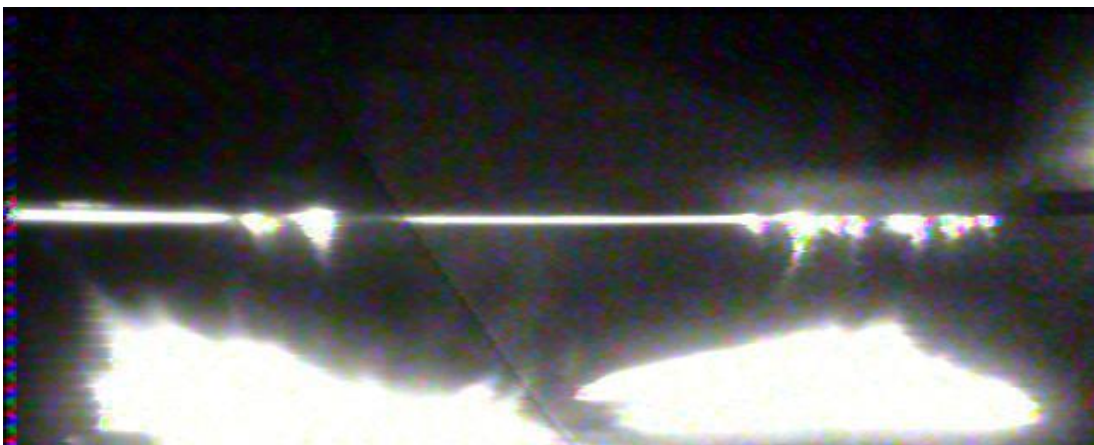


Figure C2: Image of fire beneath the conductor (corona camera)

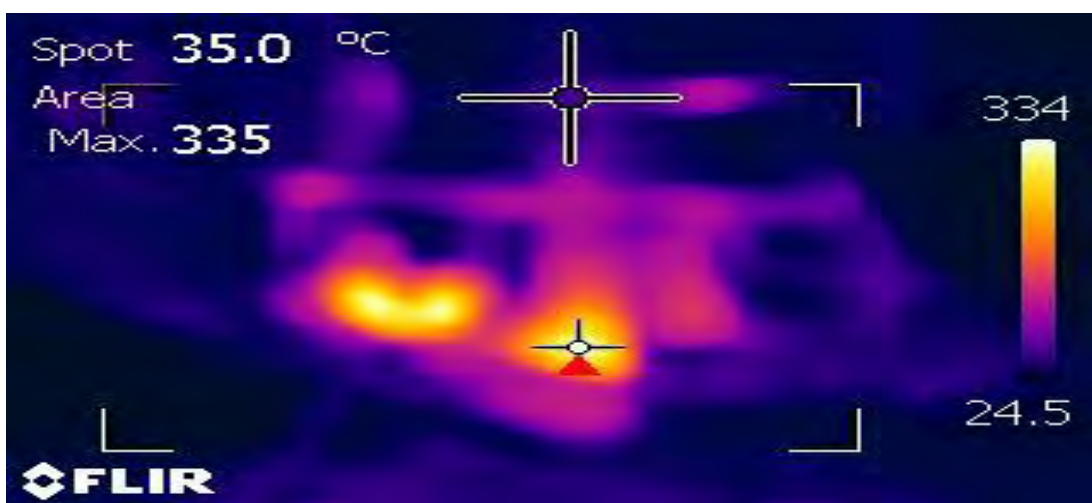


Figure C3: Image of fire beneath the conductor ( flir camera)